Cisplatin resistance is associated with altered signalling in NSCLC cells

Dissertation

zur

Erlangung des Doktorgrades (Dr. rer. nat.)

der

Mathematisch-Naturwissenschaftlichen Fakultät

der

Rheinischen Friedrich-Wilhelms-Universität Bonn

vorgelegt von

Navin Sarin

aus Monheim am Rhein

Bonn 2017

Angefertigt mit Genehmigung der Mathematisch-Naturwissenschaftlichen Fakultät der
Rheinischen Friedrich-Wilhelms-Universität Bonn

Erstgutachter: Prof. Dr. Ulrich Jaehde

Zweitgutachter: Prof. Dr. Gerd Bendas

Tag der Promotion: 21.11.2017

Erscheinungsjahr: 2018

Die vorliegende Arbeit wurde am Pharmazeutischen Institut der Rheinischen Friedrich-Wilhelms-Universität Bonn unter der Leitung von Herrn Prof. Dr. U. Jaehde angefertigt.

Meinem Doktorvater Prof. Dr. U. Jaehde danke ich für die Überlassung des interessanten Projektes, die Möglichkeit im Arbeitskreis Klinische Pharmazie zu promovieren, für sein entgegengebrachtes Vertrauen und die zahlreichen Erfahrungen, die ich während meiner Promotionszeit auch außerhalb meines Projektes sammeln konnte.

Ebenso möchte ich mich bei Prof. Dr. Gerd Bendas für die Übernahme des Koreferates und die Unterstützung des Projektes durch die Nutzung seiner Laborräume bedanken. Bei Prof. Dr. Christa Müller und Prof. Dr. Andreas Meyer bedanke ich mich für Ihr Mitwirken in der Prüfungskommission.

Herzlich möchte ich mich bei den Kooperationspartnern in der Central European Society for Anticancer Research (CESAR) für die intensiven Diskussionen und die Mitwirkung bei der Entwicklung des Projektes bedanken. Besonders sind hier Dr. Florian Rothweiler und Prof. Dr. J. Cinatl sowie Prof. Dr. M. Michaelis zu nennen, die mir bereitwillig die Zelllinien zur Verfügung gestellt haben.

Frau Dr. Anya Kalayda danke ich für Ihre Hilfsbereitschaft und Unterstützung während der gesamten Promotionszeit sowohl im Labor als auch bei der Erstellung der Arbeit und verschiedener Publikationen. Ihr Einsatz hat wesentlich zum Gelingen dieser Dissertation beigetragen.

Besonders bedanken möchte ich mich bei den Kollegen des Bundesinstituts für Arzneimittel und Medizinprodukte (BfArM), Sandra Weikhardt, Dr. Roland Frötschl und Dr. Florian Engel. Durch Ihre Unterstützung im Labor und bei der Datenauswertung sowie die Möglichkeit, einige Versuche in ihren Laboren durchführen zu können, haben Sie ebenfalls maßgeblich zum Gelingen dieser Arbeit beigetragen.

Der ganzen Laborgruppe des Arbeitskreises Klinische Pharmazie danke ich für die gute Zusammenarbeit, besonders Dr. Maximilian Kullmann für die vertrauensvolle, gegenseitige Unterstützung und das gute nachbarschaftliche Verhältnis.

Vielen Dank den Kollegen des gesamten Arbeitskreises Klinische Pharmazie für die gute Zeit und die tollen Erlebnisse. Ein besonderer Dank gilt den Kolleginnen des Büros 3.108, Dr. Stefanie Kraff, Verena Kurth und Kerstin Bitter für die freundschaftliche Unterstützung und die guten Diskussionen sowie die stete Hilfsbereitschaft.

Ein herzlicher Dank gilt den vielen kritischen Korrekturlesern meiner Arbeit, die durch ihre konstruktiven Anmerkungen die Arbeit maßgeblich weiterentwickelt haben.

Ein ganz besonderer Dank gilt meiner Familie, die auch in schwierigen Zeiten immer an mich geglaubt und mich auf meinem gesamten Lebensweg bedingungslos unterstützt hat. Der größte Dank gilt zum Abschluß meiner Frau Kathrin, die mir immer wieder den Rücken freigehalten und mich stets motiviert hat, diese Arbeit zu vollenden.

Für meine Familie

“Den Zweifel zur Lebensphilosophie zu erklären, das ist, als wählte man den Stillstand zum Transportmittel.”

Pi Patel *in* Schiffbruch mit Tiger *von* Yann Martel

Abbreviations

A	Adenosine
A549	Adenocarcinomic human alveolar basal epithelial cell line
A549^{r}CDDP^{2000}	Adenocarcinomic human alveolar basal epithelial cell line, cisplatin-resistant sub-line
AAS	Atomic absorption spectroscopy
AKT	Protein kinase B (PKB), RAC-α serine/threonine kinase
ANOVA	Analysis of variance
ApG	Adenine-phosphate-Guanine
APS	Ammonium persulfate
Atm	Ataxia telangiectasia mutated
ATP7B	Copper-transporting P-type ATPase, ß polypeptide
ATR	Ataxia telangiectasia and Rad3-related protein
BAX	BCL2-associated X protein
BCA	Bicinchoninic acid
BCL-2	Apoptosis regulator B-cell CLL/lymphoma 2
BER	Base excision repair
BRCA1, BRCA2	Breast cancer 1, early onset, Breast cancer 2, early onset
BSA	Bovine serum albumin
CAK	Cdk-activating kinases
CAT	Catalase
CBP	CREB-binding protein
CCL2	Chemokine (C-C motif) ligand 2 (monocyte chemotactic protein 1)
CDK5	Cyclin-dependent kinase 5
CDKN1A	Cyclin dependent kinase inhibitor 1A
cDNA	Complementary DNA
Chk2	Checkpoint kinase 2
cRNA	RNA derived from cDNA
CTR1	Copper transporter 1
DAPI	2-(4-amidinophenyl)-1H-indole-6-carboxamidine dihydrochloride
DMF	Dimethylformamide
DMSO	Dimethyl sulfoxide
DNA-PK	DNA-dependent protein kinase
DNER	Delta and Notch-like epidermal growth factor-related receptor

DOK1, DOK2	Docking protein 1, docking protein 2
DTT	Dithiothreitol
DYRK1B	Dual specificity tyrosine-phosphorylation-regulated kinase 1B
ECL	enhanced chemiluminescence
EDTA	Ethylenediaminetetraacetat
EGF	Epidermal growth factor
EGFR	Epidermal growth factor receptor
ELISA	Enzyme linked immuno sorbent assay
ERBB2	Erb-b2 receptor tyrosine kinase 2
ERCC1	Excision repair cross-complementation group 1
ERK	Extracellular signal-regulated kinases
FACS	Fluorescence-activated cell sorting
FCS	Foetal calf serum
FDA	Food and Drug Administration
FDR	False discovery rate
FITC	Fluorescein isothiocyanate
FL probe	FRET donor (3'-Fluroescein)
FRET	Förster resonance energy transfer
FSC	Forward-scattered light
G	Guanine
G_0-phase	Resting phase
G_1-phase	Growth phase 1
G_2-phase	Growth phase 2
GADD45a	Growth arrest and DNA-damage-inducible protein GADD45 alpha
GAPDH	Glyceraldehyde 3-phosphate dehydrogenase
GOI	Genes of interest
GpG	Guanine-phosphate-guanine
GRP78	Glucose-regulated protein, 78kDa
GSEA	Gene Set Enrichment Analysis
HCT116	Colon cancer cell species
HRas	Harvey rat sarcoma viral oncogene homolog
HRP	Horse radish peroxidase
HSP90	Heat shock protein 90
IgG	Immunoglobulin G
IMDM	Iscove’s Modified Dulbecco’s Medium

JAG2	Jagged 2
JNK1, JNK2	C-Jun N-terminal kinase 1,2
JNK3	C-Jun N-terminal kinase 3 (mitogen-activated protein kinase 10)
KEGG	Kyoto Encyclopaedia of Genes and Genomes
LC probe	FRET acceptor (LightCycler® red 640)
LIMMA	Linear model for microarray data
Lys382	Lysine at position 382 of p53
MAPK	Mitogen-activated protein kinase
MAPK10	Mitogen-activated protein kinase 10 (c-Jun N-terminal kinase 3)
MAPK14	Mitogen-activated protein kinase 14 (p38α)
MAPKAPK2	MAP kinase-activated protein kinase 2
MCP1	Monocyte chemotactic protein 1 (Chemokine (C-C motif) ligand 2)
MDM2	Mouse double minute 2 homolog
MLH1	MutL homolog 1, colon cancer, nonpolyposis type 2
MMR	Mismatch repair
M-phase	Mitosis
MRP2	Multidrug resistance-associated protein 2
MSH6	MutS homolog 6
MTT	3-(4,5-dimethylthiazol-2-yl)- 2,5-diphenyltetrazolium bromide
Mut proteins	Important components of the mismatch repair system, often mutationally inactivated
n	Number or replicates
NER	Nucleotide excision repair
NHE9	Cation proton antiporter 9 (solute carrier family 9, subfamily A)
NSCLC	Non-small cell lung cancer
p21	Cyclin dependent kinase inhibitor 1A
p300	E1A binding protein p300
p38α	Mitogen-activated protein kinase 14
p53	Tumour protein p53
PAGE	Polyacrylamide gel electrophoresis
pAtm	Phosphorylated ataxia telangiectasia mutated
PBS	phosphate buffered saline
PCNA	Proliferating cell nuclear antigen
PDIA1, PDIA3	Protein disulfide-isomerase A1, protein disulfide-isomerase A3
pEC_{50}	Negative decimal logarithm of EC_{50}

PI	Propidium iodide
PI3K	Phosphatidylinositol-4,5-bisphosphate 3-kinase
POLH	DNA polymerase eta
PP2A	Protein phosphatase 2 alpha
PS	Phospholipid phosphatidylserine
PTK2B	Protein tyrosine kinase 2 beta
PVDF	Polyvinylidene fluoride
QC	Quality control
QSP	Quantitative and Systems Pharmacology
Rac1	Ras-related C3 botulinum toxin substrate 1
Ras	Rat sarcoma viral oncogene homolog
RASA1	RAS p21 protein activator 1
REV3	DNA polymerase zeta subunit
RIPA	Radioimmunoprecipitation assay
RKO	Colon cancer cell species
ROS	Reactive oxygen species
RT-PCR	Reverse transcriptase polymerase chain reaction
SD	Standard deviation
SDS	Sodium dodecyl sulphate
SDS-PAGE	Sodium dodecyl sulphate polyacrylamide gel electrophoresis
SEM	Standard error of mean
SIP	Stress inducible protein (Tumour protein p53 inducible nuclear protein 1)
SLC12A3	Solute carrier family 12, subfamily A, member 3
SLC9A9	Solute carrier family 9, subfamily A, member 9 (cation proton antiporter 9)
S-phase	Synthesis phase
SSC	Side-scattered light
SYBR Green I	N',N'-dimethyl-N-[4-[(E)-(3-methyl-1,3-benzothiazol-2-ylidene)methyl]-1-phenylquinolin-1-ium-2-yl]-N-propylpropane-1,3-diamine
TBS	Tris-buffered saline
TBS-T	Tris-buffered saline with Tween®-20
TEMED	Tetramethylethylenediamine
Thr18, Thr55	Threonine at position 18 and 55 of p53
Tip60	K(lysine) acetyltransferase 5
TMB	3,3’,5,5’-Tetramethylbenzidin
TP53INP1	Tumour protein p53 inducible nuclear protein 1 (Stress inducible protein)

Tris	2-Amino-2-hydroxymethyl-propane-1,3-diol (Tris(hydroxymethyl)aminomethane)
VDAC1	Voltage-dependent anion-selective channel protein 1
VEGFR	Vascular endothelial growth factor receptor
Wnt4	Wingless-type mouse mammary tumour virus integration site family, member 4
XPC	Xeroderma pigmentosum, complementation group C

1 Introduction

1.1 Non-small cell lung cancer (NSCLC) and treatment

Lung carcinomas are one of the leading cancer diseases in Germany. It is the most frequent cause of death with a mortality rate of 25 % in men and the third-leading cause of death with a mortality rate of 14 % in women with cancer (1). A very poor prognosis is reflected in relatively low 5-year survival rates with 21 % in women and 16 % in men. Lung cancer is divided into three main types: An adenocarcinoma is diagnosed in one third of all cases, whereas one fourth accounts for squamous cell carcinoma and small cell lung carcinoma, respectively (2). Adenocarcinomas, squamous cell carcinomas and large cell carcinomas belong to the non-small cell lung carcinomas (NSCLC). This histological WHO classification is based on biological behaviour, prognosis and therapy options. The therapy depends on stage and time of diagnosis of the tumour. Curative resection is, if possible, the first-line treatment in stages I-IIIb after neo-adjuvant and following adjuvant chemotherapy. If the tumour is diagnosed rather late in stage IV with multiple metastases, which is the case in approx. 40 % of NSCLC, only palliative chemotherapy is possible. The type of chemotherapy depends on the genetic status of the tumour cells. If the tumour shows an activating deletion mutation in Exon 19 or a L858R mutation in Exon 21 of the Epithelial Growth Factor Receptor (EGFR) (5-15 % of NSCLC patients in Europe and USA), patients benefit from a therapy with targeted drugs. Gefitinib and erlotinib, targeting the EGFR and inhibiting its tyrosine kinase activity show a remission rate of 70 % and a disease control rate of 90 % with a significantly better progression-free survival compared to standard chemotherapy, which is a platinum-based treatment in combination with radiation or e.g. taxans, gemcitabine, vinorelbin or pemetrexed. Using the standard therapy, remission rates of 15 to 30 % and a mean progression-free survival of 3 to 5 months can be achieved (3).

1.2 Cisplatin

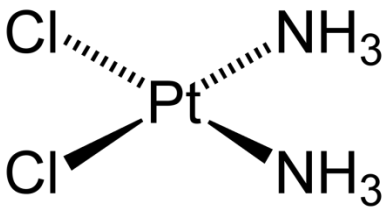

Figure 1 Molecular structure of cisplatin (4).

Cisplatin (cis-Diamminedichloroplatinum(II)) is one of three widely used platinum-containing chemotherapeutic agents used to treat solid tumours. Its chemical structure is shown in Figure 1. It was first synthetized in 1845 by Michele Peyrone (5). The cytotoxic effect of platinum was discovered by chance by Barnett Rosenberg in 1965 (6–8). Cisplatin is an uncharged, cis-configured, square-planar platinum(II) complex, which has to be administered intravenously. At first it was approved in 1978 by the FDA to treat testicular and bladder cancer. In addition, it is used today against other solid neoplasms like bladder, ovarian, lung and head and neck cancer. Many patients initially experience a therapeutic response and disease stabilisation. During further treatment, nearly every tumour develops a chemoresistance against cisplatin. This drawback is accompanied by severe adverse effects like nephrotoxicity, neurotoxicity and ototoxicity. Reduction of toxicity was the rationale behind the development of several cisplatin analogues described elsewhere (9–12). Because of the high potency and the lack of alternatives, cisplatin is still the backbone of many chemotherapeutic combination treatments in lung cancer (13).

1.2.1 Mode of action

Cisplatin elicits its cytotoxic effects through binding to DNA. This leads either to successful repair of DNA damage by several mechanisms or the irreversible activation of programmed cell death. Prior to DNA binding, cisplatin has to be activated by exchanging one or both chloride ligands for water. The aquation takes place in the cytosol resulting in a highly active diaquacomplex. Due to several nucleophilic binding and detoxification partners like glutathione, metallothionine and different proteins abundantly present in the cytosol, less than 10 % of cisplatin entering the cell eventually reaches the nucleus (14). Here, cisplatin reacts with different functional groups of the DNA, whereas the interaction with N7-sites of purine bases is predominant leading to bifunctional 1,2-intrastrand ApG (adenine-phosphate-guanine) or GpG (guanine-phosphate-guanine) crosslinks occurring in 80 to 95 % of all lesions (15). The less abundant crosslinks are 1,3-intrastrand GpG crosslinks (5-6 %), interstrand GpG crosslinks (2-5 %) and monofunctional links with e.g. proteins (2-3 %) (14) (Figure 2). These lesions lead to activation of several DNA damage response pathways including repair mechanisms and apoptosis induction.

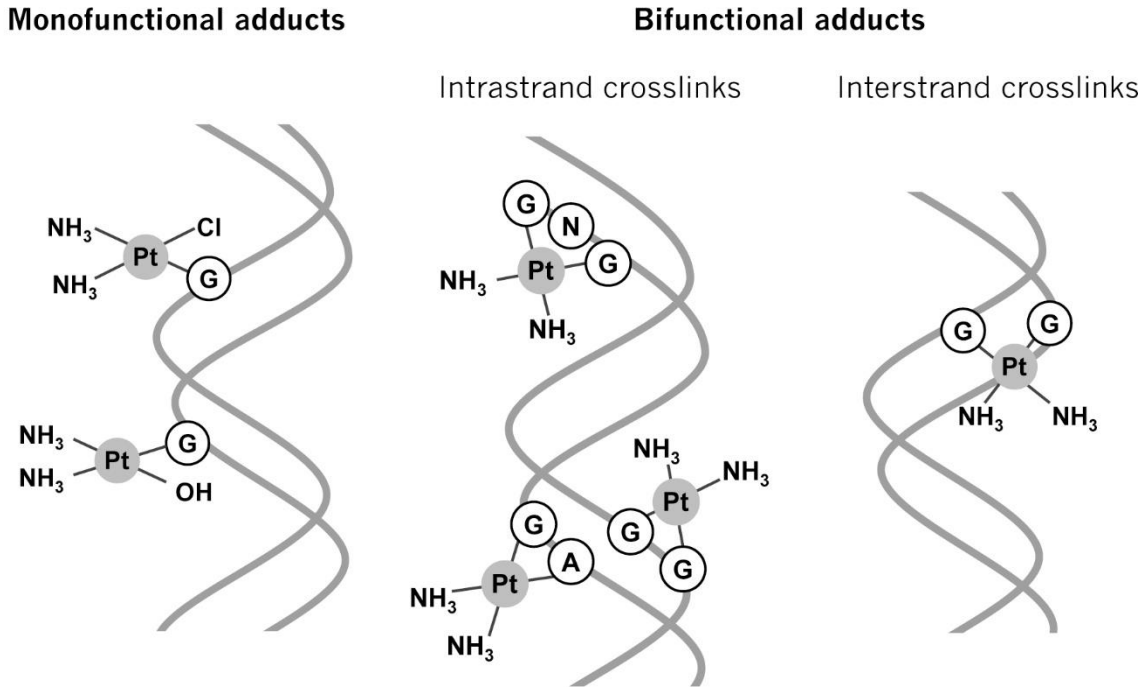

Figure 2 Cisplatin-DNA adducts (A: adenosine, G: guanosine, N: any nucleoside) (16).

1.3 Repair mechanisms and apoptosis induction

1.3.1 Cell response to DNA damage

DNA damage recognition involves over 20 candidate proteins, which bind to the damaged DNA site leading either to DNA repair and cell survival or to apoptosis (15). First of all, the mismatch repair (MMR) system has to be mentioned, which is a highly conserved, strand-specific repair mechanism. After replication, Mut proteins recognise unmatched or mismatched DNA base pairs and initiate their excision. DNA base pairs are then resynthesized by DNA polymerases. The cisplatin-DNA adducts interfere with MMR proteins and hinder them to repair these DNA lesions completely (futile repair). This instability in the mechanism leads to apoptosis, initiated by MMR (17). Lesions caused by cisplatin are apparently not repaired by the MMR, but loss of this system contributes to chemoresistance (18), because cells can survive in spite of DNA damage. The second repair mechanism of DNA is the nucleotide excision repair (NER). DNA lesions altering the helical structure (e.g. cisplatin binding) and interfering with replication and translation are recognised by several proteins of the xeroderma pigmentosum group, like XPC. After marking the lesion and recruiting other proteins, like the excision repair cross-complementation group 1 (ERCC1), the area is unwound and excised. Again DNA polymerases fill up the resulting gap (19). Cisplatin-DNA adducts are mostly repaired by this mechanism, which is enhanced in platinum-resistant cells (18, 20). Other repair mechanisms like the base excision repair (BER) are of minor importance in cisplatin-DNA adduct

excision (18). Another mechanism to deal with DNA-damaging agents is the replicative bypass. Here some DNA polymerases have the ability to synthesize ignoring the damaged site. Cells can proceed the cell cycle to G2 phase and repair the damaged site before entering mitosis. Enhanced replicative bypass can be seen in many chemoresistant cell lines (18).

1.3.2 Cellular stress affecting p53

P53 is the most important tumour suppressor protein and centrally involved in cellular stress response. It influences cell cycle, apoptosis and DNA repair depending on its activation at different amino acid sites. P53 is mutated in more than 50 % of lung cancers. With a mutation frequency of 42 %, it is one of the most frequently mutated genes leading to loss of function and unregulated cancer cell growth (21). Structurally, p53 consists of 393 amino acids and can be divided into several functional domains. The N-terminal transactivation domain and the proline-rich region are binding sites for several interacting proteins of the transcription machinery, like transcriptional co-activators p300 or CREB-binding proteins (CBP) and the major regulator Murine Double Minute 2 (MDM2). Proteins may compete for similar binding sites, making the p53 activation dependent of their concentration and binding affinity. This process is very complex, as the activation involves multiple phosphorylation sites at the N-terminus of p53. The functional domain of DNA binding is located in the centre of the protein, which is bound by a flexible linker to the C-terminal tetramerisation domain, making p53 bind to DNA as a tetramer. The rest of the C-terminus seems to be intrinsically disordered, but may undergo ordering after binding to specific proteins. Most of posttranslational modifications, like acetylation, ubiquitination, phosphorylation, sumoylation, methylation and neddylation seem to take place here and regulate p53 function, next to export or binding signals (22).

1.3.3 Modifications of p53 in stress response

P53 is consecutively expressed in a cell and kept on low protein levels by continuous degradation. Following cell stress, modifications of p53 especially at Ser-, Thr- and Lys-residues take place, leading to stabilisation of p53 and its accumulation in the nucleus. Different stress stimuli lead to different activation profiles of p53 and consequently to different functions. Phosphorylation and acetylation in response to DNA damage is still not fully understood. Several protein kinases like Chk2, Cdk-activated kinases CAK, the PI3K members Atm, ATR and DNA-PK phosphorylate p53 at serines and threonines in the N-terminal and C-terminal domains and strongly contribute to its activation (23) (Figure 3).

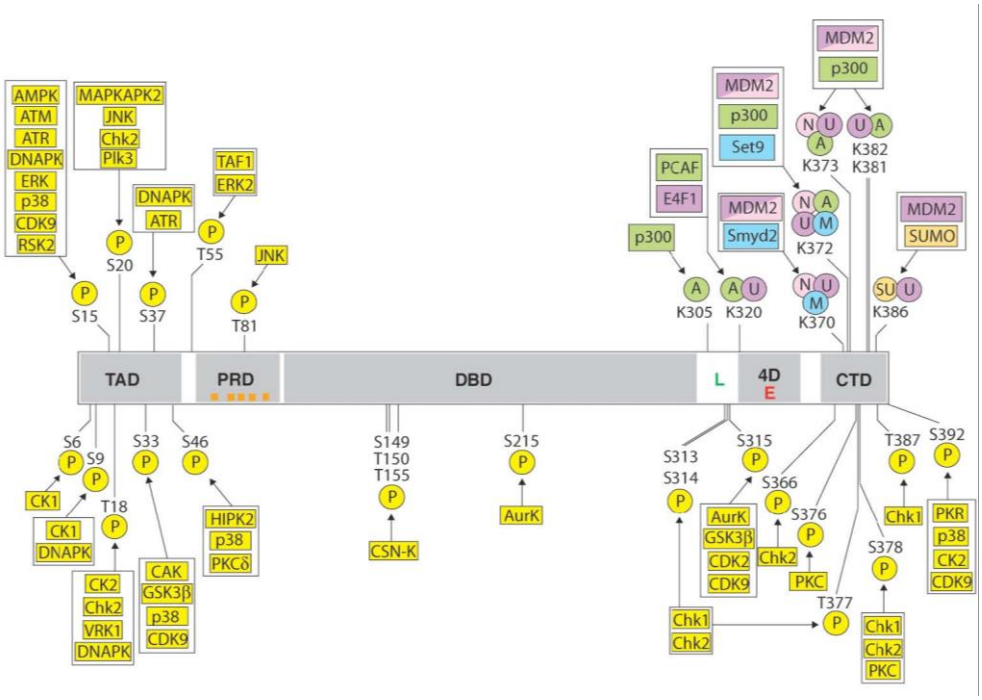

Figure 3 Map and post-translational modifications of human p53. Structure of p53: TAD, transactivation domain; PRD, proline-rich domain; DBD, DNA-binding domain; L, linker; 4DE, tetramerisation domain; CTD, C-terminal domain. Specific residues are modified as shown, with phosphorylation (P) in yellow, acetylation (A) in green, ubiquitylation (Ub) in purple, neddylation (N) in pink, methylation (M) in blue and sumoylation (SU) in brown. Proteins responsible for these modifications are shown in matching colours: AMPK, adenosine monophosphate-activated protein kinase; Atm, ataxia telangiectasia mutated; ATR, ataxia telangiectasia and Rad3-related protein; AurK, Aurora kinase A; CAK, CDK-activating kinase; CDK, cyclin-dependent kinase; CHK, checkpoint kinase; CK, casein kinase; CSNK, cop-9 signalosome associated kinase complex; DNAPK, DNA-dependent protein kinase; ERK, extracellular signal-regulated kinase; GSK3beta, glycogen synthase kinase 3beta; HIPK2, homeodomain-interacting protein kinase 2; JNK, c-Jun NH2-terminal kinase; MAPKAPK2, mitogen-activated protein kinase-activated protein kinase 2; p38, p38 kinase; PCAF, p300/CBP associated factor; PKC, protein kinase C; PKR, double stranded RNA-activated kinase; PLK3, pol-like kinase 3; RSK2, ribosomal S6 kinase 2; SET9, SET9 methyltransferase; SMYD2, SET/MYND domain-containing methyltransferase 2; SUMO, small ubiquitin-like modifier 1; TAF1, TATA-binding protein-associated factor 1; VRK1, vaccinia-related kinase 1 (24).

1.4 Platinum resistance

Typically, drug resistance is not restricted to a single mechanism but is the result of an accumulation of several mechanisms. Galuzzi et al. (13) classified these into four categories:

- Pre-target resistance, preventing the binding of cisplatin to its target by reduced cellular accumulation or binding to cytoplasmic structures;
- On-target resistance, by tolerating or repairing cisplatin-DNA adducts;
- Post-target resistance, by several alterations or defects in signalling pathways responding to DNA damage; and

- Off-target resistance, by mechanisms, which are not directly related to cisplatin binding but altered upon the development of resistant phenotypes (Figure 4).

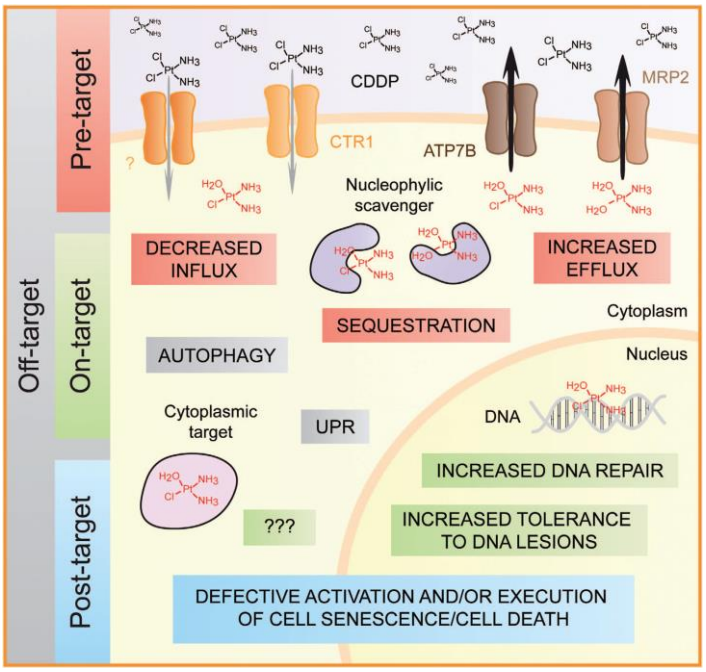

Figure 4 Different mechanisms of cisplatin resistance (25).

1.4.1 Pre-target resistance

Pre-target resistance paraphrases every detoxification mechanism that targets cisplatin before binding to the nuclear target DNA. These mechanisms can on one hand reduce the cytoplasmic pool of cisplatin, through decreased influx or increased efflux or on the other hand lead to sequestration of activated cisplatin. Beside passive diffusion, it is well believed that cisplatin also enters the cell via active transport. Major influx transporters are copper transporters, especially CTR1, whereas major efflux transporters are ATP7B and MRP2. Alterations in their expression profile, subcellular localisation or functionality are associated with different cisplatin-resistant cancer models. Sequestration takes places, when aquated platinum species bind to nucleophilic substances, like glutathione, methionine, metallothioneins and other cysteine-rich proteins, acting as scavengers and reducing the level of active cisplatin in cancer cells (13).

1.4.2 On-target resistance

On-target resistance includes resistant mechanisms directly connected to cisplatin's mode of action, the binding to nuclear DNA. Here resistant cells show alterations in different repair mechanisms, like increased proficiency in nuclear excision repair (NER), defects in the mismatch repair (MMR), increased activity of translesion synthesis (replicative bypass), increased homologous recombination

and binding of cisplatin to cytoplasmic components that are involved in extranuclear cytotoxicity of cisplatin. In the latter case it is still not clear, whether these mechanisms belong to on-target or post-target resistance (25).

As mentioned above, most of cisplatin-DNA adducts are removed by the NER system. Consequently, a higher activity of this repair mechanism can lead to chemoresistance against cisplatin, as shown in several preclinical cancer models (13), especially in NSCLC (26). Reduced expression of XPC and ERCC1, two central proteins in DNA damage recognition and excision of DNA lesions correlates with survival or response to cisplatin-based therapies (13). It is not sure, if increased activity of ERCC1 corresponds with higher activity of NER in patients and if overexpression of ERCC1 enhances cisplatin resistance. Low expression of ERCC1 resulted in higher response to platinum-based chemotherapy and higher median survival. So this protein could be a future biomarker for elucidating cisplatin sensitivity (27).

Recognition of DNA lesions by cisplatin is often done by the MMR system. MMR-related proteins, like MSH2 and MLH1 try to repair mismatch due to cisplatin-DNA adducts and induce a proapoptotic signal when failing to repair the damage (28). Mutations in these proteins or reduced expression can often be found in cisplatin-resistant cells. Defects in MLH1 and MSH6, other proteins of the MMR-system lead to higher activity of the translesion synthesis (29), which is another mechanism of on-target resistance. Here DNA replication is not stopped by a cisplatin-induced lesion, but proceeds until the arrest is induced in later cell cycle phases to start DNA repair. Several specific DNA polymerases show high activity, whereas the up-regulation of e.g. DNA polymerase POLH correlates with shorter survival in NSCLC patients (30). Defects in POLH or REV3, another polymerase, sensitise cells to cisplatin (31).

The third mechanism of on-target resistance is homologous recombination, which usually tries to repair cisplatin-induced double-strand breaks in the S phase of the cell cycle. Here two proteins, BRCA1 and 2, often mutated in different cancer types, seem to play a major role in chemoresistance. BRCA1/2-deficient cancer cells show a higher sensitivity to cisplatin. Especially the development of resistance in those cells seems interesting, because some cancer cells try to compensate the BRCA1/2 deficiency by secondary mutations leading to cisplatin resistance (32).

Last but not least, several extra-nuclear binding partners have been identified, like mitochondrial DNA, the mitochondrial anion channel, VDAC1 and cytosolic components, like HSP90 or myosin IIa, GRP78 or PDIA1/3. In mitochondria, it was shown that cisplatin leads to changes in the respiratory chain, which could be one possible extra-nuclear effect. For this reason, it remains unclear, whether these interactions lead to a cytotoxic effect and should be classified as on-target resistance mechanisms (25).

1.4.3 Post-target resistance

Post-target resistance addresses all mechanisms recruited after binding of cisplatin to DNA being involved in the complex network of signalling cascades activated after DNA damage recognition. These changes in signalling lead to alterations in cell senescence or cell death signals and are involved in chemoresistance to different extents. The most prominent alteration in signalling is the inactivation of p53, which occurs in several cancer entities (33). The presence of p53-mediated apoptosis signalling is crucial for anticancer therapy, as it correlates directly with response to treatment (34). Besides this role in development of chemoresistance, the loss of p53-gene regulation is involved in the cancerogenesis process. Mutations of p53 occur in almost half of human cancers, leading to loss of functions or to overactivation in context of cell cycle control, apoptosis signalling, stress-independent p21 activation, angiogenesis, cell growth and proliferation (35).

The second important signalling pathway may be pro-apoptotic signal transduction mediated by the mitogen-activated protein kinase (MAPK) family members, including extracellular related kinases (ERK1/2), mitogen-activated protein kinases p38 and c-Jun N-terminal kinases (JNK). All family members of the MAPK have a plenitude of regulatory functions in human cells. Among others, these kinase pathways lead to activation of p53 and apoptosis signalling. The role of these kinases in cisplatin resistance is still not clear. In some cells, activation of MAPK led to higher cisplatin sensitivity, whereas in other studies inhibition of MAPK led to higher sensitivity to cisplatin. Some researchers concluded, that chemoresistance against cisplatin is independent of MAPK (15).

In addition to these complex networks, a lot of factors activated either by DNA damage or oxidative stress in mitochondria influence resistance against cisplatin. Among others, the functional status of BCL-2 family members (BCL-2-like proteins, BAX-like proteins), caspases, cell death receptors, which together execute the apoptotic cell death, PI3K signalling and Survivin pathways may contribute to cisplatin sensitivity or resistance (36). All these mechanisms, described elsewhere, contribute to post-target resistance.

1.4.4 Off-target resistance

Sensitivity of cancer cells can also be influenced by off-target mechanisms, which are not directly connected to cisplatin's mode of action. These are alterations of survival signals or detoxification partners without direct activation by cisplatin. For example, overexpression of ERBB2, one of the EGFR family members, contributes to cisplatin resistance by sending a pro-survival signal via the antiapoptotic AKT1-signaling pathway. Consequence is a cell cycle arrest by up-regulation of the cyclin-dependent kinase inhibitor p21 enabling the cell to repair cisplatin-DNA lesions (37). Another resistance mechanism is the activation of DYRK1B, a nuclear protein kinase, which induces the

expression of antioxidant enzymes to cope with reactive oxygen species, which might be induced by cisplatin. The same idea may be also true for glutathione, which was already mentioned in the pre-target section. GSH also binds reactive oxygen species and in consequence makes cells less sensitive to cell death signals (13). More general mechanisms contributing to cisplatin resistance are autophagy, including mechanisms of sequestration and lysosomal degradation (38) and the heat-shock response, where cells are enabled to survive high temperatures and which is also activated in cell-stressing conditions (39).

In conclusion, the comprehensive knowledge of cytoplasmic and nuclear actions of cisplatin and a resistance scheme with multifactorial activation of several mechanisms mentioned above, drives research to a systems pharmacology approach. This is supposed to lead to holistic models of the cell's reaction to cisplatin for better understanding of the mechanisms underlying chemoresistance.

1.5 Systems pharmacology

Systems pharmacology was discussed extensively in a NIH white paper by the Quantitative and Systems Pharmacology (QSP) Workshop Group in 2011. Here the authors consider that systems pharmacology is an emerging discipline with different definitions in academia and industry: Academia generally defined it as an extension of classical pharmacology by systems biology: "systems pharmacology involves the application of systems biology approaches, combining large-scale experimental studies with model-based computational analyses, to study drug activities, targets, and effects" (40) or "…the quantitative analysis of the dynamic interactions between drug(s) and a biological system… (that) aims to understand the behaviour of the system as a whole, as opposed to the behaviour of its individual constituents" (41). On the other side, industry defines systems pharmacology as modelling of physiological processes by parameters of pharmacokinetics and pharmacodynamics in response to drug treatment. The resulting working definition, combining both sides of the story was developed by the working group as follows: "Quantitative and Systems Pharmacology is an emerging discipline focused on identifying and validating drug targets, understanding existing therapeutics and discovering new ones. The goal of QSP is to understand, in a precise, predictive manner, how drugs modulate cellular networks in space and time and how they impact human pathophysiology. QSP aims to develop formal mathematical and computational models that incorporate data at several temporal and spatial scales; these models will focus on interactions among multiple elements (biomolecules, cells, tissues etc.) as a means to understand and predict therapeutic and toxic effects of drugs" (42). This will involve classical well-known pharmacology, systems biological approaches (like protein networks in a whole cell system), large

scale studies (-omics technologies: genomics, transcriptomics, proteomics, metabolomics…) and model-based computational analysis of experimental data.

The two basic approaches, systems biology and classical pharmacology are originally of horizontal integration in a system. This means that they refer to analysing the drug target, multiple receptors, signalling networks or metabolites at one time point, because molecules often react with multiple components of a system. Additionally, this involves the issue that even in precisely targeted therapies the consequences of a perturbation can be rather complex, involving different states of activity in time and space. Systems pharmacology adds the vertical integration to the complex. Here multiple spatial and temporal scales at different levels of biological complexity are analysed by multi-omics approaches. This involves data on the reaction to a molecule in a defined system, like cells, tissues, organs, patients or populations. Vertical integration can be a bottom-up, top-down, or middle-out approach. For example, in relation to systems pharmacology and genome medicine, a bottom-up approach would be based on experimental and clinical analysis. By computational biology this is leading to the prediction and characterisation of new targets from biochemistry and cell physiology experiments and at the end the network analysis of the therapeutic intervention. A top-down approach would come from a clinical diagnosis by genetic and genomic testing, computational processing of experimental data, leading to information for personalised medicine like personalised dosing or a combination therapy and reaching again the network analysis of the therapeutic intervention (Figure 5). Middle-out approaches would start at any level, wherever information is available and add data to both directions.

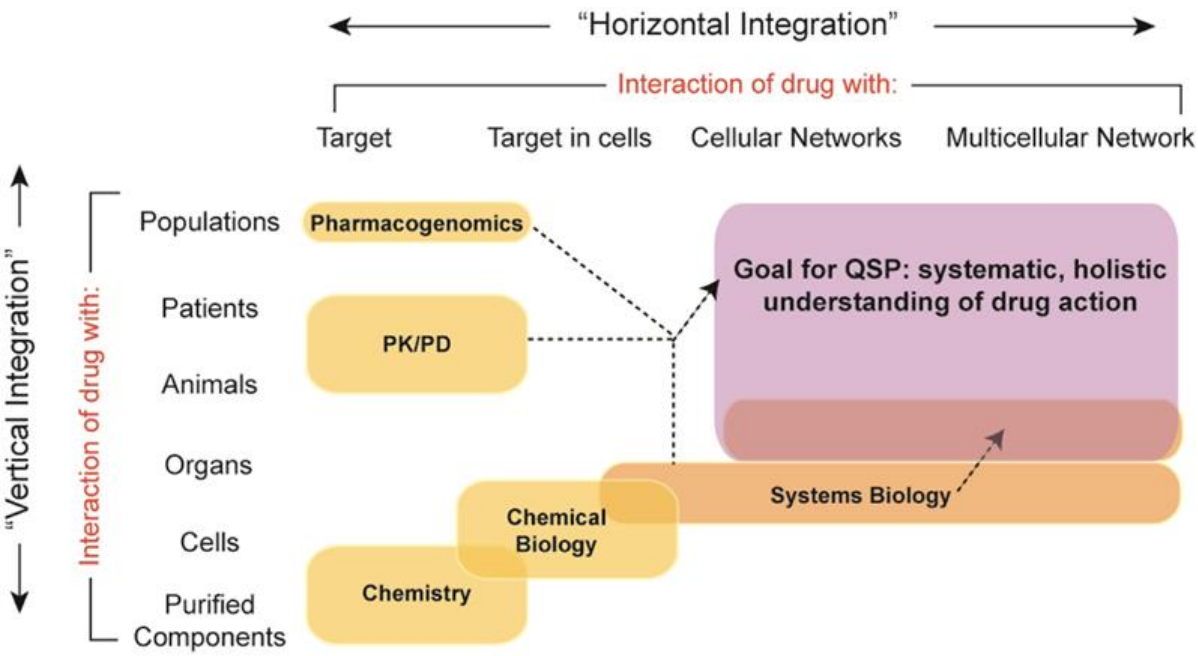

Figure 5 Horizontal and vertical integration in systems biology and pharmacology including also changes in physiological complexity and changes in time scales (from seconds and minutes to years and lifespans). The goal for QSP is to bring network-level understanding of drugs to the complex physiology of patient responses. The arrows denote trend lines (42).

The selection of a system should be carefully considered in context of the issue (Figure 6). As the clinical analysis of a human could be too complex, the system analysed can be outlined on a lower level at the beginning. Even at molecular level an enzyme or a receptor can be analysed as a system reacting to different perturbations in different ways. A bottom-up approach then can also be the upscaling from a receptor or enzyme to a network level and further on to a tissue or organ level.

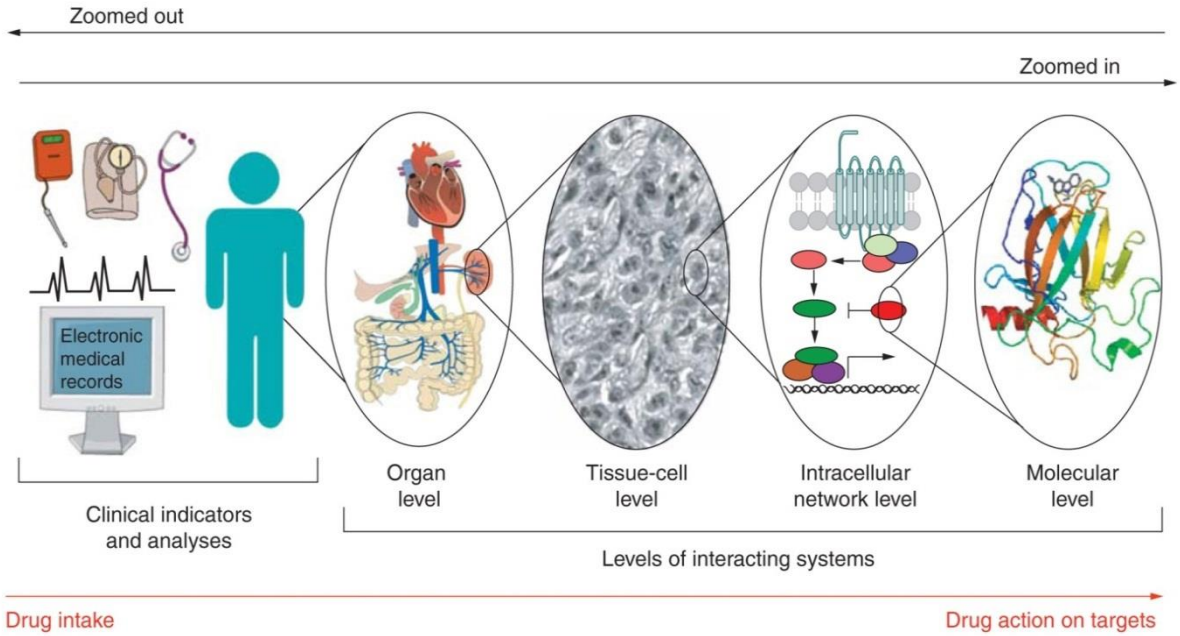

Figure 6 Possibilities of defining a system for systems pharmacological approaches, modified from (43).

These experimental data should in the end be condensed in a multi-scale temporal and spatial model, to reflect an integrated picture of therapeutic and toxic effects of drugs. The modells could lead to new hypothese, which should be proofed experimentally. The final step is to link the mechanistic models of protein or gene networks to pharmacokinetics and pharmacodynamics in organs or patients.

2 Aim and objectives

This project aimed at characterising the resistance mechanisms against cisplatin in non-small lung cancer cells using a systematic approach. Therefore, this piece of work was intended to be the first one in a series of systems pharmacology projects in our working group.

A newly established cisplatin-resistant non-small cell lung cancer cell line (A549^{r}CDDP^{2000}) was characterised in comparison to its parental cell line (A549) regarding its reaction to cisplatin treatment including cytotoxicity tests, cellular platinum accumulation, cisplatin DNA-adduct formation, apoptosis induction and cell cycle status after treatment with equimolar and equitoxic cisplatin concentrations. As p53 is the crucial player in DNA-damage response and apoptosis-inducing pathways, this key protein and connected relevant up- and downstream players like pAtm, XPC, MDM2, GADD45a and p21 were analysed at the transcriptome and proteome level. The first step towards systems pharmacology was then done using a data-driven bottom-up approach. Here, the whole transcriptome served as a starting point to identify additional genes altered upon cisplatin exposure in sensitive and resistant cells using a whole genome array. After evaluation of these differentially expressed genes with RT-PCR, the next higher level of vertical integration within the cells was added: The key candidates were analysed additionally on protein level by Western blots to elucidate their contribution to the previously measured endpoints. Finally, the data were compiled in a signalling model to describe the differences in reaction to cisplatin treatment in both cell lines.

3 Materials and methods

3.1 Chemicals and reagents

10x Blocking Agent	Agilent Technologies, Santa Clara, USA
25x Fragmentation Buffer	Agilent Technologies, Santa Clara, USA
2x GEx HI-RPM Hybridisation Buffer	Agilent Technologies, Santa Clara, USA
AccuMax	PAA, Pasching, Österreich
Acrylamide 30 % [m/V]	AppliChem GmbH, Darmstadt
AffinityScript-RT	Agilent Technologies, Santa Clara, USA
AKT antibody (rabbit polyclonal IgG)	Cell Signalling, Danvers, USA
Ammonium persulfate (APS)	AppliChem GmbH, Darmstadt
Anti-rabbit poly-HRP	Thermo Fisher Scientific, Oberhausen
Argon 4.6	Air Product, Hattingen
BCA™ protein assay kit (Novagen®):	Merck KGaA, Darmstadt
Albumin standard ampoules (2 mg/mL bovine serum albumin)	
Reagent A (bicinchoninic acid)	
Reagent B (4 % cupric sulfate)	
BD Pharmingen™ FITC Annexin V Apoptosis Detection Kit	BD Biosciences, San Jose, USA
Binding buffer	BD Biosciences, San Jose, USA
Blocking buffer	R&D Systems, Minneapolis, USA
Boric acid	Fluka Chemie, Neu-Ulm
Bovine serum albumin (BSA)	Sigma-Aldrich, Steinheim
Bromophenol blue	AppliChem GmbH, Darmstadt
CASYton, isotonic diluting solution	Schärfe System, Reutlingen
CCL2 antibody (rabbit polyclonal IgG)	Aviva Systems Biology, San Diego, USA
Cisplatin	Sigma-Aldrich, Steinheim
Cisplatin-DNA adduct antibody	Merck Millipore, Darmstadt
Cobalt(II) sulfate heptahydrate	Sigma-Aldrich, Steinheim
Denaturation Cell Extraction Buffer	Life Technologies, Carlsbad, USA
Dithiothreitol (DTT)	Applichem, Darmstadt
dNTP Desoxynucleotide Mix	Agilent Technologies, Santa Clara, USA
DOK1 antibody (rabbit polyclonal IgG)	GeneTex, Irvine, USA
DuoSet®IC	R&D Systems, Minneapolis, USA

Human Phospho-p53 (S15) Kit	
Electrophoresis buffer, 10 x [25 mM Tris base, 192 mM glycin, 0.1 % sodium dodecyl sulfate]	Bio-Rad Laboratories GmbH, München
Ethanol 96-100 % [V/V]	Merck KGaA, Darmstadt
Ethylenediaminetetraacetic acid (EDTA), disodium salt dihydrate	Sigma-Aldrich, Steinheim
Fluoromount™ aqueous mounting medium	Sigma-Aldrich, Steinheim
Foetal calf serum (FCS)	Sigma-Aldrich, Steinheim
Formaldehyde 37 % [m/V]	Riedel de Haën AG, Seelze
GAPDH antibody (rabbit polyclonal IgG)	GeneTex, Irvine, USA
Glucose monohydrate	Sigma-Aldrich, Steinheim
Glycerol 100 % [V/V]	Applichem GmbH, Darmstadt
Glycine	Grüssing GmbH, Filsum
Goat anti-mouse HRP antibody (polyclonal IgG)	Santa Cruz Biotechnology, Inc., Heidelberg
Goat anti-mouse poly-HRP antibody (polyclonal IgG)	Thermo Fisher Scientific, Oberhausen
Goat anti-rabbit antibody (polyclonal IgG)	SouthernBiotech, Birmingham, USA
Goat anti-rabbit HRP antibody (polyclonal IgG)	Santa Cruz Biotechnology, Inc., Heidelberg
Goat anti-rabbit poly-HRP antibody (polyclonal IgG)	Thermo Fisher Scientific, Oberhausen
HRas antibody (rabbit polyclonal IgG)	GeneTex, Irvine, USA
HRP substrate	R&D Systems, Minneapolis, USA
Hydrochloric acid [0.1 M and 1.0 M]	Riedel de Haën AG, Seelze
Hydrochloric acid 37 % [m/V]	Merck KGaA, Darmstadt
IMDM Medium	PAN Biotech
Isopropanol 100 % [V/V]	Merck KGaA, Darmstadt
JNK3 antibody (rabbit polyclonal IgG)	GeneTex, Irvine, USA
Leupeptin hemisulfate	Sigma-Aldrich GmbH, Steinheim
L-Glutamin solution [200 mM]	Sigma-Aldrich, Steinheim
LightCycler 480® SYBR Green I Master Mix	Roche Diagnostics, Rotkruez, Switzerland
MDM2 antibody (rabbit polyclonal IgG)	GeneTex, Irvine, USA
MDM2 antibody (rabbit polyclonal IgG)	GeneTex, Irvine, USA
Methanol	Merck KGaA, Darmstadt
Mouse monoclonal p53 coating antibody	Sigma-Aldrich, Steinheim
My-Budget RNA Mini Kit	Bio-Budget Technologies GmbH, Krefeld

Nitric acid 65 % [V/V], suprapur	Merck KGaA, Darmstadt
Non-fat dry milk powder	Carl Roth GmbH & Co. KG, Karlsruhe
Oligo dT-Promoter Primer	Agilent Technologies, Santa Clara, USA
p21 antibody (rabbit polyclonal IgG)	GeneTex, Irvine, USA
p21 antibody (rabbit polyclonal IgG)	Santa Cruz Biotechnology, Inc., Heidelberg
p38 antibody (rabbit polyclonal IgG)	GeneTex, Irvine, USA
p53-HRP antibody (mouse polyclonal IgG)	Santa Cruz Biotechnology, Inc., Heidelberg
pAKT antibody (rabbit polyclonal IgG)	Cell Signalling, Danvers, USA
pAtm antibody (mouse polyclonal IgG)	Santa Cruz Biotechnology, Inc., Heidelberg
Penicillin-streptomycin solution [10,000 I.E./mL, 10 mg/mL]	Sigma-Aldrich, Steinheim
Pepstatin A	Sigma-Aldrich, Steinheim
Pierce™ ECL Western blotting Substrate (luminol/enhancer, peroxide buffer)	Thermo Fisher Scientific Inc., Rockford, USA
Pierce™ BCA Protein Assay Kit	Life Technologies, Carlsbad, USA
Potassium chloride	Merck KGaA, Darmstadt
Potassium dihydrophosphate	Fluka Chemie GmbH, Neu-Ulm
PP2A antibody (rabbit polyclonal IgG)	Bethyl Laboratories, Montgomery, USA
Propidium iodide	Sigma-Aldrich, Steinheim
Protease Inhibitor Cocktail	Sigma-Aldrich, Steinheim
ProteinMarker V	Peqlab GmbH, Erlangen
PTK2B antibody (rabbit polyclonal IgG)	GeneTex, Irvine, USA
PureLink™ Rnase A	Life Technologies, Carlsbad, USA
QIAamp® DNA Mini Kit	Quiagen, Hilden
Ribonuclease A (RNAse)	Sigma-Aldrich, Steinheim
RNasin® Ribonuclease Inhibitors	Agilent Technologies, Santa Clara, USA
RNA Spike-In Kit	Agilent Technologies, Santa Clara, USA
RNeasy® Mini Kit	Qiagen N.V., Hilden
SCL9A9 antibody (rabbit polyclonal IgG)	MBL, Nagoya, Japan
Sodium azide	Fluka Chemie, Neu-Ulm
Sodium chloride	Fluka Chemie, Neu-Ulm
Sodium desoxycholate	Sigma-Aldrich, Steinheim
Sodium dodecyl sulfate (SDS)	Applichem GmbH, Darmstadt
Sodium hydrophosphate	Applichem GmbH, Darmstadt
Sodium hydroxide [0.1 M and 1.0 M]	Riedel de Haën AG, Seelze

Sodium orthovanadate	Applichem GmbH, Darmstadt
Stop solution sulphuric acid	R&D Systems, Minneapolis, USA
T7 RNA Polymerase	Agilent Technologies, Santa Clara, USA
Tetramethylethylenediamine (TEMED)	Applichem GmbH, Darmstadt
Tris(hydroxymethyl)aminomethane (Tris base)	Applichem GmbH, Darmstadt
Tris(hydroxymethyl)aminomethane-Hydrochloride (Tris-HCl)	Applichem GmbH, Darmstadt
Triton® X-100	Sigma-Aldrich, Steinheim
Trypsin-EDTA solution [0.5 g porcine trypsin and 0.2 g EDTA in 100 ml]	Sigma-Aldrich, Steinheim
Tween®-20	Applichem GmbH, Darmstadt
Ultrapure water	Obtained by Purelab Plus™ system, Elga Labwater, Celle
Whole Genome Array SurePrint G3 Human GE V2 8x60K Kit	Agilent Technologies, Santa Clara, USA
Wnt4 antibody (rabbit polyclonal IgG)	GeneTex, Irvine, USA
α-Actin antibody (mouse polyclonal IgG)	Santa Cruz Biotechnology, Inc., Heidelberg
β-Actin (C4) antibody (mouse polyclonal IgG)	Santa Cruz Biotechnology, Inc., Heidelberg

3.2 Buffers and solutions

Phosphate-buffered saline (PBS)	
Sodium chloride	8.0 g
Potassium chloride	0.2 g
Sodium hydrophosphate dihydrate	1.44 g
Potassium dihydrophosphate	0.24 g
Ultrapure water	ad 1000.0 mL
pH adjusted to 7.4 using sodium hydroxide or hydrochloric acid	

Cisplatin stock solution [5 mM]	
Cisplatin	1.5 mg
Sodium chloride solution 0.9 %	1.0 mL

3-(4,5-Dimethylthiazol-2-yl)-2,5-diphenyltetrazolium bromide (MTT) solution [5 mg/mL]

MTT	50 mg
PBS	5.0 mL

DAPI stock solution [1 mg/mL]

DAPI	1 mg
Methanol	1000 µL

DAPI working solution [5 µg/mL]

DAPI stock solution	5 µL
Ultrapure water	ad 1000 µL

3.2.1 SDS-PAGE and Western blot

Cell lysis

RIPA lysis buffer

Tris-HCl (pH 7.6)	3.939 g
NaCl	8.766 g
Triton X-100	100 g
Sodium desoxycholate	10 g
SDS	1 g
EDTA	0,292 g
Ultrapure water	ad 1000.0 mL

Activated Na_3VO_4 solution*,**	10 µL
Leupeptin solution [5 mg/mL in ultrapure water]**	2 µL
Pepstatin A solution [2 mg/mL in DMSO]**	5 µL
Protease inhibitor cocktail**	1 µL

* Activation: Solution of sodium orthovanadate [10 mM] in ultrapure water, pH adjusted to 10 and solution boiled yielding a clear solution. After cooling down, pH readjusted to 10.

** added shortly before usage.

SDS polyacrylamide gel electrophoresis

Ammonium persulfate (APS) solution [10 %]

APS	100 mg
Ultrapure water	ad 1000.0 µL

Dithiothreitol (DTT) solution [3.2 M]

DTT	49.4 mg
Ultrapure water	ad 1000.0 µL

Electrode buffer

Glycin	14.4 g
Tris-Base	3 g
SDS	1 g
Ultrapure water	Ad 1000.0 mL

Loading buffer

Stacking gel buffer	1.75 mL
Glycerol	1.5 mL
Sodium dodecyl sulfate solution (see below)	5 mL
Bromphenol blue solution*	1.25 mL

* Saturated bromphenol blue solution in ultrapure water containing 0.1 % ethanol

Sodium dodecyl sulfate (SDS) solution [10 %]

SDS	1.0 g
Ultrapure water	ad 10.0 mL

Stacking gel (5 %)

Acrylamide 30 %	833 µL
Stacking gel buffer (see below)	625 µL
Ultrapure water	3445 µL
SDS 10 %	50 µL
TEMED*	5 µL
APS 10 %*	20.8 µL

* Added last for initiation of polymerisation

Stacking gel buffer (pH 6.8)

Tris base	12.11 g
Ultrapure water	ad 100.0 mL

pH adjusted to 6.8

Separating gel (10%)

Acrylamide 30 %	5000 µL
Stacking gel buffer (see below)	5625 µL
Ultrapure water	4093 µL
SDS 10 %	150 µL
TEMED*	27 µL
APS 10 %*	105 µL

* Added last for initiation of polymerisation

Separating gel buffer (pH 8.8)

Tris base	12.11 g
Ultrapure water	ad 100.0 mL

pH adjusted to 8.8

Western blot

Tris-buffered saline (TBS)

Sodium chloride	4 g
Tris base	0.6 g
Ultrapure water	ad 500.0 mL

pH adjusted to 7.3 using hydrochloric acid

Tris-buffered saline with Tween®-20 (TBS-T) solution

Tween®-20	1.6 mL
TBS	ad 800.0 mL

Blocking solution

Non-fat dry milk powder	5 g
TBS-T solution	ad 100.0 mL

Transfer buffer

Glycine	14.4 g
Tris base	3 g
Methanol	200.0 mL

Ultrapure water	ad 1000.0 mL

pH adjusted to 8.2 to 8.4 using hydrochloric acid

Antibody solutions for detection of proteins

Primary antibody p38 solution (1:500)

Sodium azide	10 mg
BSA	500 mg
p38 antibody	40 µL
TBS-T solution	10.0 mL

Primary antibody HRas solution (1:500)

Sodium azide	10 mg
BSA	500 mg
HRas antibody	40 µL
TBS-T solution	10.0 mL

Primary antibody DOK1 solution (1:500)

Sodium azide	10 mg
BSA	500 mg
DOK1 antibody	40 µL
TBS-T solution	10.0 mL

Primary antibody CCL2 solution (1:2000)

Sodium azide	10 mg
BSA	500 mg
CCL2 antibody	5 µL
TBS-T solution	10.0 mL

Primary antibody PTK2B solution (1:333)

Sodium azide	10 mg
BSA	500 mg
PTK2B antibody	30 µL
TBS-T solution	10.0 mL

Primary antibody MDM2 solution (1:1000)

Sodium azide	10 mg
BSA	500 mg
MDM2 antibody	10 µL
TBS-T solution	10.0 mL

Primary antibody JNK3 solution (1:333)

Sodium azide	10 mg
BSA	500 mg
JNK3 antibody	30 µL
TBS-T solution	10.0 mL

Primary antibody SLC9A9 solution (1:333)

Sodium azide	10 mg
BSA	500 mg
SLC9A9 antibody	30 µL
TBS-T solution	10.0 mL

Primary antibody p21 solution (1:333)

Sodium azide	10 mg
BSA	500 mg
p21 antibody)	30 µL
TBS-T solution	10.0 mL

Primary antibody Wnt4 solution (1:1000)

Sodium azide	10 mg
BSA	500 mg
Wnt4 antibody	10 µL
TBS-T solution	10.0 mL

Secondary anti-rabbit antibody solution (1:10000)

Non-fat dry milk powder	0.5 g
Anti-rabbit IgG horseradish peroxidase-conjugated antibody	1 µL
TBS-T solution	10.0 mL

3.3 Equipment

3.3.1 Instruments

Accu-jet® pipetting controller	Brand GmbH & Co., Wertheim
AllPrep DNA/RNA Mini Kit	Qiagen N.V., Hilden
Autosampler PSD 100	Varian, Darmstadt
BD FACScalibur™	BD Biosciences, San Jose, USA
Casy®1 cell counter, Modell TT	Schärfe System, Reutlingen
Centrifuge Mikro 200R	Hettich GmbH & Co. KG, Tuttlingen
Centrifuge Universal 32R	Hettich GmbH & Co. KG, Tuttlingen
DYNEX MRXe microplate reader	Magellan Bioscience, Chelmsford, USA
Finnpipette® (10-100 µL, 100 – 1000 µL)	Thermo Electron GmbH, Dreieich
Gel Doc ™ XR+ System	Bio-Rad Laboratories GmbH, München
Graphite Tube Atomisator GTA 100	Varian, Darmstadt
Handystep®	Brand GmbH & Co., Wertheim
Hybridisation Oven	Agilent Technologies, Santa Clara, USA
Incubator Thermo	Thermo Electron GmbH, Dreieich
InoLab® pH level 2 pH Meter	WTW GmbH, Weilheim
Kern 770 analytical balance	Kern & Sohn GmbH, Balingen-Frommern
Kern EW analytical balance	Kern & Sohn GmbH, Balingen-Frommern
Laminar air flow work bench	Heraeus Holding GmbH, Hanau
LightCycler 480®	Roche Diagnostics, Rotkreuz, Switzerland
MT Classic AB135-S analytical balance	Mettler-Toledo GmbH, Giessen
Multiskan EX® microplate reader	Thermo Electron GmbH, Dreieich
NanoDrop™ N-1000	Thermo Fisher Scientific, Oberhausen
Nikon A1 Eclipse Ti confocal microscope	Nikon, Kingston, UK
Probes Master LC 480	Agilent Technologies, Santa Clara, USA
PURELAB Plus system	ELGA LabWater, Celle
Shaker KS 15 control	Edmund Bühler GmbH, Hechingen
Slot Blot Manifold	GE Healthcare, Solingen
Spectrometer SpectrAA® Zeeman 220	Varian, Darmstadt
SurePrint G3 Human GE V2 8x60K	Agilent Technologies, Santa Clara, USA
SureScan Microarray Scanner System	Agilent Technologies, Santa Clara, USA
Transferpette® S (0,5-100µL, 10-100 µL, 100-1000 µL)	Brand GmbH & Co., Wertheim

Transferpette®-12 electronic (10-100 µL, 30-300 µL)	Brand GmbH & Co., Wertheim
Ultrasonic bath Sonorex® Super RK 103 H	Bandelin, Berlin

3.3.2 Consumables

Blotting paper (cellulose), 7 x 10 cm	Sigma-Aldrich GmbH, Steinheim
Casy® tubes	Schärfe System, Reutlingen
Cell culture flasks 25, 75, 175 cm^2	Sarstedt AG & Co., Nümbrecht
Cell scraper	Sarstedt AG & Co., Nümbrecht
Cryovials	Sarstedt AG & Co., Nümbrecht
Disposable syringe (10 mL)	B. Braun Melsungen AG, Melsungen
Glass Pipettes	Labomedic GmbH, Bonn
Graphite tubes	Varian (Agilent Technologies), Darmstadt
Hybond nitrocellulose membranes	GE Healthcare, Solingen
Microscope slides	Carl Roth GmbH & Co., Karlsruhe
Pasteur pipettes	Brand GmbH & Co., Wertheim
Petri dishes	Greiner Labortechnik, Frickenhausen
Pipette tips	Brand GmbH & Co., Wertheim
Platinum hollow cathode lamps (UltrAA® lamps)	Varian (Agilent Technologies), Darmstadt
Reaction tubes (0.5, 1.5, 2 mL)	Greiner Labortechnik, Frickenhausen
Roti®-PVDF (Polyvinylidene fluoride) membrane	Carl Roth GmbH & Co.KG, Karlsruhe
Sample vials (2 mL, conical)	Varian (Agilent Technologies), Darmstadt
Tissue culture plates, 6 wells	Sarstedt AG & Co., Nümbrecht
Tissue culture plates, 96 wells	Sarstedt AG & Co., Nümbrecht

3.3.3 Software

Ascent Software (for Multiskan EX®)	Thermo Electron Inc., Dreieich
AIDA Image Analyzer 4	Raytest, Straubenhardt
BD CellQuest™	BD Biosciences, San Jose, USA
Feature Extraction V 10	Agilent Technologies, Santa Clara, USA
Flowing Software V 2.5	Turku Centre for Biotechnology, Finland
GeneSpring GX 13.1	Agilent Technologies, Santa Clara, USA
Graph Pad Prism® 6.00	GraphPad Software, San Diego, USA
HTSanalyzeR	Bioconductor, Roswell Park Cancer Institute, Buffalo, USA

Image Lab™ 5.2.1	Bio-Rad Laboratories GmbH, München
Microsoft® Excel 2010	Microsoft Corporation, Redmond, USA
NIS-Elements software	Nikon, Kingston, UK
SpectrAA® 220, Version 2.20	Varian, Darmstadt

3.4 Cell culture

3.4.1 Cell lines

In this study, the human adenocarcinoma derived non-small cell lung cancer cell line A549, sensitive to cisplatin (Figure 7) and its newly developed cisplatin-resistant sub-line A549^{r}CDDP^{2000} were used. The sensitive cells were explanted from a 58-year old Caucasian male and cultivated in 1972 by Giard et al. (44). The A549 cell line was obtained from ATCC (Manassas, VA, USA) and its cisplatin-resistant sub-line A549^{r}CDDP^{2000} was derived from the Resistant Cancer Cell Line (RCCL) collection (www.kent.ac.uk/stms/cmp/RCCL/RCCLabout.html). The sub-line had been established by adapting A549 cells in the presence of increasing concentrations of cisplatin until the target concentration of 2000 ng/mL cisplatin as described previously (45).

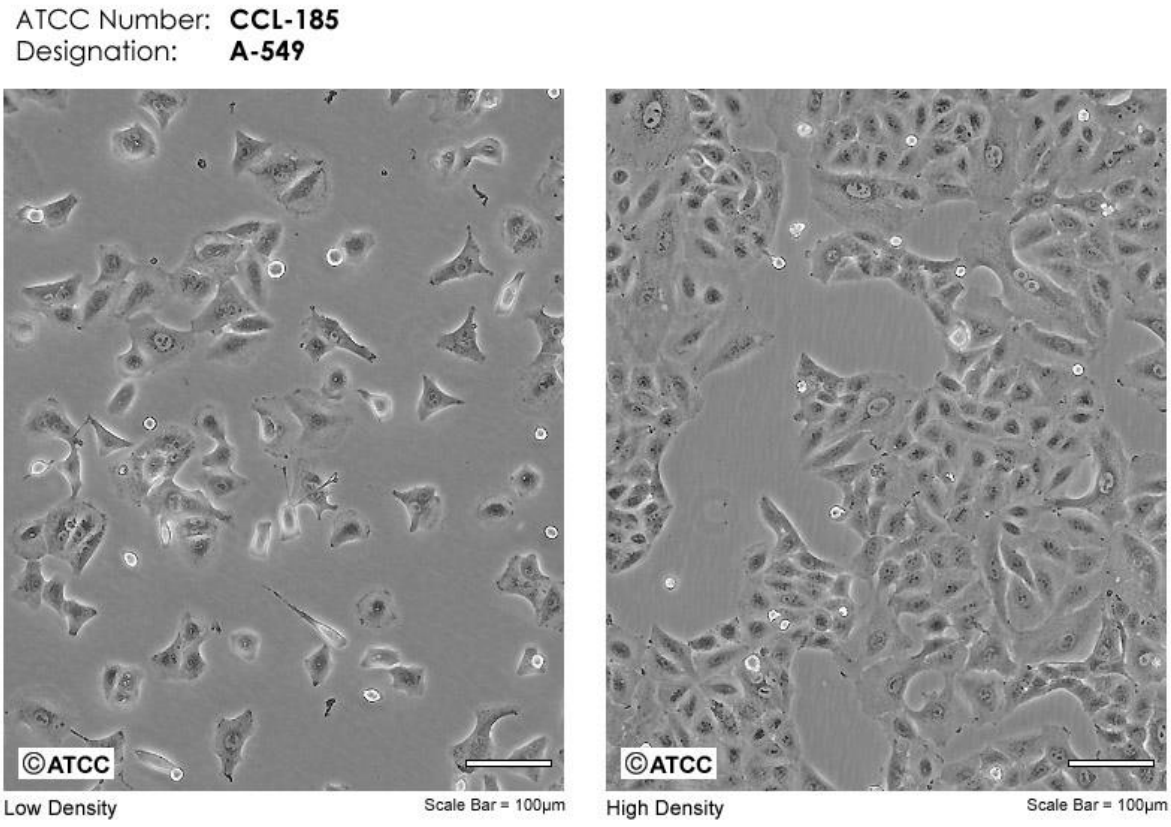

Figure 7 Image of A549 cells (46).

3.4.2 Cultivation and cell experiments

A549 cells were grown in IMDM medium containing 4 mM L-glutamine, supplemented with 10 % foetal calf serum (FCS), 100 I.E./mL penicillin and 0.1 mg/mL streptomycin. The medium of the A549^{r}CDDP^{2000} cells additionally contained 2000 ng/mL cisplatin. Cells were cultivated as monolayers in a humidified atmosphere at 37 °C and 5 % CO_2. Cell growth, morphology and viability of cells were checked regularly by a light microscope. Cells were grown until a confluence of 80 % and either sub-cultivated (approx. every third day) or used for an experiment. Backups of each cell line were suspended in FCS with 10 % DMSO and stored in liquid nitrogen. For each experiment, cells were counted and allowed to attach overnight, experienced 4 h of serum starvation and were subsequently treated with cisplatin for 24 h in IMDM medium without any supplements. The cisplatin concentrations used were cell line-dependent and based on the respective EC_{10} (concentrations, which produce 10 % of the maximum possible response). Both cell lines were treated with 11 µM cisplatin (EC_{10} of sensitive cell line). The resistant sub-line was also treated with 34 µM cisplatin (the respective EC_{10}). In the following, equimolar treatment refers to treatment of the sensitive and resistant cell line with 11 µM cisplatin and equitoxic treatment refers to treatment of the sensitive cell line with 11 µM cisplatin and the resistant cell line with 34 µM cisplatin.

3.4.3 Test for mycoplasma contamination

Mycoplasma is a genus of small (0.22 to 2 µm), wall-less bacteria, which are able to grow on different substrates and cultivated cells. A contamination with mycoplasma can lead to genetic changes and death of cells. The A549 and A549^{r}CDDP^{2000} cells were therefore routinely checked for an infection with mycoplasma. Detection was performed using the fluorescence dye DAPI (2-(4-amidinophenyl)-1H-indole-6-carboxamidine dihydrochloride), which binds to cellular DNA and mycoplasma DNA. DAPI was detected by fluorescence microscopy after exciting with ultraviolet light through a blue filter. Cells were cultivated on microscope slides in a Petri dish for three days without medium change in IMDM without antibiotic supplements. After washing once with PBS, cells were fixed with methanol and subsequently incubated with 5 µg/mL DAPI working solution at room temperature for 5 min. Afterwards, slides were washed twice with 2 mL methanol and Fluoromount™ aqueous mounting medium was used to fix cover slips on the slides. Analysis was performed using a Nikon A1 Eclipse Ti confocal laser scanning microscope. A mycoplasma contamination would be visible as blue pointed shades around the cell nucleus. During the experimental period of this study, no contaminations were detected as shown in Figure 8.

a) b)

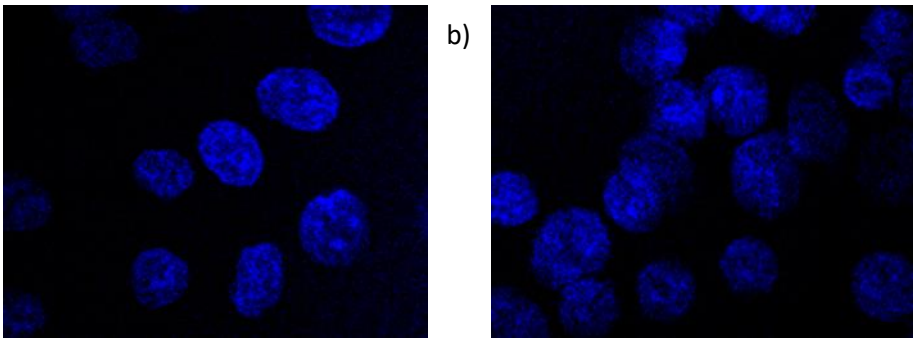

Figure 8 Representative fluorescence image of a negative test for mycoplasma contamination in a) A549, passage 59 and b) A549^{r}CDDP^{2000}, passage 104. The DNA is indicated in blue.

3.5 Cytotoxicity assay (MTT)

3.5.1 Principle

The MTT assay was performed to determine the cytotoxicity of cisplatin in the cells. Cisplatin concentrations that resulted in 90 % cell viability relative to an untreated control (EC_{10}) were determined. The underlying principle is the formation of insoluble violet formazan crystals from 3-(4,5-dimethylthiazol-2-yl)-2,5-diphenyltetrazolium bromide (MTT) through mitochondrial dehydrogenases. With increasing concentrations of the drug, the viability and with it the mitochondrial activity of the cells decrease, leading to reduced formation of the violet formazan product. Its concentration can be measured in an UV spectrometer, as the absorption is proportional to the amount of formazan formed. This analysis results in a sigmoidal concentration-response curve with the turning point giving the pEC_{50} value (concentration which produces 50 % of the maximum possible response). This assay was performed as presented elsewhere (47, 48).

3.5.2 Procedure

8000 cells per well were seeded in a 96-well microtiter plate in 80 µL IMDM and kept at 37 °C and 5 % CO_2 overnight. The outer wells of the microtiter plate were filled with PBS (Table 1). Four hours before treatment, medium was changed to 80 µL non-supplemented IMDM in accordance to other experiments. Cell treatment was performed by adding cisplatin dissolved in 20 µL 0.9 % NaCl in different concentrations, leading to the indicated end-concentrations in each well (Table 1). Each concentration was tested in triplicates and control samples were treated with 0.9 % NaCl. Following 24 h of incubation, 20 µL of MTT solution [5 mg/mL dissolved in phosphate buffered saline] were added for 1 h at 37 °C and 5 % CO_2. Then, the medium was removed, and formazan crystals were dissolved in 100 µL DMSO. Absorbance of the converted dye was measured at 595 nm with background subtraction at 690 nm using a Multiwell-Reader Multiskan EX®.

Table 1 Scheme of 96-well plate with concentrations of cisplatin used for the MTT assay, PBS: phosphate buffered saline; CTR: control.

Cisplatin concentration [µM]												
	1	2	3	4	5	6	7	8	9	10	11	12
A	PBS	PBS	PBS	PBS	PBS	PBS	PBS	PBS	PBS	PBS	PBS	PBS
B	PBS	CTR	0.5	1	5	10	30	50	70	100	500	PBS
C	PBS	CTR	0.5	1	5	10	30	50	70	100	500	PBS
D	PBS	CTR	0.5	1	5	10	30	50	70	100	500	PBS
E	PBS	CTR	0.5	1	5	10	30	50	70	100	500	PBS
F	PBS	CTR	0.5	1	5	10	30	50	70	100	500	PBS
G	PBS	CTR	0.5	1	5	10	30	50	70	100	500	PBS
H	PBS	PBS	PBS	PBS	PBS	PBS	PBS	PBS	PBS	PBS	PBS	PBS

The resulting pEC_{50} values were estimated using the software GraphPad Prism™. Concentration-effect curves were calculated by non-linear regression (settings: no comparison, constraint: 'BOTTOM must be greater than 0.0', no weighting, consider each replicate Y value as an individual point) based on a four-parameter logistic Hill equation (49). The resistance factor was calculated by dividing the EC_{50} of the resistant cell line by the EC_{50} of the respective sensitive cell line.

3.6 Protein quantification

3.6.1 Principle

In the experiment measuring intracellular platinum accumulation, platinum had to be referred to cellular platinum content instead of cell count, as different growth characteristics of sensitive and resistant cells could not ensure an equal number of cells after attachment over night for treatment. Besides that, total cellular protein content had to be determined to load equal amount of proteins into the pockets of the SDS gel electrophoresis. Cellular protein concentration was determined using the bicinchoninic acid assay (BCA™ Protein Assay Kit) according to the manufacturer's instructions (50). A validation with respect to calibration curve linearity, working range, precision, accuracy, lower limit of quantification has been reported previously in our group (4, 51).

Different amino acids in proteins reduce Cu^{2+} to Cu^{+} quantitatively, which can react with two molecules bicinchoninic acid to form a violet chelate complex (Figure 9). This complex can be analysed with an UV spectrometer. The absorption measured with an UV spectrometer at 562 nm is proportional to the concentration of the chelate complex and therefore proportional to the protein quantity. The quantification was done in a 96-well microtiter plate with calibration curve standards and quality control samples on each plate. Every sample was measured in triplicate.

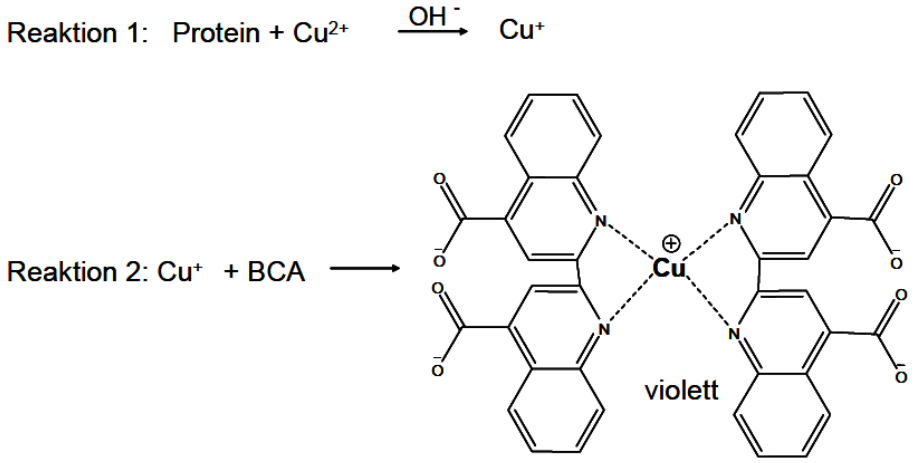

Figure 9 Chemical reaction underlying the protein quantification with the BCA assay (51).

3.6.2 Standard solutions and quality control samples

Six standard solutions for generating a calibration curve were measured on each 96-well plate in triplicates. Solutions were prepared dissolving BSA-containing protein standard (2 mg/mL) provided by the manufacturer in sterile ultrapure water according to Table 2. To assure the quality of the measurement, quality control samples in three different concentrations in the calibration range were measured in triplicates on each 96-well plate. Quality control samples were prepared by diluting BSA-containing protein standard of a different batch according to Table 2.

Table 2 Standard solutions and quality control samples for protein quantification using the BCA assay.

	Volume BSA [µL]	Volume ultrapure [µL]	Protein concentration [µg/mL]
Standard solution			
S1	50	1950	50
S2	75	1925	75
S3	100	1900	100
S4	200	1800	200
S5	300	1700	300
S6	400	1600	400
Quality control samples			
QC1	150	1850	150
QC2	250	1750	250
QC3	350	1650	350

3.6.3 Sample preparation

For cellular platinum accumulation experiments, 20 µL of cell sample were lysed with 10 µL of 1 M NaOH in an ultrasonic bath for 30 min. After centrifugation, 10 µL of 1 M HCl were used for neutralisation and lysate was diluted with 40 µL of ultrapure water (dilution factor 4). From this dilution, proteins were quantified in triplicate in a 96-well plate. Standard solutions and quality control samples were treated in the same way than the cell samples, diluted as well with 10 µL of 1 M NaOH and 10 µL of 1 M HCl, but subsequently not diluted with 40 µL of ultrapure water.

To perform protein quantification for SDS gel electrophoresis, 20 µL of cell lysate were diluted with 80 µL of ultrapure water (dilution factor 5). Afterwards, proteins were again quantified in triplicate in a 96-well plate. 25 µL of standard solutions and quality control samples were added without any further preparation.

For both ways of preparation, a 50:1 mix of BCA working reagent A (BCA) and BCA working reagent B ($CuSO_4$) was prepared and 200 µL were added to each well containing 25 µL of a cell sample. The plate was incubated 15 – 30 min at 60°C. Absorbance was subsequently recorded at 570 nm using a Multiwell-Reader Multiskan EX®.

Microsoft® Excel 2010 was used to perform linear regression based on the mean of triplicates and to calculate protein concentration. Calibration curve was accepted when at least four of the standard solutions show a deviation of ≤ 15 % from the nominal value (20 % at lower limit of quantification) and two of the quality control samples show a deviation of ≤ 15 % of the nominal value. Correlation coefficient (r) had to be ≥ 0.99 (weight 1/x).

3.7 Cellular platinum accumulation

Cellular platinum accumulation was measured to evaluate differences in platinum uptake in the cell lines, which may contribute to resistance development. 2.5×10^5 sensitive cells and 5×10^5 of the resistant sub-line per well were seeded in 6-well plates and left at 37 °C and 5 % CO_2 overnight. After 4 h of serum starvation and treatment with cisplatin for 24 h, cells were washed with ice-cold PBS, trypsinised and centrifuged for 4 min at 1500 x g in 2 mL Eppendorf tubes. Cells were reconstituted in 1.0 mL PBS and 20 µL of the solution were taken aside for protein quantification. The cell pellet was washed again with PBS and stored at -20°C until platinum quantification.

After lysing the cell pellet in 50 µL concentrated HNO_3 at 80 °C for 1 h, measurement of the total platinum content was performed using flameless atomic absorption spectrometry. The method was described elsewhere (52) and used in a modified way, according to the validation performed in our group (53). Briefly, at the beginning of every measurement a calibration curve between 5 and 50 ng platinum/mL was recorded. During measurement run, quality was assured by measuring different quality control samples with 10, 20 and 40 ng platinum/mL. The diluted sample was injected into a graphite tube with an autosampler. After vaporisation and atomisation, platinum absorption was measured at 265.9 nm and 2700 °C. Every sample was measured at least in duplicate but maximal four times depending on the precision of each measurement. The cellular platinum content was referred to the cellular protein quantity, which was determined using the BCA assay as described in section 3.6.

Microsoft® Excel 2010 was used to perform linear regression based on the mean of replicates and to calculate platinum concentration which was referred to cellular protein content. Calibration curve of platinum measurement was accepted when standard solutions showed a deviation of ≤ 15 % from the nominal value (20 % at lower limit of quantification) and at least two of the quality control samples showed a deviation of ≤ 15 % of the nominal value.

3.8 Cisplatin-DNA adducts

Cisplatin-DNA adducts were measured by immunoblotting. After 4 h of serum starvation and treatment with different concentrations of cisplatin for 24 h, total DNA was isolated with the AllPrep® DNA/RNA Mini Kit. 1 µg of DNA was dissolved in Tris/EDTA (TE) buffer and denatured at 95 °C for 10 min. Subsequently, the DNA was spotted on Hybond™ nitrocellulose membranes with a slot blot manifold by a vacuum of 35 kPa. After denaturation with 0.4 M NaOH for 45 min on a drenched filter paper the binding sites at the membranes were blocked with 5 % (w/v) non-fat dry

milk in Tris-buffered saline with 0.1 % (v/v) Tween-20 (≙ TBS-T) overnight at 4 °C. Subsequently, the membranes were incubated with the antibody against cisplatin-DNA adducts, diluted 1:1000 in TBS-T with 5 % (w/v) non-fat dry milk powder, for 2 h at room temperature to detect 1,2-d(GG) DNA intrastrand cross links. The membranes were washed three times with TBS-T followed by incubation with the secondary HRP-coupled antibody (1:1000). Antibody complexes were detected using the enhanced chemiluminescence (ECL) reagent and densitometric analysis was carried out using the AIDA^{TM} 4 software.

3.9 Cell cycle analysis with flow cytometry

3.9.1 Principle

Flow cytometry is a laser-based technology used in cell sorting or cell counting. Small particles like cells or nuclei are separated in a fluid stream and pass a laser beam, which is diffracted and subsequently detected as side-scattered light (SSC) and forward-scattered light (FSC). SSC provides information about the granularity of the cells and FSC about the size of cells. Additionally, specific cell components tagged with a fluorescence dye can be detected by emitting fluorescence after excitation with the laser. For cell cycle analysis, cellular DNA content is analysed, as it differs in different cell cycle phases. Cellular DNA is therefore tagged with the intercalating fluorescent dye propidium iodide (PI). PI binds to DNA without any sequence preference and in a stoichiometric manner, resulting in a proportional ratio of DNA to fluorescence.

3.9.2 Cell cycle phases

The cell cycle can be divided into two major phases: the mitosis (M phase), where one cell divides into two genetically similar daughter cells and the interphase between mitosis. The interphase again is divided into three phases: the G_1 phase, where the cell grows, produces RNA and proteins and prepares for DNA synthesis; the S phase, where DNA is replicated and the G_2 phase, where the cell grows further and prepares itself for mitosis. Additionally, there is a phase called G_0, where cells rest and do not proceed for dividing. The DNA content of every phase differs during cell cycle. After DNA replication in the G_2/M phase, the DNA content is twice as high as before replication in the G_0/G_1 phase. The DNA content in the S phase should be somehow in between the other phases, because the cells start with replication here.

3.9.3 Procedure

5×10^5 sensitive cells and 1×10^6 cells of the resistant sub-line were seeded into 25 cm² flasks and kept at 37 °C and 5 % CO_2 overnight. After 4 h of serum starvation and cisplatin treatment for 24 h,

the supernatant was collected and cells were washed once with PBS, harvested with AccuMax and transferred to the consolidated supernatants. Subsequently, cells were centrifuged 5 min at 200 x g, the supernatant was discarded and cells were fixed with 79 % ethanol for 24 h at 4 °C. After fixation, cells were centrifuged for 5 min at 1400 x g, washed with PBS and incubated with 100 µg/ml RNase A for 30 min at room temperature. After staining with 5 µL propidium iodide (0.1 mg/mL in PBS) samples were analysed using the flow cytometer FACSCalibur™ and evaluated with BD CellQuest™.

3.10 Apoptosis assay

3.10.1 Principle

Cells that undergo apoptosis show several morphologic changes such as loss of plasma membrane symmetry and attachment. Loss of plasma membrane symmetry is reflected in the translocation of phospholipid phosphatidylserine (PS) from the inner to the outer side of the membrane. Outside the plasma membrane PS can be specifically bound by Annexin V, which is conjugated to the detectable fluorochrome fluorescein isothiocyanate (FITC). Combined with the vital dye propidium iodide (PI), which is only able to enter the cell at later apoptotic/necrotic stages where the cell membrane is permeable, this assay distinguishes between early apoptotic cells (Annexin V-FITC positive, PI negative) and late apoptotic/necrotic cells (Annexin V-FITC positive, PI positive).

3.10.2 Procedure

The apoptosis assay was performed using the BD Pharmingen™ FITC Annexin V Apoptosis Detection Kit according to the manufacturer's instruction. 2.5×10^5 sensitive cells and 5×10^5 cells of the resistant sub-line per well were seeded into 6-well plates and kept at 37 °C and 5 % CO_2 overnight. Additionally to the cisplatin treatment with 11 µM and 34 µM, cells were treated with 0.4 µM and 0.8 µM of actinomycin D as a positive control. These concentrations were defined by a pre-evaluation experiment. After 4 h of serum starvation and 24 h treatment, trypsinised cells were added to previously collected supernatant centrifuged for 4 min at 1500 × g and washed twice with PBS. Supernatant was exchanged against 500 µL binding buffer (included in BD Pharmingen™ FITC Annexin V Apoptosis Detection Kit). 5 µL PI and 5 µL Annexin V-FITC were added to 100 µL of the resulting solution. After 15 min of incubation on ice, the solution was diluted with 300 µL binding buffer and analysis was performed using the flow cytometer FACSCalibur™ and evaluated using the Flowing Software V 2.5.

3.11 Whole genome array

Total ribonucleic acid RNA was isolated from both treated and untreated cell lines using the my-Budget RNA Mini Kit or the RNeasy® Mini Kit through different spin columns according to the manufacturer's instructions. Isolated RNA was stored at -80°C until analysis was performed.

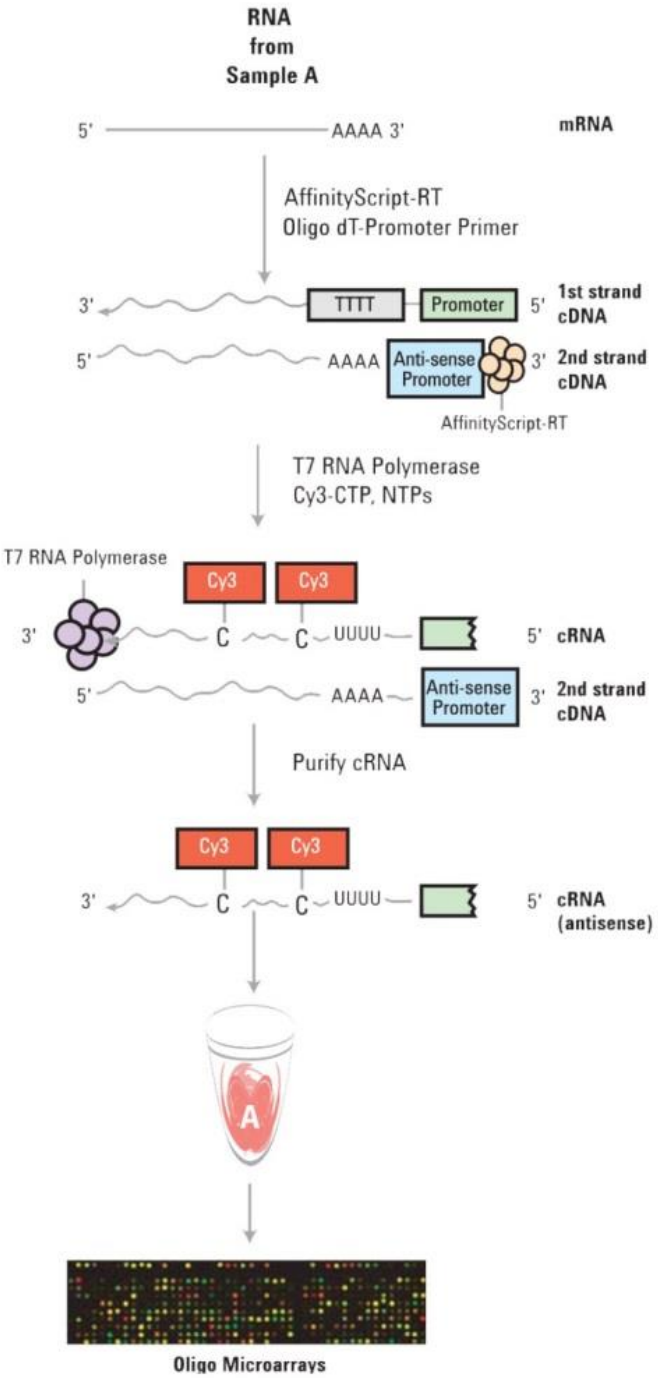

Figure 10 Flow chart of sample preparation for the whole genome array according to the manual of the SurePrint G3 Human GE V2 8x60K Kit (54).

The transcriptome was then analysed using the Whole Genome Array SurePrint G3 Human GE V2 8x60K Kit according to the manufacturer's instruction (Figure 10). Total RNA was transcribed to cDNA using AffinityScript-RT, Oligo dT-Promoter Primer and T7 RNA Polymerase and labelled using the RNA Spike-In Kit (positive controls) including Cyanin 3-CTP (Cy3) dye. After purifying the labelled/amplified cRNA using the RNeasy® Mini Kit, cRNA was quantified spectrophotometrically (UV/VIS) using a NanoDrop™ ND-1000. 40 µL of equivalent amounts of Cy3-labelled cRNA in 10x Blocking Agent and 25x Fragmentation Buffer, diluted with 2x GEx HI-RPM Hybridisation Buffer (all included in the SurePrint G3 Human GE V2 8x60K Kit) were loaded on the gaskets of the microarray slide and kept at 65 °C for 17 h with 10 rpm of agitation. After washing twice with different washing buffers (included in the SurePrint G3 Human GE V2 8x60K Kit), the microarray was read out with the SureScan Microarray Scanner System to measure immunofluorescence intensity. The data were analysed by the Feature Extraction software and the multiples of differentially expressed genes were calculated.

3.12 Gene expression analysis

3.12.1 Principle

Gene expression analysis was performed using real-time quantitative PCR: Firstly, the cDNA needs to be denaturised at 95 °C and split into single strands (denaturation phase), secondly, the primers bind to DNA at a primer-specific annealing temperature (hybridisation phase), thirdly, DNA polymerases need to elongate the missing DNA strand at a polymerase-specific temperature (68 – 72 °C), starting at the 3'-end of the primer which serves as a starting point of the complementary strand (polymerisation phase). Theses phases are executed in recurring cycles.

Real-time qPCR adds a detection phase to each cycle of the PCR, where quantification of the amplified product is performed. Depending on the method, this takes place at the end of the hybridisation phase (fluorescent reporter probe method) or at the end of each cycle after polymerisation (SYBR Green method).

3.12.2 Fluorescent reporter probe method

The fluorescent reporter probe method relies on Förster resonance energy transfer (FRET). Two specific fluorophore oligonucleotides, one bound to a FRET donor and one bound to a FRET acceptor bind next to each other to the target cDNA. If bound, both fluorochromes are close enough, so that energy, created by a light source at defined wave length, can be absorbed by the FRET donor and transferred to the FRET acceptor. The FRET acceptor then emits the energy as light of higher wave length. The intensity of the emitted light is proportional to the amplified target cDNA.

RNA was isolated using the RNeasy® Mini Kit and quantified with a NanoDrop™ N-1000. Subsequently, cDNA synthesis was performed for 60 min at 42 °C. Reaction mixture was composed of 2 µl water, 1.5 µl 10 x buffer, 1.1 µl $MgCl_2$ (25 mM), 1.5 µl dithiothreitol (100 mM), 1.5 µl dNTP (2,5 mM), 0.6 µl RNasin® (20 units/µl), 0,3 µl oligo-dt-primer and murine leukaemia virus reverse transcriptase (50 units/µL) (55). RT-PCR was then performed with Probes Master LC 480 according to the manufacturer's instructions. Hybridisation probes and primers were purchased from TIB MOLBIOL and are described in Table 3. PCR efficiency was evaluated by analysis of four different cDNA concentrations (1:10 to 1:10000) and results were corrected accordingly.

Table 3 Description of hybridisation probes and primers for PCR analysis using the fluorescent reporter probe method.

Gene	**p53**	**SIP**
Forward primer	GCTGCTCAGATAGCGATGGTCT	CGGTACCATTGGGCCAACTA
Reverse primer	GTACAGTCAGAGCCAACCTCAG	GCTGAGAAACCAGTGCAAGTATCTA
LC probe	LC640-TCTGTCATCCAAATACTCCACACGC-PH	CCACAAACATTTTATTCAGCCTCTGG-PH
FL probe	GCACCACCACACTATGTCGAAAAGT-FL	TGGTTGGAGGAAGAACTGACTTCA-FL
Annealing temp. [°C]	57	57
Gene	**Actin**	**GADD45A**
Forward primer	AGCCTCGCCTTTGCCGA	AAGCTGCTCAACGTCGACC
Reverse primer	CTGGTGCCTGGGGCG	CGTCACCAGCACGCAGT
LC probe	LC640-CGACGACGAGCGCGGCGATATC-PH	LC640-AGCCACATCTCTGTCGTCGTCCTCGT-PH
FL probe	TTGCACATGCCGGAGCCGTTG--FL	CTGGATCAGGGTGAAGTGGATCTGCA--FL
Annealing temp. [°C]	61	58
Gene	**XPC**	**p21**
Forward primer	CGATGGGGATGACCTCAGG	GAGGCCGGGATGAGTTG
Reverse primer	TTTCTTCCTCTTCTTCATTGCTG	GAGTGGTAGAAATCTGTCATGCTG
LC probe	LC640-TGTGCCTTCTTGAGGTCACTTGG-PH	LC640-GTCTTGTACCCTTGTGCCTCGCTC-PH
FL probe	CATGGTAGCCCCTCTCTTCAGATG-FL	GAGGAAGACCATGTGGACCTGTCAC-FL
Annealing temp. [°C]	57	58
Gene	**MDM2**	
Forward primer	CAGATGAATTATCTGGTGAACGA	
Reverse primer	AAACTGAATCCTGATCCAACC	
LC probe	LC640-TGTTGTGAAAGAAGCAGTAGCAGTGA-PH	
FL probe	CTGGCTCTGTGTGTAATAAGGGAGAT-FL	
Annealing temp. [°C]	53	

LC Probe: FRET acceptor with LightCycler® red emitting light at 640 nm, FL Probe: FRET donor with 3'-Fluroescein

3.12.3 SYBR Green method

This method uses the fluorescence dye SYBR Green I (N',N'-dimethyl-N-[4-[(E)-(3-methyl-1,3-benzothiazol-2-ylidene)methyl]-1-phenylquinolin-1-ium-2-yl]-N-propylpropane-1,3-diamine), which intercalates in double-stranded DNA or binds to the minor groove of DNA in a stoichiometric manner. The intensity of the fluorescence is again proportional to the amplified target DNA. At the end of the amplification cycles, a melting curve is recorded to validate the applied method and primers. The amplified product melts at one, for the fragment specific temperature, where the double strand is denaturised to two single strands. This leads to the release of SYBR Green I and a change in fluorescence intensity.

Whole cellular RNA was isolated after treatment using the my-Budget RNAse Mini Kit and quantified with a Nanodrop™ N-1000. Subsequent cDNA synthesis was performed as described above in section 3.11 (55). According to the manufacturer's instructions, the following RT-PCR was performed with LightCycler® 480 SYBR Green I Master Mix. Primers were purchased from Life Technologies, USA and are described in Table 4. Quality of the PCR was proven by recording the melting curve of each DNA product. PCR efficiency was evaluated by analysis of four different cDNA concentrations (1:10 to 1:10000) and results were accordingly corrected.

Table 4 Description of primers for PCR analysis using the SYBR Green method.

Gene	Forward Primer Sequence (5' to 3')	Reverse Primer Sequence (5' to 3')	Annealing Temp. [°C]	Product Length [b]
P38	TGCCGCTGGAAAATGTCTCA	GTTGTTCAGATCTGCCCCCA	60	357
HRAS	TGGACGAATACGACCCCACT	CCAACGTGTAGAAGGCATCC	60	393
DOK1	TCTACCTGAGAAGGACGGCA	TCCAGGCACAGTCCAACATC	60	365
CCL2	CGCCTCCAGCATGAAAGTCT	TGTCTGGGGAAAGCTAGGGG	60	372
PTK2B	TTGCCATGGAGCAAGAGAGG	GACCTTTTCAGCCTCCCACA	60	341
MDM2	CCTAAGCCAGACGGGGACTA	TCCACCCATAAAGCGCAACT	60	483
JNK3	AAGCACCTCCATTCTGCTGG	GGAAGGTGAGTCCCGCATAC	60	397
SLC9A9	TCCCCTGGAACTTTCAGCAC	GTTGTAGTCAGCGGAGGACC	60	418
CDKN1A	CCGTCTCAGTGTTGAGCCTT	GCCAGTGTCTCCCTCCTAGA	60	388
WNT4	TCGTGCCTGCGTTCGCT	GTCAGAGCATCCTGACCACTG	60	459

b = nucleotides

3.12.4 Data analysis

Results of the real-time qRT-PCR are presented as fold change relative to untreated control to display the effects of cisplatin. Additionally, the results are presented as absolute data, displaying also the expression levels of untreated controls. The quantitative endpoint for real-time PCR is the threshold cycle (C_t). The C_t is defined as the PCR cycle at which the fluorescent signal of the reporter dye crosses an arbitrarily placed threshold (56). There is an inverse correlation between C_t and the

amount of amplicon: The earlier the threshold is crossed, the higher is the amount of the target gene in the sample. However, using a relative quantification, the data is referred to an internal reference gene ($\Delta C_t = C_{t\ (reference)} - C_{t\ (gene\ of\ interest)}$). Calculation is done by using the widely accepted comparative C_t method (56, 57).

Fold change is calculated as follows by considering the efficiency (E) of the PCR reaction (Equation 1). Here the C_t value of the gene of interest is referred to the internal reference gene and the untreated control ($\Delta\Delta C_t$):

Equation 1

$$\textbf{Fold change} = \frac{\mathbf{E_{gene\ of\ interest}}^{\mathbf{C_{t_{control}} - C_{t_{treated}}}}}{\mathbf{E_{reference\ gene}}^{\mathbf{C_{t_{control}} - C_{t_{treated}}}}}$$

Results for the presentation as absolute data are calculated as follows by assuming, that the efficiency of the PCR = 2 (Equation 2). This means that amplicons are doubled in each cycle of the PCR reaction. Here the C_t value of the gene of interest is only referred to the internal control gene:

Equation 2

$$\textbf{Individual datapoint} = 2^{-\mathbf{C_{t_{reference\ gene}} - C_{t_{gene\ of\ interest}}}}$$

3.13 SDS-PAGE and Western blot

3.13.1 Principle

Analysis of expression of different signalling proteins was performed using Western blot after separation by SDS-polyacrylamide gel electrophoresis (SDS-PAGE). Proteins were detected with specific antibodies and visualised by a chemiluminescence reaction with horseradish peroxidase.

The SDS-PAGE was done according to the discontinued method of Lämmli (58). Here the proteins are filled in pockets in a stacking gel, were the samples are condensed to build up a continuous dye front. The separation takes place in a separation gel with different polyacrylamide concentration, depending on the size of the proteins. Due to the loading of the sample in an SDS-containing loading buffer, the proteins react with a constant amount of SDS. This results in protein-SDS complexes with the same charge/size ratio, making the proteins move in an electric field to the anode, depending on their size.

3.13.2 Sample preparation

Cellular proteins were extracted using RIPA buffer (50 mM Tris-HCl (pH 7.6), 150 mM NaCl, 1 % Triton X-100, 1 % sodium desoxycholate, 0.1 % SDS, 1 mM EDTA) with protease inhibitors (pepstatin, leupeptin, protease inhibitor cocktail, 1 mM activated Na_3VO_4, 1 mM NaF). Protein concentrations were determined using the bicinchoninic acid assay (BCA) and samples were diluted to a final concentration of 30 µg protein/20 µL for every gel pocket. The samples were denaturised at 95 °C for 5 min in loading buffer, containing DTT to reduce disulphide bonds.

3.13.3 Gel electrophoresis and Western blot

Gels were casted starting with the separating gel requiring a polymerisation time of 15 min, being covered with isopropanol to build a plain phase boundary between the gels. Afterward the stacking gel was casted on top and combs were inserted for 30 min to form the sample pockets. After loading 20 µL of samples, electrophoresis was run for 40 – 60 min at 200 V in electrode buffer. Afterwards the two gel parts were separated and the separating gel was kept in transfer buffer for the Western blot procedure. For quantitative detection, proteins were transferred to a PVDF membrane using a semi-dry tank blot method. According to the manufacturer's instruction, the PVDF membrane was equilibrated 20 sec in methanol and kept in transfer buffer. Afterwards a sandwich of fiberpads, separating gel and PVDF membrane was built and proteins were transferred in transfer buffer for 1 h at 100 V and 350 mA. PVDF membrane was blocked after protein transfer with 5 % (w/v) not-fat dry milk powder in Tris-buffered saline (TBS) with 0.1 % (v/v) Tween-20 (≙ TBS-T) for 1 h at room temperature. Subsequently, the membranes were incubated overnight at 4 °C with primary antibodies diluted according to Table 5 and washed three times for 10 min with TBS-T. Afterwards, incubation with the primary antibody against the housekeeping protein for 10 min at room temperature followed. Subsequently after washing again twice with TBS-T for 10 min, incubation with a secondary HRP-conjugated antibody for 1 h at room temperature was performed before detection.

Table 5 Dilution of antibodies used for detection of proteins by Western blot.

Antibody	Dilution
anti-mouse HRP	1:2000
anti-mouse poly-HRP	1:5000
anti-rabbit HRP	1:2000
anti-rabbit poly-HRP	1:5000
CCL2	1:2000
DOK1	1:500
goat anti-rabbit	1:10000
HRas	1:500
JNK3	1:333
MDM2	1:1000
p21	1:200
p38	1:500
p53-HRP	1:200
pAtm	1:200
SIP	1:1000
α-Actin	1:1000

3.13.4 Visualisation of proteins

Antibody complexes were detected with Pierce™ ECL Western blotting Substrate, which is converted into a light-emitting substrate by horseradish peroxidase. Densitometric read-out was performed with Bio-Rad Gel Doc™ XR+ System and analysis was carried out using Image Lab™ Software 5 or Image Analyzer 4 software. Protein signals were normalised to the housekeeping protein GAPDH or α-Actin. Experiments showed reproducibly that α-actin is expressed twofold higher in sensitive cells than in the resistant cells. Because some proteins were not detectable in untreated cells and therefore a fold-of-control analysis was not possible the normalisation to α-actin had to be modified to keep the densitometric analysis of sensitive and resistant cells comparable. Therefore those proteins were normalized to α-actin/2 in sensitive cells. Protein data are presented relative to untreated control referring each treated sample to the corresponding control on the same blot after normalisation. Additionally, the protein data are presented as absolute values only after normalisation (integrated signal intensity of each sample/control). Besides that, the concentrations dependent propensity was looked at, where the comparison of absolute data points between treated cells and control cells revealed a fold change > 2 and the error bars did not overlap.

3.14 Statistical analysis

Statistical analyses were performed with Prism® V6, except for the microarray experiments. A value was only excluded from the analysis if Grubbs' outlier test (extreme studentised deviate) determined it as an outlier, based on the significance level α = 0.05.

3.14.1 Statistical analysis of cell experiments

EC_{50} values, resulting from the viability assay were assumed to be log-normally distributed (49). Statistical significance was in this case tested using two-sided Student's t-test for independent samples. For the cisplatin accumulation and DNA-adduct formation experiments, the means of each independent experiment were calculated and compared between groups by a one-way ANOVA.

To analyse whether gene/protein expression was induced by cisplatin, the differences between treated and untreated cells was analysed using a one-way ANOVA with Bonferroni's multiple comparison post-test.

Differences were considered to be statistically significant with a p-value < 0.05 and are indicated in the diagrams. Experiments were performed at least in triplicates on different days and are presented as mean ± standard error of the mean (SEM), describing the accuracy of estimating the mean.

3.14.2 Statistical analysis of the microarray experiment

Statistical analysis of the array data was performed using GeneSpring GX, Vers. 13.1. For normalisation, data was analysed with the Linear Model for Microarray data (LIMMA), a linear model-based technique (59). A quantile normalisation was applied, to exclude systematic differences between spots of different array slides. Student's t-test was used to calculate statistically significant differentially expressed genes (DEG). Cut-off p-value was < 0.05 and cut-off fold change was > 2. Subsequently a Gene Set Enrichment Analysis (GSEA) of all differentially expressed genes was performed with respect to Gene Ontology terms (GO) and the Kyoto Encyclopedia of Genes and Genomes (KEGG) pathways using HTSanalyzeR (60–63). Array data were pre-processed via background correction (exponential convolution method) and quantile normalisation (64, 65). GSEA is a widely used method comparing the mapping of genes to a defined GO term with a ranking of these genes, e.g. via logarithmic fold change. The GSEA method calculates a score assessing the statistical significance of term enrichments with respect to the ranking of genes. Dose- and resistance-induced gene expression changes were analysed for statistical significances again using LIMMA. The overall significance of the signature of differentially expressed genes was assessed via a global test (66).

4 Results

4.1 Cisplatin cytotoxicity

The concentration-response curves of cisplatin show differences between the sensitive and resistant cells. Cisplatin cytotoxicity was markedly reduced in the A549^{r}CDDP^{2000} cells (pEC_{50} = 4.262 ± 0.171; mean ± SD, n=12) compared to the A549 cell line (pEC_{50} = 4.522 ± 0.144; n=11) after 24 h treatment. Based on the sigmoidal concentration-response curves, 90 % viability concentrations (EC_{10} values) were determined as 11 µM in A549 and 34 µM in A549^{r}CDDP^{2000} cells (Figure 11, see Appendix A). These values result in a resistance factor of approximately 3.

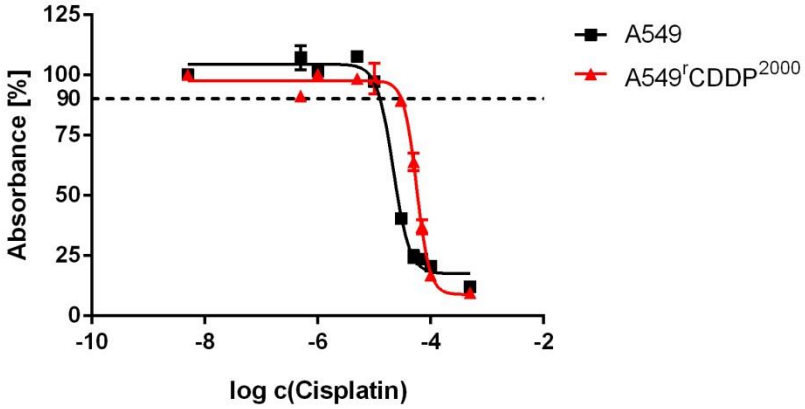

Figure 11 Representative sigmoidal concentration-response curve of cisplatin in A549 and A549^{r}CDDP^{2000} cells. Survival is expressed in terms of % of absorbance of untreated cells as mean ± SD.

4.2 Cellular platinum accumulation

To assess cisplatin uptake, the intracellular platinum concentration was measured in both cell lines (Figure 12). The intracellular platinum content was significantly ($p < 0.05$) reduced in A549^{r}CDDP^{2000} cells (0.051 µmol platinum/g protein, SEM = 0.004; n = 31) compared to A549 cells (0.066 µmol platinum/g protein, SEM = 0.005; n = 33) after treating both cell lines with equimolar concentrations of 11 µM cisplatin. After treating the resistant cells with an equitoxic concentration of 34 µM, the accumulated platinum content raised to 0.158 µmol platinum/g protein (SEM = 0.013; n = 29), which was significantly ($p < 0.0001$) higher than the sensitive cells treated with the equitoxic concentration of 11 µM (see Appendix B).

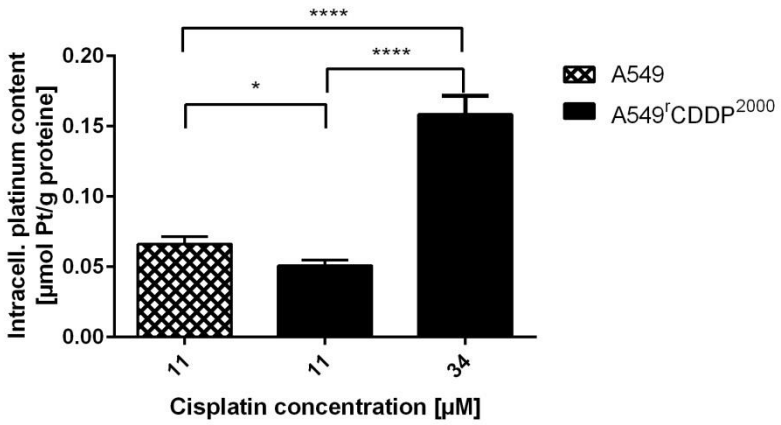

Figure 12 Cellular platinum accumulation, n ≥ 29 in A549 and A549^{r}CDDP^{2000} cells, treated with 11 µM or 34 µM cisplatin for 24 h and presented as mean ± SEM.

4.3 Cisplatin-DNA adduct formation

After treatment with equimolar concentrations of cisplatin, the A549^{r}CDDP^{2000} cells showed a lower, not significantly different level of Cisplatin-DNA adducts. The equitoxic concentrations led to a not significantly increased adduct formation in A549^{r}CDDP^{2000} cells after 4 h treatment compared to A549 cells. After 24 h treatment, resistant cells showed a similar DNA platination as after 4 h, whereas a not significantly increase in cisplatin-DNA adduct formation was observed in sensitive cells over time. These data indicate that A549^{r}CDDP^{2000} cells acquired resistance mechanisms that reduce DNA platination, e.g. by repair mechanisms, in comparison to A549 cells. At equitoxic concentrations, cellular platinum accumulation was about 3-fold higher in A549^{r}CDDP^{2000} cells than in A549 cells. However, the higher intracellular ciplatin content did not result in enhanced cisplatin-DNA adduct formation (Figure 13, see Appendix C).

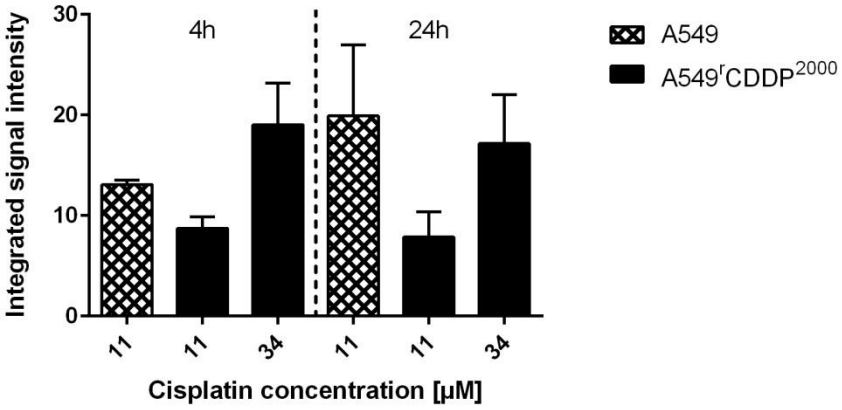

Figure 13 Cisplatin-DNA adduct formation, n = 3, in A549 and A549^{r}CDDP^{2000} cells, treated with 11 µM or 34 µM cisplatin for 4 h and 24 h presented as mean ± SEM.

4.4 Cell cycle analysis

The results of the flow cytometric cell cycle analysis are shown in Figure 15. A549 cells treated with 11 µM cisplatin showed a significant decrease of the cell fraction in the G_1/G_0 phase compared to equitoxic (34 µM) and equimolar (11 µM) cisplatin treatment in A549^{r}CDDP^{2000} cells (Figure 15A). A more striking difference was observed in the G_2/M-phase, where A549 cells treated with 11 µM showed a significant level of cell cycle arrest compared to that of A549^{r}CDDP^{2000} cells, treated with either equimolar or equitoxic concentrations (Figure 15C). Thus, A549^{r}CDDP^{2000} cells seem to have a mechanism to suppress DNA damage-induced G_2/M arrest. There was a non-significant increase in the cell fraction found in the S-phase of resistant cells after treatment with cisplatin compared to that of the sensitive ones (Figure 15B, see Appendix D).

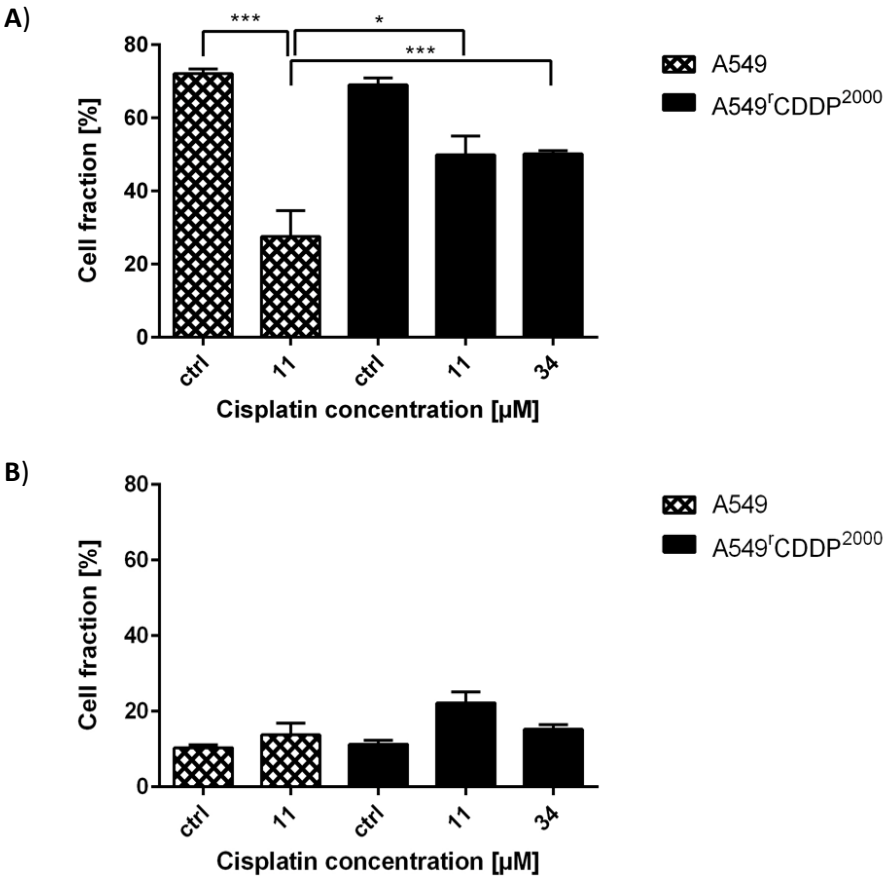

Figure 14A/B Cell cycle analysis (n = 3) of cell fraction presented in % of the total cell population in **A**) the G_1/G_0-phase, **B**) the S-phase in A549 and A549^{r}CDDP^{2000} cells as untreated controls (ctrl) or after treatment with 11 µM or 34 µM cisplatin presented as mean ± SEM.

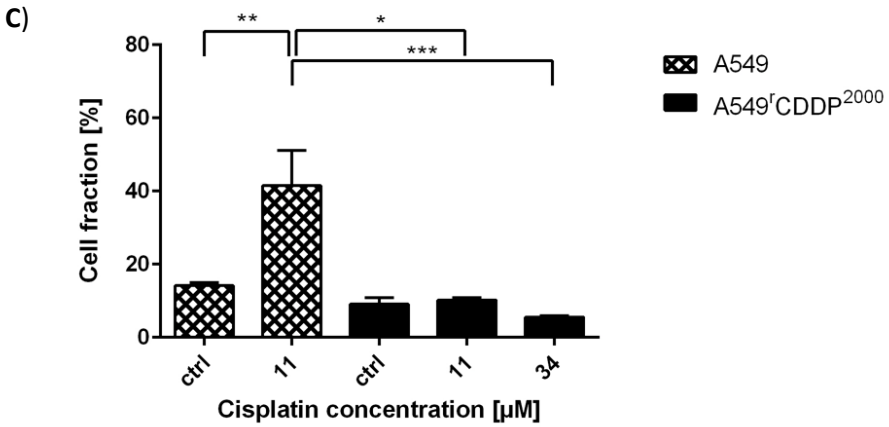

Figure 15C Cell cycle analysis (n = 3) of cell fraction presented in % of the total cell population in the G_2/M-phase in A549 and A549^{r}CDDP^{2000} cells as untreated controls (ctrl) or after treatment with 11 µM or 34 µM cisplatin presented as mean ± SEM.

4.5 Apoptosis induction

After treatment with 11 µM cisplatin, apoptosis was markedly induced in A549 cells. A549^{r}CDDP^{2000} cells exhibited significantly less apoptotic cells in response to treatment with equimolar concentrations of cisplatin compared to A549 cells. A549^{r}CDDP^{2000} cell treatment with 34 µM cisplatin resulted in a tendency towards more apoptotic cells compared to 11 µM cisplatin exposure. However, the number of apoptotic cells was still lower compared to sensitive cells treated with the equitoxic concentration of 11 µM (Figure 16A). Similar results were obtained by the quantification of the number of cells in the SubG_1-phase (Figure 16B, see Appendix E).

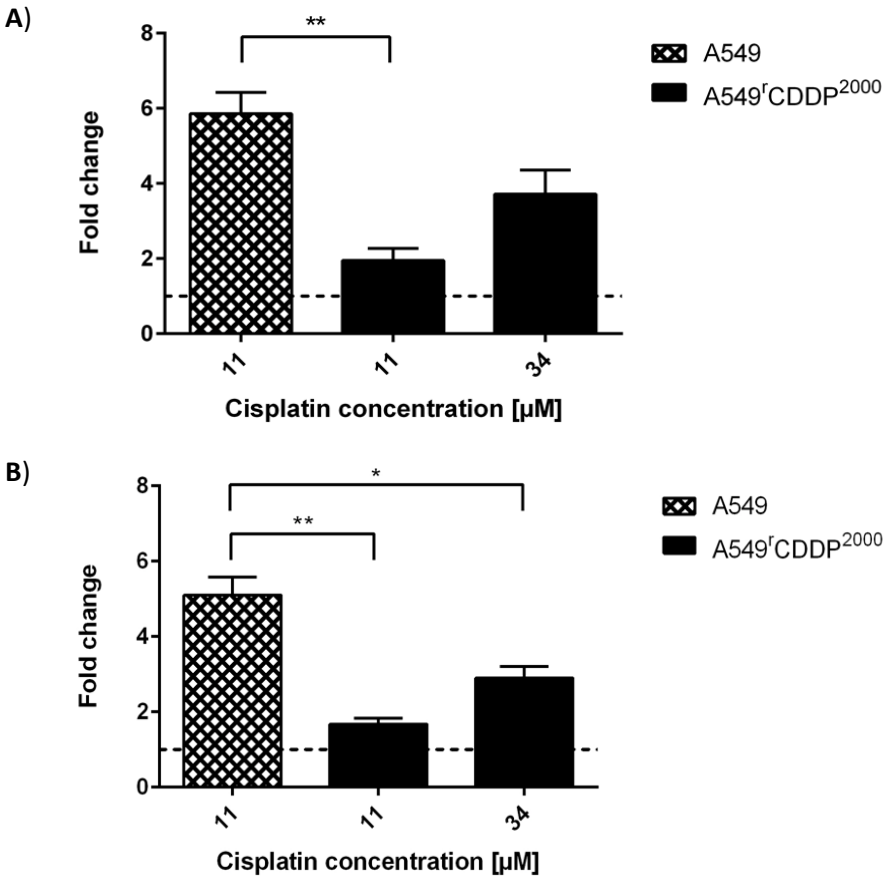

Figure 16 Apoptosis analysis with **A**) FITC Annexin, n ≥ 3 and **B**) cell count in SubG1 phase, n = 3, as fold change related to untreated controls in A549 and A549^{r}CDDP^{2000} cells, presented as mean ± SEM.

4.6 Response of the p53 system

As the results presented in the previous three sections suggested that cisplatin-resistant cells may feature alterations in DNA damage response (see section 4.3, 4.4, 4.5), p53-mediated signalling was investigated in more detail. P53 plays a major role in DNA damage response, apoptosis and cell cycle regulation. Key players of the downstream signalling of p53 were investigated at the mRNA and protein level in order to determine differences in p53 signalling in response to cisplatin treatment between A549 and A549^{r}CDDP^{2000} cells. As expected, because of a minor role of changes in p53 transcription and mainly regulation on protein level (67), p53 expression was not changed after cisplatin treatment but showed a significantly ($p < 0.01$) higher baseline level in resistant cells compared to sensitive ones (Figure 17A). There was a significant accumulation ($p < 0.05$) of the total protein in cisplatin-treated sensitive cells compared to resistant cells treated with 11 µM cisplatin ($p < 0.01$) or with 34 µM cisplatin ($p < 0.001$). Absolute data revealed that only cisplatin treatment in sensitive cells resulted in a significant increase in protein accumulation. Equitoxic cisplatin treatment

induced a similar increase of p53 protein expression in A549 and A549^{r}CDDP^{2000} cells (Figure 17B/C, see Appendix F).

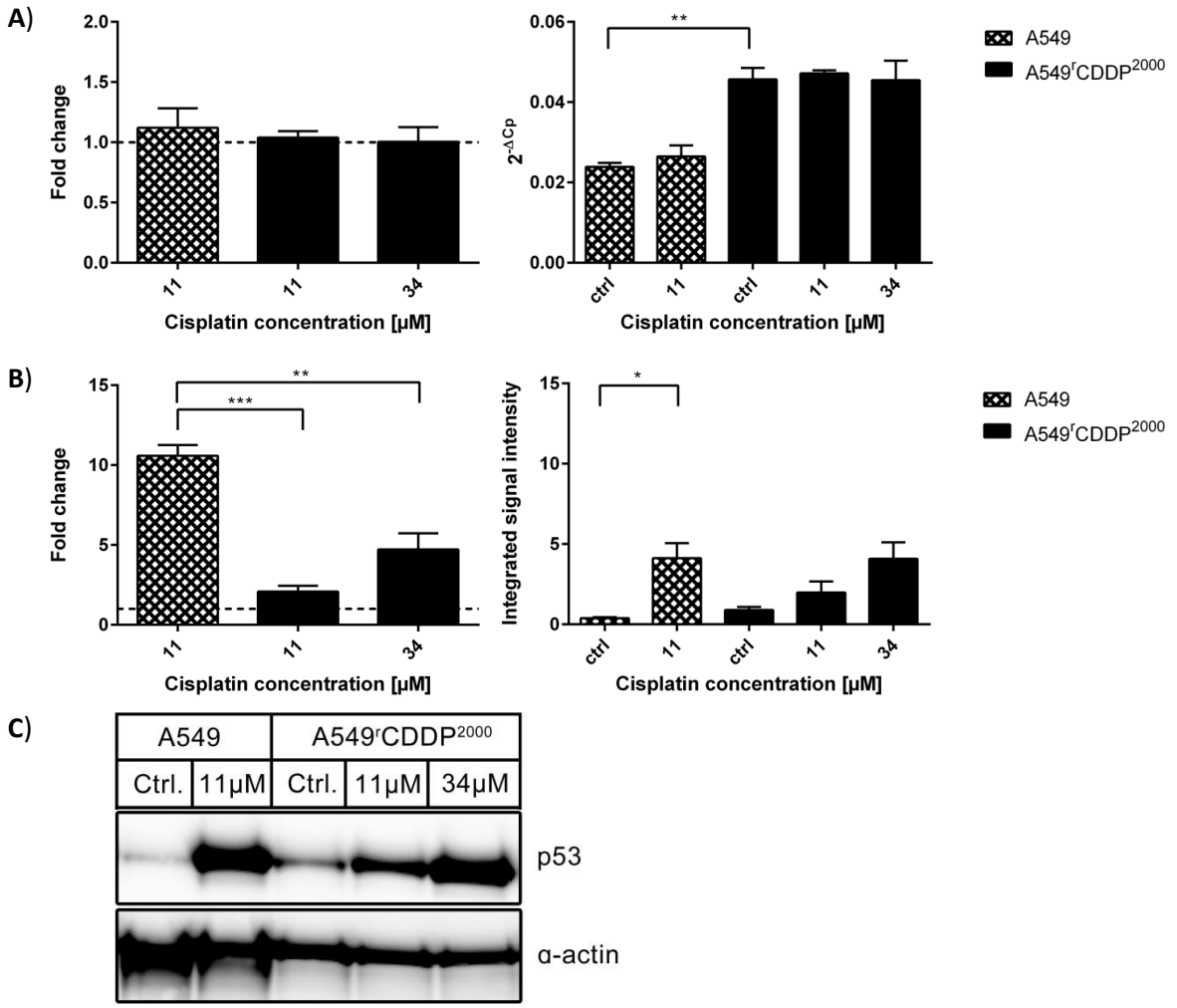

Figure 17 Analysis of **p53** in **A**) RT-PCR (n = 3) as fold change relative to untreated control (ctrl) and absolute data, **B**) Western blot (n = 3) as fold change and integrated signal intensity normalised to the housekeeper α-actin in A549 and A549^{r}CDDP^{2000} cells, presented as mean ± SEM, **C**) one representative Western blot with A549 cells untreated, A549 cells treated with 11 µM cisplatin, A549^{r}CDDP^{2000} cells untreated, A549^{r}CDDP^{2000} cells treated with 11 µM cisplatin and A549^{r}CDDP^{2000} cells treated with 34 µM cisplatin.

Upstream of p53, the DNA damage recognition protein Ataxia Telangiectesia mutated (Atm) protein showed a higher induction in relative protein level in sensitive cells compared to A549^{r}CDDP^{2000} cells. This difference in extent of induction was, however, not significant. In sensitive cells the activation was significant compared to the untreated control ($p < 0.05$) after treatment with 11 µM cisplatin whereas it was not significant in resistant cells (Figure 18A, see Appendix G).

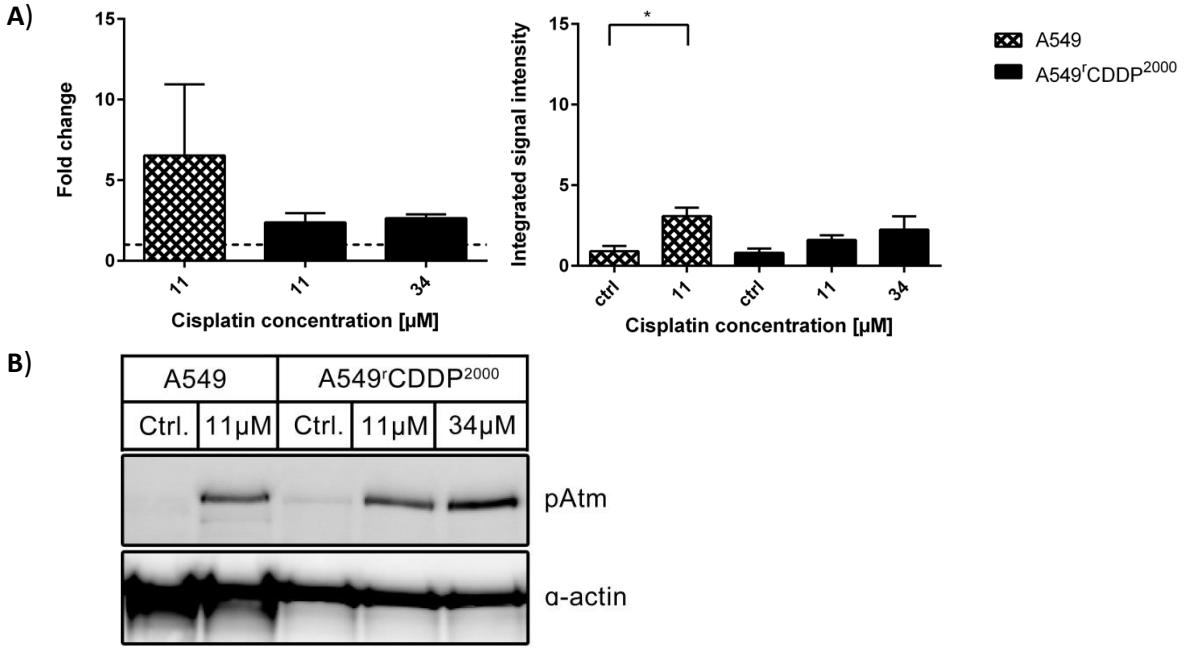

Figure 18 Analysis of **pAtm** in **A**) Western blot (n = 3) as fold change and integrated signal intensity normalised to the housekeeper α-actin in A549 and A549^{r}CDDP^{2000} cells, presented as mean ± SEM, **B**) one representative Western blot with A549 cells untreated, A549 cells treated with 11 µM cisplatin, A549^{r}CDDP^{2000} cells untreated, A549^{r}CDDP^{2000} cells treated with 11 µM cisplatin and A549^{r}CDDP^{2000} cells treated with 34 µM cisplatin.

Mouse double minute 2 homolog (MDM2) protein, a p53 target and endogenous p53 antagonist was significantly up-regulated at mRNA level ($p < 0.05$) after 24 h treatment with equitoxic cisplatin concentrations in both cell lines (Figure 19A). Levels of mRNA were comparable in sensitive and resistant cells. The level of induction in fold change compared to control was significantly higher in sensitive cells compared to equimolar ($p < 0.001$) and equitoxic ($p < 0.001$) treatment in resistant cells. No significant changes in MDM2 protein expression were observed in both cell lines after cisplatin treatment (Figure 19B, see Appendix H).

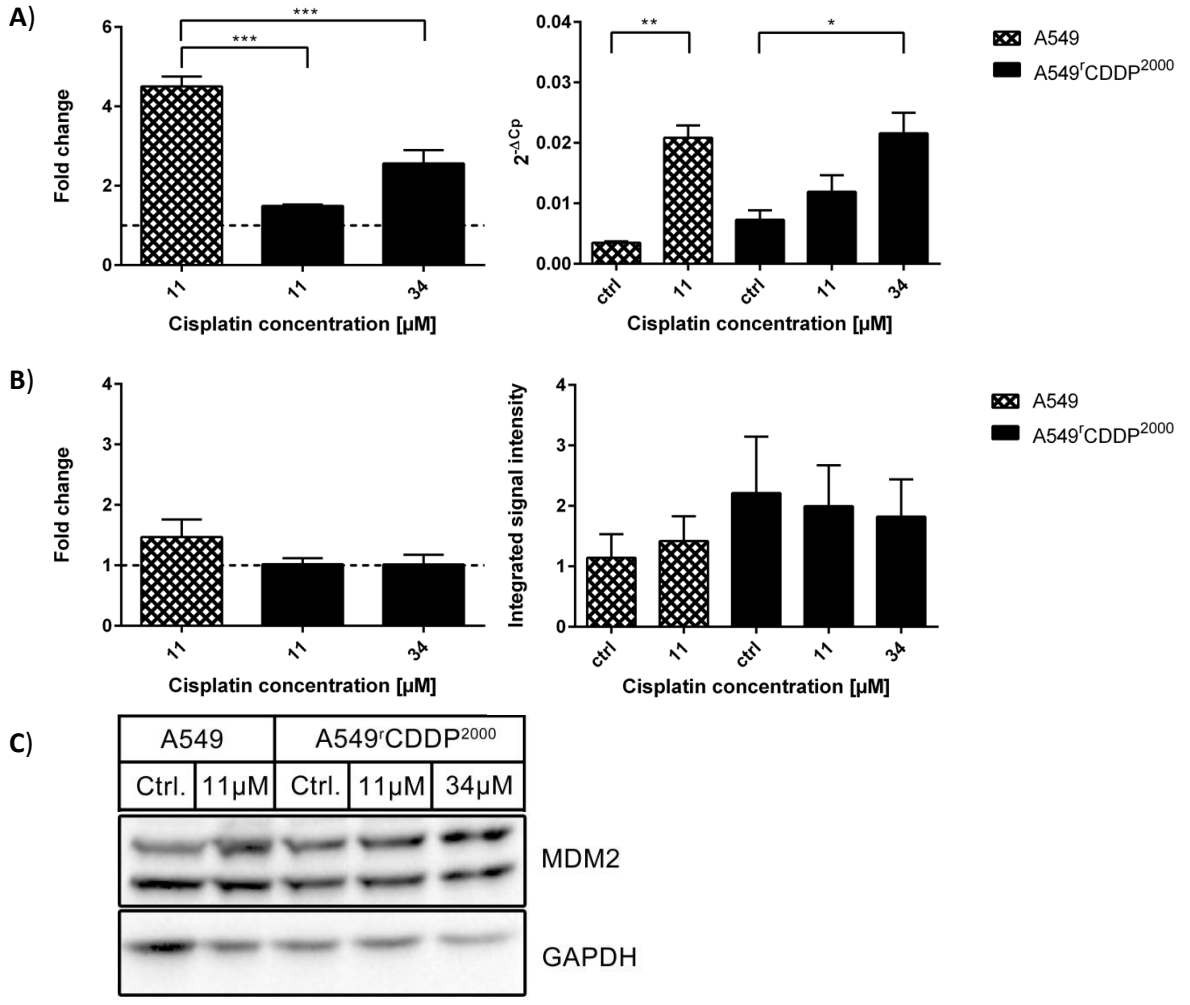

Figure 19 Analysis of **MDM2** in **A**) RT-PCR (n = 3) as fold change related to untreated controls (ctrl) and absolute data, **B**) Western blot (n = 7) as fold change and integrated signal intensity, normalised to the housekeeper GAPDH in A549 and A549^{r}CDDP^{2000} cells, presented as mean ± SEM, **C**) one representative Western blot with A549 cells untreated, A549 cells treated with 11 µM cisplatin, A549^{r}CDDP^{2000} untreated, A549^{r}CDDP^{2000} cells treated with 11 µM cisplatin and A549^{r}CDDP^{2000} cells treated with 34 µM cisplatin. According to the manufacturer's instruction both bands of MDM2 were quantified.

The mRNA of p21, a protein involved in regulation of the cell cycle, was significantly higher in fold change after 11 µM cisplatin treatment in sensitive cells ($p < 0.01$) and after 34 µM cisplatin treatment in resistant cells ($p < 0.05$) compared to 11 µM cisplatin treatment in resistant cells (Figure 20A). It was significantly ($p < 0.05$) up-regulated at mRNA level upon all treatment conditions and in both cell lines. On protein level, no significant changes were observed (Figure 20B, see Appendix I).

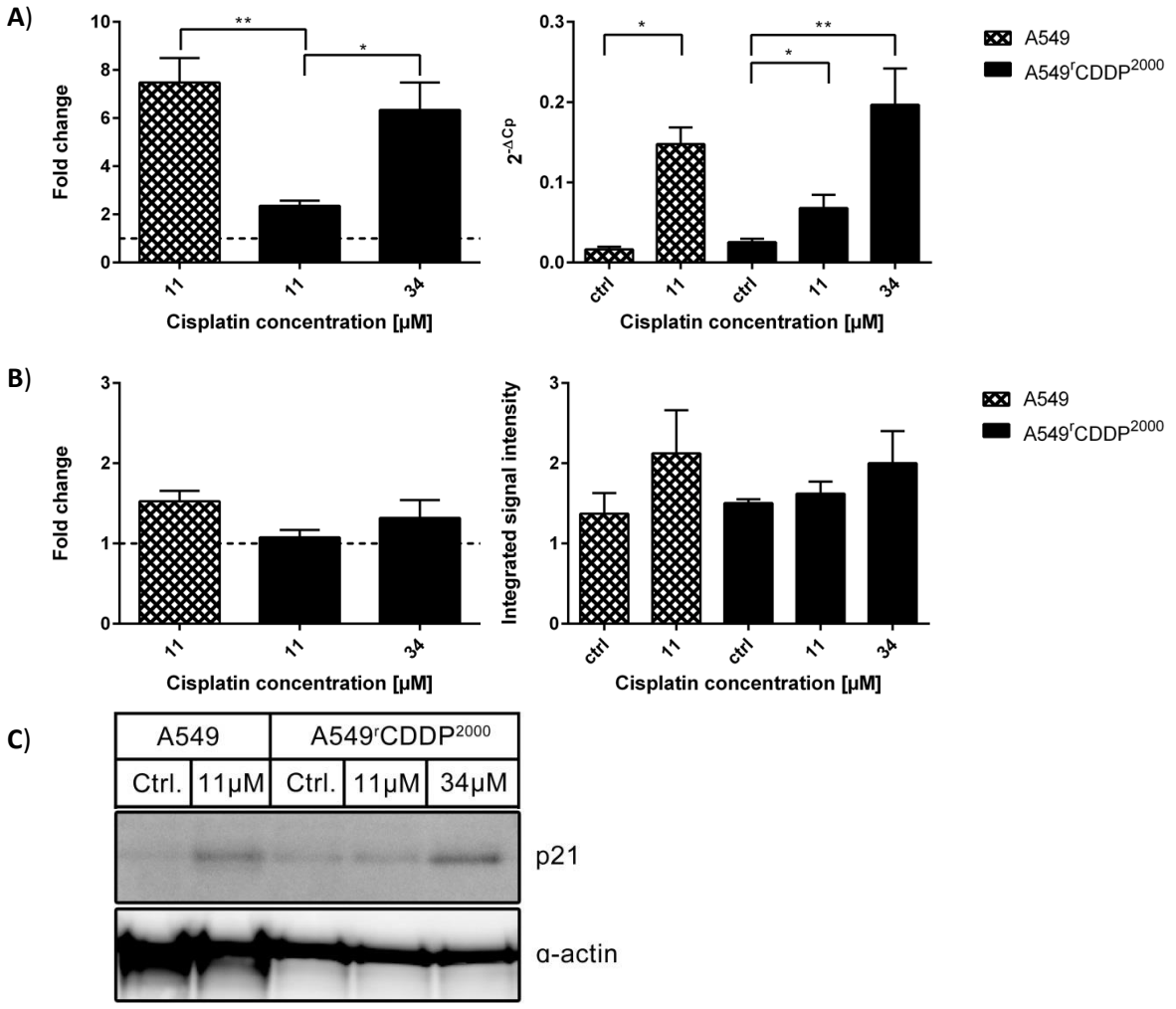

Figure 20 Analysis of **p21** in **A**) RT-PCR (n = 3) as fold change related to untreated controls (ctrl) and absolute data, **B**) Western blot (n = 3) as fold change and integrated signal intensity, normalised to the housekeeper α-actin in A549 and A549^{r}CDDP^{2000} cells, presented as mean ± SEM, **C**) one representative Western blot with A549 cells untreated, A549 cells treated with 11 µM cisplatin, A549^{r}CDDP^{2000} untreated, A549^{r}CDDP^{2000} cells treated with 11 µM cisplatin and A549^{r}CDDP^{2000} cells treated with 34 µM cisplatin.

Relative mRNA levels of SIP, a stress-induced protein and another upstream activator (cofactor) of p53, were significantly ($p < 0.05$) increased in sensitive cells after treatment with cisplatin in contrast to to resistant cells (Figure 21A). These results were not transferred to the protein level, where no regulation of protein expression was observed. Baseline levels of SIP differed significantly between both cell lines (Figure 21B, see Appendix J).

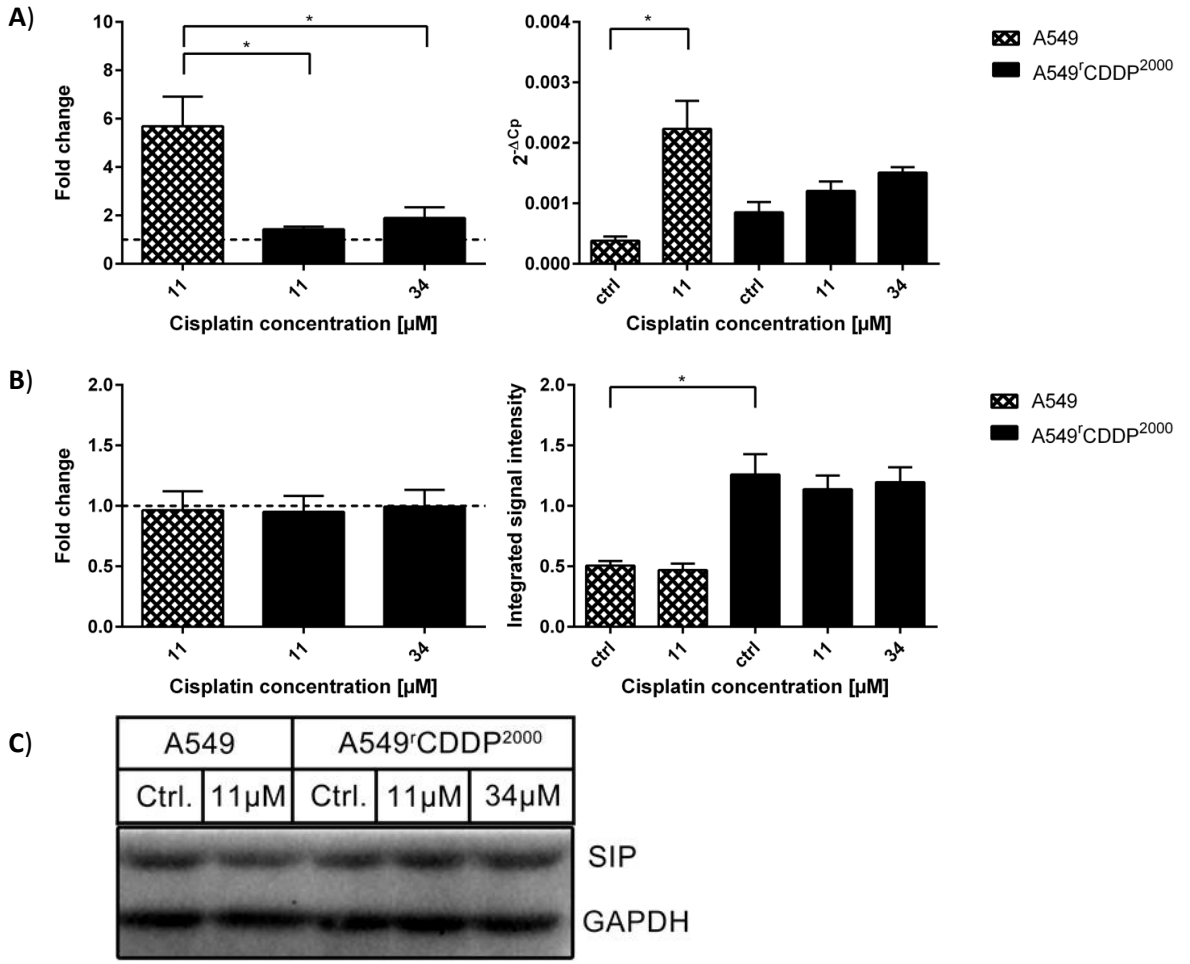

Figure 21 Analysis of **SIP** in **A**) RT-PCR (n = 3) as fold change relative to untreated controls (ctrl) and absolute data, **B**) Western blot (n = 5) as fold change and integrated signal intensity, normalised to the housekeeper GAPDH in A549 and A549^{r}CDDP^{2000} cells, presented as mean ± SEM, **C**) one representative Western blot showing A549 cells untreated, A549 cells treated with 11 µM cisplatin, A549^{r}CDDP^{2000} cells untreated, A549^{r}CDDP^{2000} cells treated with 11 µM cisplatin and A549^{r}CDDP^{2000} cells treated with 34 µM cisplatin.

Xeroderma pigmentosum, complementation group C (XPC) mRNA, which encodes a member of the nucleotide excision repair system and is a downstream effector of p53, was significantly up-regulated in fold change in sensitive cells after cisplatin treatment ($p < 0.05$). The induction of XPC mRNA expression was significantly stronger in sensitive cells compared to resistant cells treated with equimolar ($p < 0.01$) and equitoxic ($p < 0.05$) cisplatin concentrations (Figure 22A). On protein level, XPC showed no significant changes after treatment with cisplatin (Figure 22B, see Appendix K).

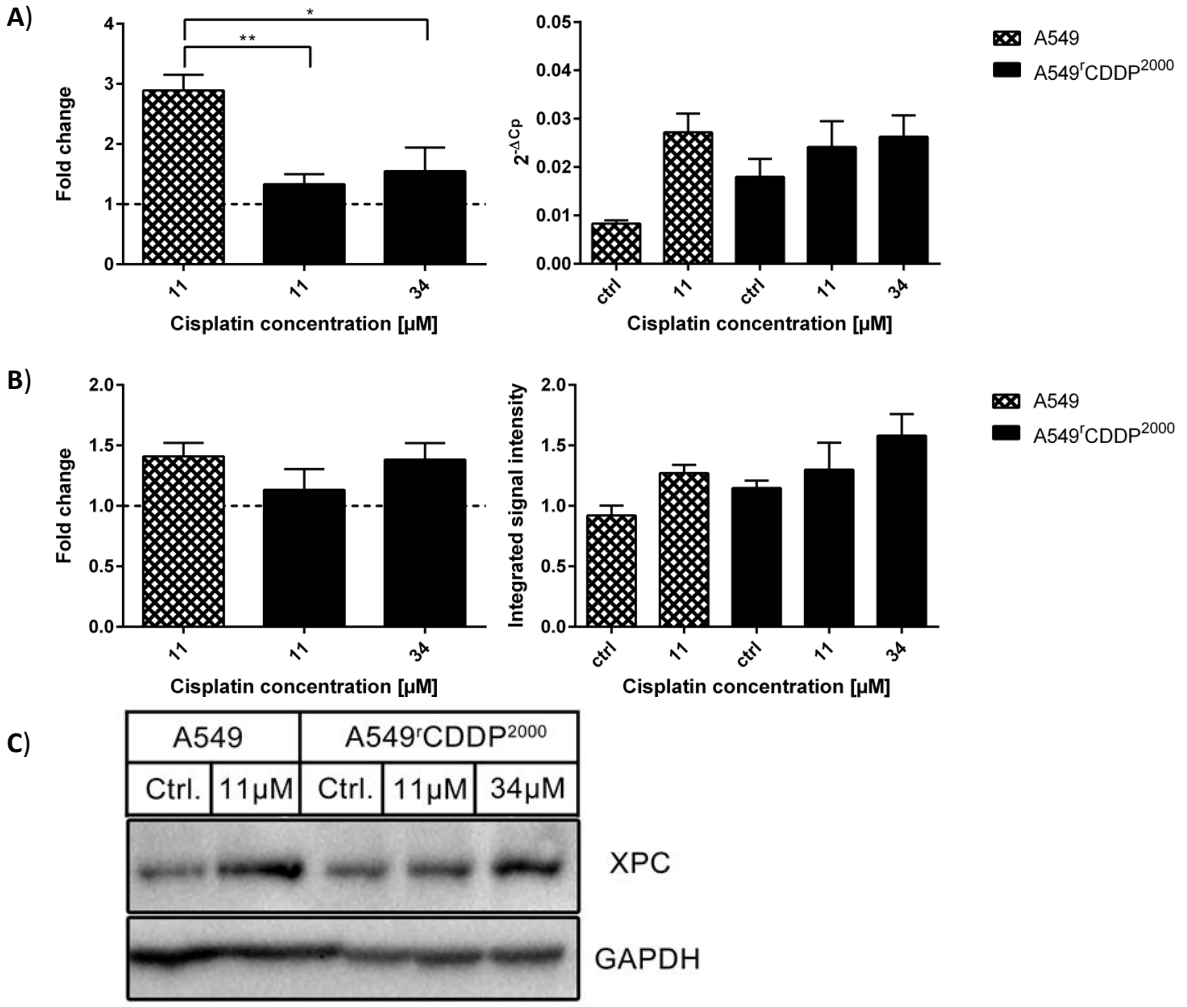

Figure 22 Analysis of **XPC** in **A**) RT-PCR (n = 3) as fold change related to untreated controls (ctrl) and absolute data, **B**) Western blot (n = 5) as fold change and integrated signal intensity, normalised to the housekeeper GAPDH in A549 and A549^{r}CDDP^{2000} cells, presented as mean ± SEM as well, **C**) one representative Western blot with A549 cells untreated, A549 cells treated with 11 µM cisplatin, A549^{r}CDDP^{2000} cells untreated, A549^{r}CDDP^{2000} cells treated with 11 µM cisplatin and A549^{r}CDDP^{2000} cells treated with 34 µM cisplatin.

The growth arrest and DNA-damage-inducible protein GADD45 alpha (GADD45a), which in general is a downstream effector of p53 with impact on checkpoint kinases and an inducer of cell cycle arrest, showed a significantly different expression upon treatment with 11 µM cisplatin in A549 cells compared to A549^{r}CDDP^{2000} cells treated with an equimolar concentration (Figure 23A). At the protein level, however, no significant differences between treated and untreated cells were observed (Figure 23B, see Appendix L).

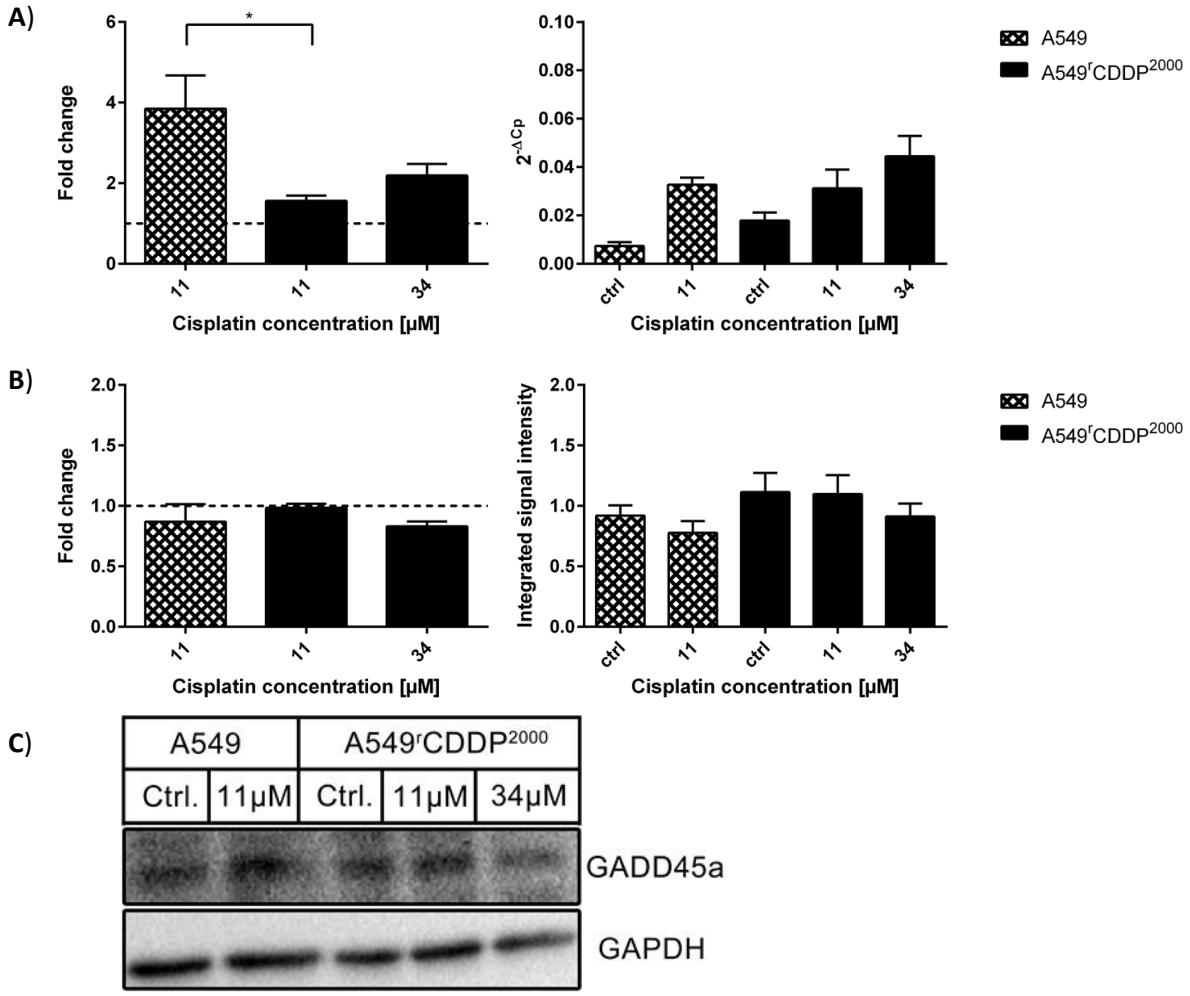

Figure 23 Analysis of **GADD45a** in **A**) RT-PCR (n = 3) as fold change related to untreated controls (ctrl) and absolute data, **B**) Western blot (n = 4) as fold change and integrated signal intensity, normalised to the housekeeper GAPDH in A549 and A549^{r}CDDP^{2000} cells, presented as mean ± SEM, **C**) one representative Western blot with A549 cells untreated, A549 cells treated with 11 µM cisplatin, A549^{r}CDDP^{2000} cells untreated, A549^{r}CDDP^{2000} cells treated with 11 µM cisplatin and A549^{r}CDDP^{2000} cells treated with 34 µM cisplatin.

4.7 Transcriptome analysis and array validation

4.7.1 Differentially expressed genes

To perform a first step towards systems pharmacology, a more systematic approach was needed. Here a data-driven approach was chosen investigating the transcriptome of both cell lines in different treatment situations in a whole genome array. Processing of array data is shown in Figure 24. After extracting differentially expressed genes a Gene Set Enrichment Analysis (GSEA) was carried out in order to identify key pathways altered in response to cisplatin treatment (62). The set of differentially expressed genes was then reduced to those involved in the identified pathways and further validated via qPCR and Western blot.

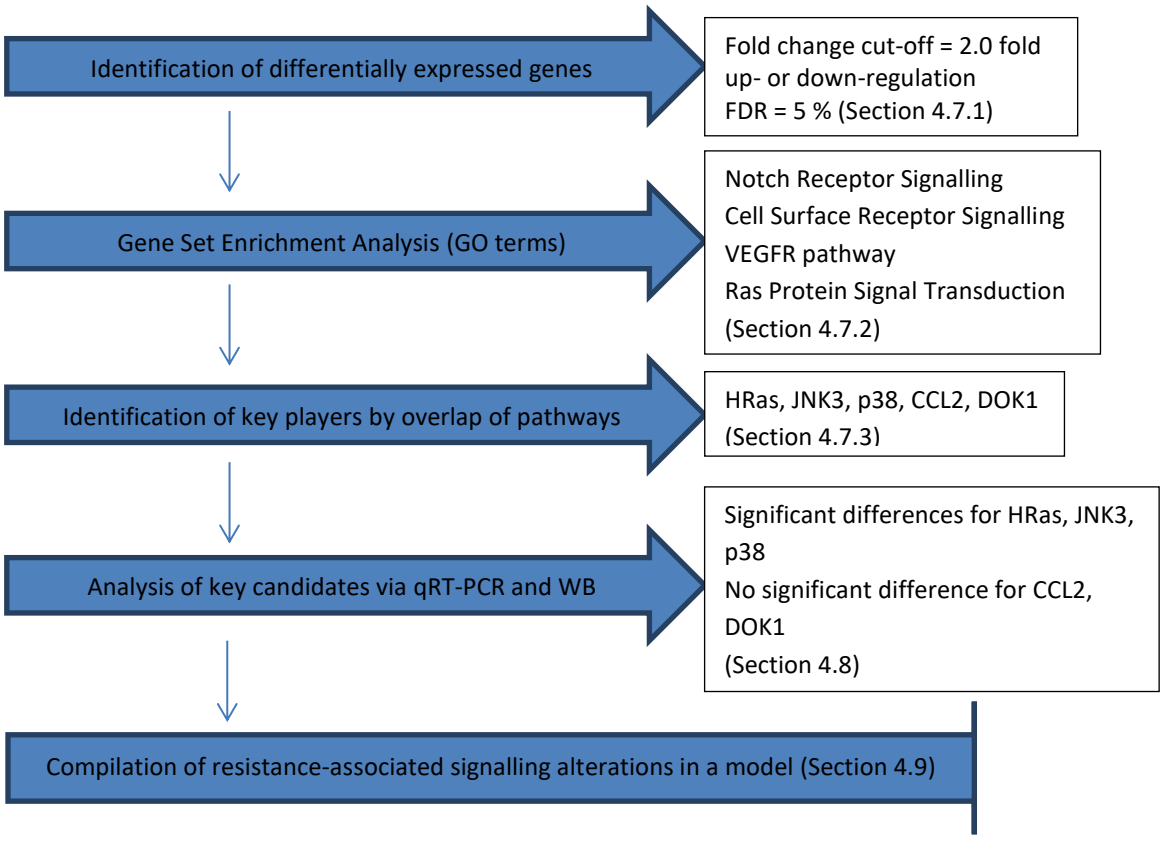

Figure 24 Flow diagram of array data processing (FDR = false discovery rate; WB = Western blot; GO terms = Gene ontology terms).

The number of differentially expressed genes in the different treatment situations with at least 2.0 fold up- or down-regulation and a false discovery rate of 5 % in A549 and A549^{r}CDDP^{2000} cells can be found in Table 6.

Table 6 Number of differentially expressed genes, compared as treatment condition vs. treatment control with at least 2-fold up- or down-regulation and a false discovery rate below 5 %.

Treatment control vs.	Treatment condition	Number of differentially expressed genes
A549, control	A549^{r}CDDP^{2000}, control	3697
A549, 11 µM cisplatin	A549^{r}CDDP^{2000}, 11 µM cisplatin	4394
A549^{r}CDDP^{2000}, control	A549^{r}CDDP^{2000}, 11 µM cisplatin	27
A549^{r}CDDP^{2000}, control	A549^{r}CDDP^{2000}, 34 µM cisplatin	708
A549, control	A549, 11 µM cisplatin	1191
A549, 11 µM cisplatin	A549^{r}CDDP^{2000}, 34 µM cisplatin	3670

The generated heat map of differentially expressed genes shows a clear clustering between the different treatment conditions and cell types based on an average linkage clustering using Pearson's correlation distance (Figure 25).

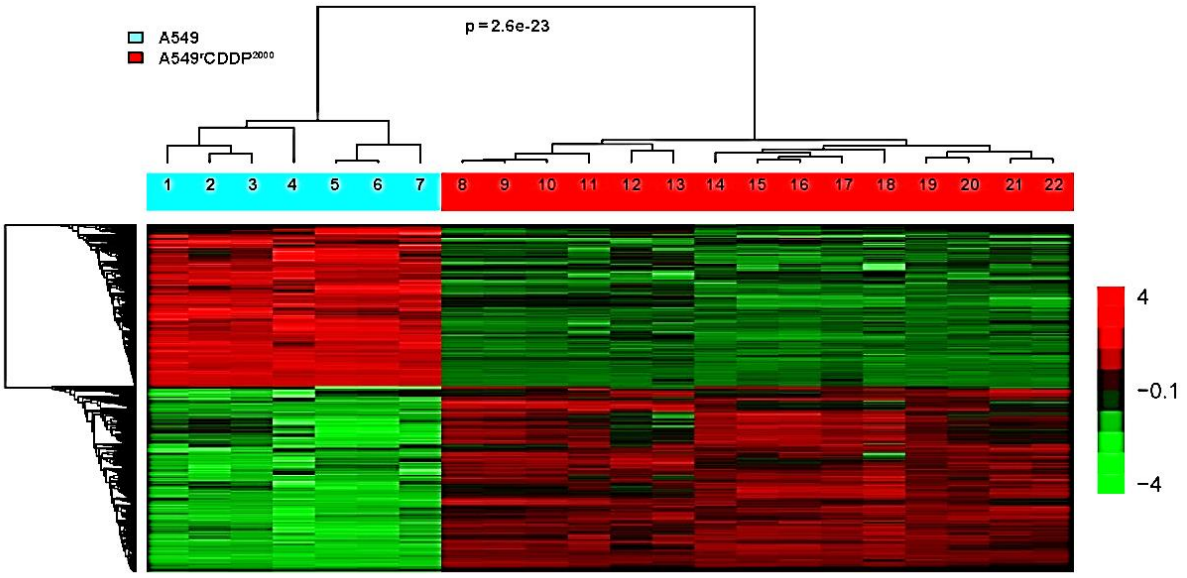

Figure 25 Heat map of the whole transcriptome, regulated genes with fold change cut-off at 2.0 and a false discovery rate of 5 % of all replicates in sensitive and resistant cells. Numbers above lanes indicate: 1, 2, 3, 4: A549 untreated control; 5, 6, 7: A549 treated with 11 µM cisplatin; 8, 9, 14, 15, 16: A549^{r}CDDP^{2000} untreated control; 10, 11, 17, 18, 19: A549^{r}CDDP^{2000} treated with 11 µM cisplatin; 12, 13, 20, 21, 22: A549^{r}CDDP^{2000} treated with 34 µM cisplatin.

The tree structure on top of the heat map indicates that A549 cells and A549^{r}CDDP^{2000} cells cluster in two different groups independent of treatment. This shows that the adaptation to cisplatin over a long time changes the expression pattern more than a single treatment with a higher concentration.

In the resistant cells, the difference in expression is concentration-dependent, as cells treated with the higher concentration cluster on the outer right side of the heat map. Furthermore, the number of differentially expressed genes caused by acute cisplatin exposure is larger in sensitive cells than in the resistant cells, even with the higher dose (Table 6).

The technical validation of the microarray was performed by real time qRT-PCR with 10 significantly up- or down-regulated genes in all three different treatment conditions using the SYBR Green method with the LightCycler® 480. The results of the qRT-PCR were consistent with the microarray data, so that they were accepted as successfully validated. As shown in Figure 26, the analysis of genes in real time qRT-PCR (on the right side) shows the same pattern of up-regulation and down-regulation as the data evolved from the microarray analysis (on the left side, only significant fold changes depicted for visualisation) (see Appendix M).

4.7.2 Gene Set Enrichment Analysis

After the previously described identification of differentially expressed genes a Gene Set Enrichment Analysis (GSEA) was performed. 12 GO and KEGG terms, respectively, were found to be statistically significant (FDR < 5 %) associated with cisplatin treatment: actin filament bundle assembly, cell surface receptor signalling pathway, cytokine-mediated signalling pathway, cytoplasmic microtubule organisation, hematopoietic progenitor cell differentiation, negative regulation of osteoblast differentiation, NOTCH receptor signalling, oocyte maturation, Ras protein signal transduction pathway, regulation of proteolysis, response to testosterone stimulus, and VEGFR signalling pathway. The number of differentially expressed genes annotated with all of these 12 terms was far too large for further analysis. Therefore, the analysis was focused on those terms, for which a contribution to the mode of action of cisplatin or a possible involvement in chemoresistance has been described in the literature, namely the NOTCH receptor signalling (68–70), the VEGFR signalling pathway (71, 72), the cell surface receptor signalling pathway (71–78) and the Ras protein signal transduction pathway (79–82).

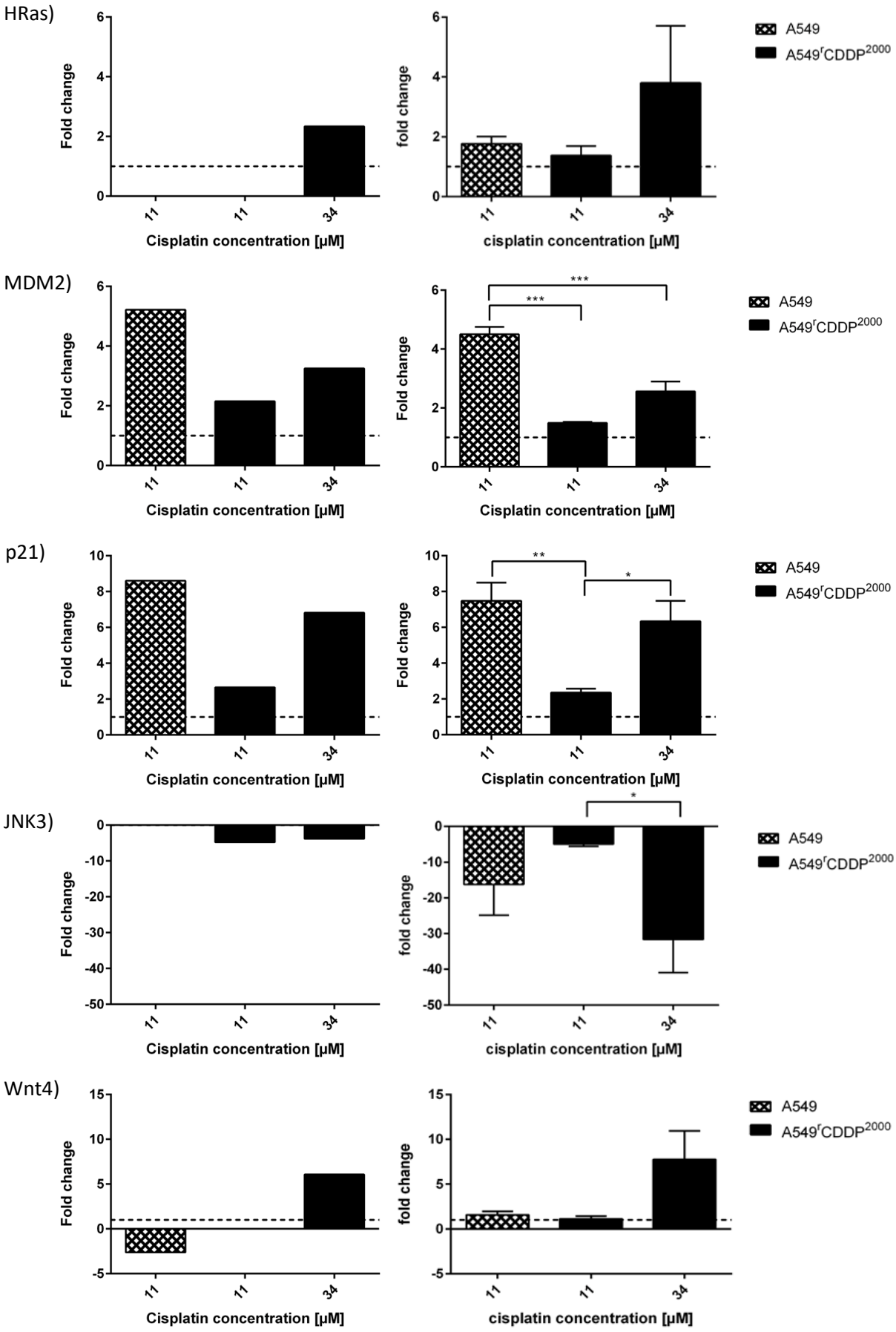
HRas)
MDM2)
p21)
JNK3)
Wnt4)
Fold change
fold change
Cisplatin concentration [µM]
cisplatin concentration [µM]
11
34
A549
A549rCDDP2000
***
**
*

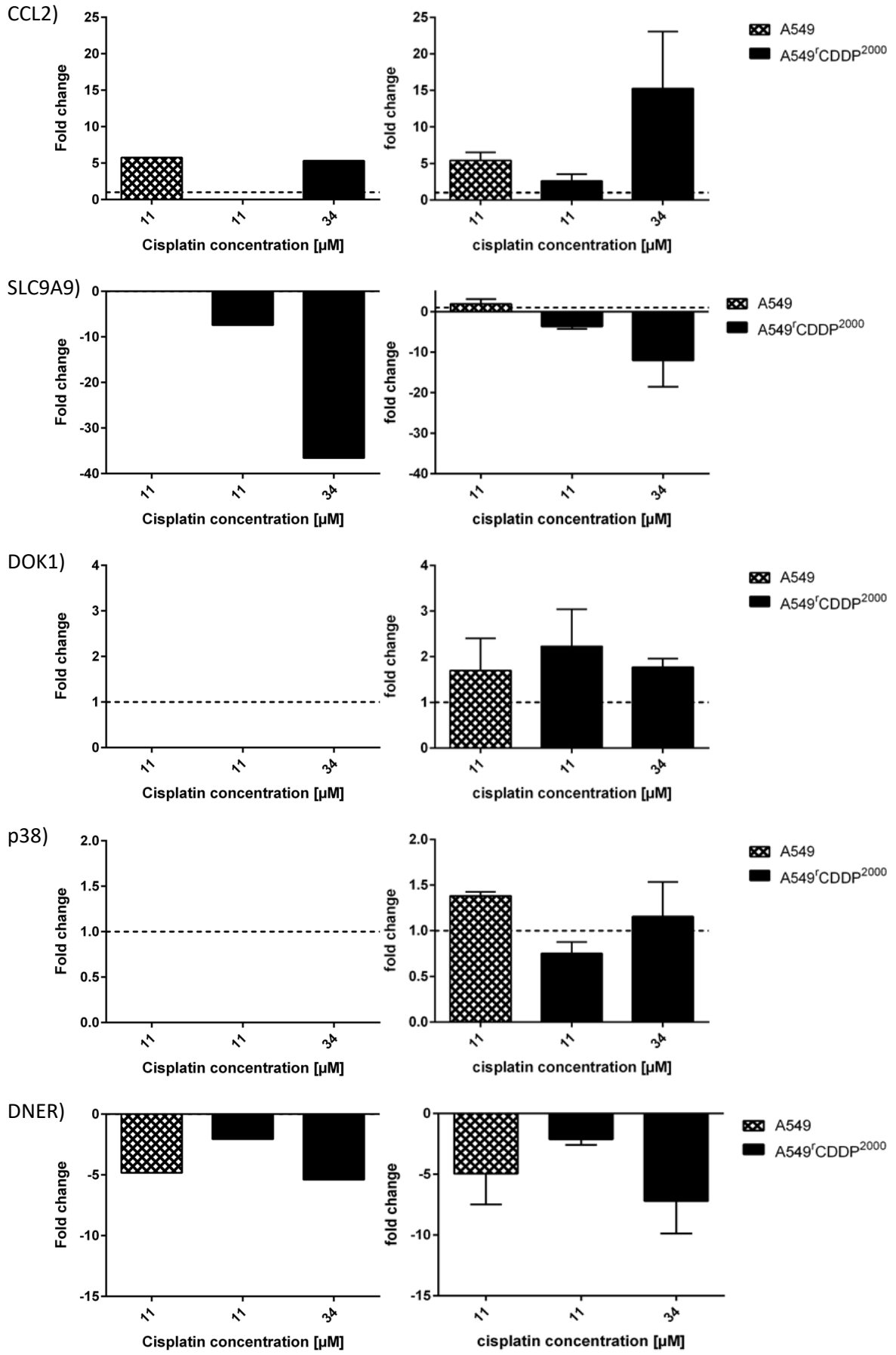

Figure 26 Comparison of array data, n = 3 (left) to PCR data, n = 3, presented as mean ± SEM (right); displayed as fold change with respect to untreated controls in A549 and A549^{r}CDDP^{2000} cells.

4.7.3 Identification of key players

Importantly, the four identified gene sets are not independent but share a number of differentially expressed genes (Figure 27). The numbers in the fields of the diagram indicate the number of genes which were found in the indicated pathway. The yellow sections indicate those overlapping genes which were found in at least two pathways and because of this were chosen for further analysis.

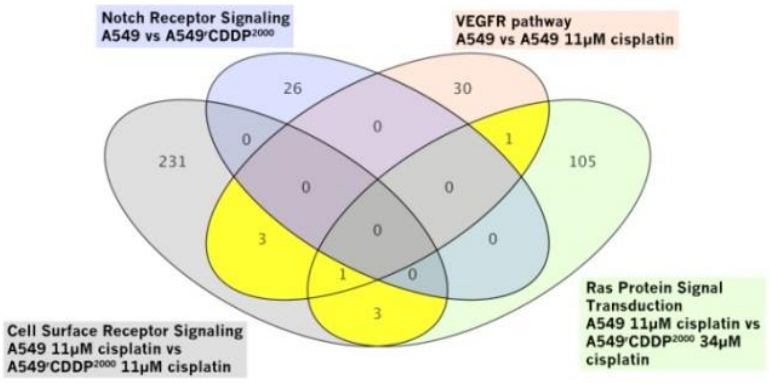

Figure 27 Venn diagram showing differentially expressed genes annotated with respective GO and KEGG terms: The yellow sections indicate those genes which were chosen for validation.

These shared genes comprise: HRas, p38, CCL2, DOK1, DOK2, PTK2B and a highly similar transcript variant, and MAPKAPK2. For further investigation, we decided to investigate only one isoform of DOK, DOK1, because of the high similarity between both forms. As MAPKAPK2 is directly associated downstream to p38 and directly regulated by p38, we decided to analyse only p38 as the superordinate mitogen-activated protein kinase (83–85). Both isoforms of PTK2B were not included in the validation because it was shown that they are mostly highly expressed in the central nervous system and in megakaryocytes (86, 87). Moreover, it appeared interesting to include JNK3 in further analysis as well, because HRas signalling reaches the nucleus via phosphorylation of JNK (88–90) and JNK3 was found to be differentially regulated on the microarray. This data-driven method thus identified the following five key players for further evaluation: HRas, JNK3, p38, CCL2 and DOK1.

4.8 Protein expression of identified key players in comparison to gene expression

After the whole-transcriptomic analysis, the identified genes were evaluated at the mRNA level by qPCR and at the protein level by Western blot analysis. Both, mRNA and protein levels are shown in Figure 28 to Figure 32 next to each other for a better comparison.

Expression at mRNA level of HRas, a member of the oncogenic Ras-family, was not altered after cisplatin exposure in both cell lines. In resistant cells, only a hint to an up-regulation after treatment with 34 µM cisplatin was observed (Figure 28A). At the protein level, the cisplatin-sensitive cells differed from resistant ones: Sensitive cells showed no changes, whereas resistant cells showed a significant ($p < 0.05$) reduction of protein content in fold change after treatment with 11 µM and 34 µM cisplatin relative to sensitive cells after cisplatin treatment (Figure 28B, see Appendix N). Presented as absolute data, this reduction in protein content is visible as well. However, in this case the difference is not significant.

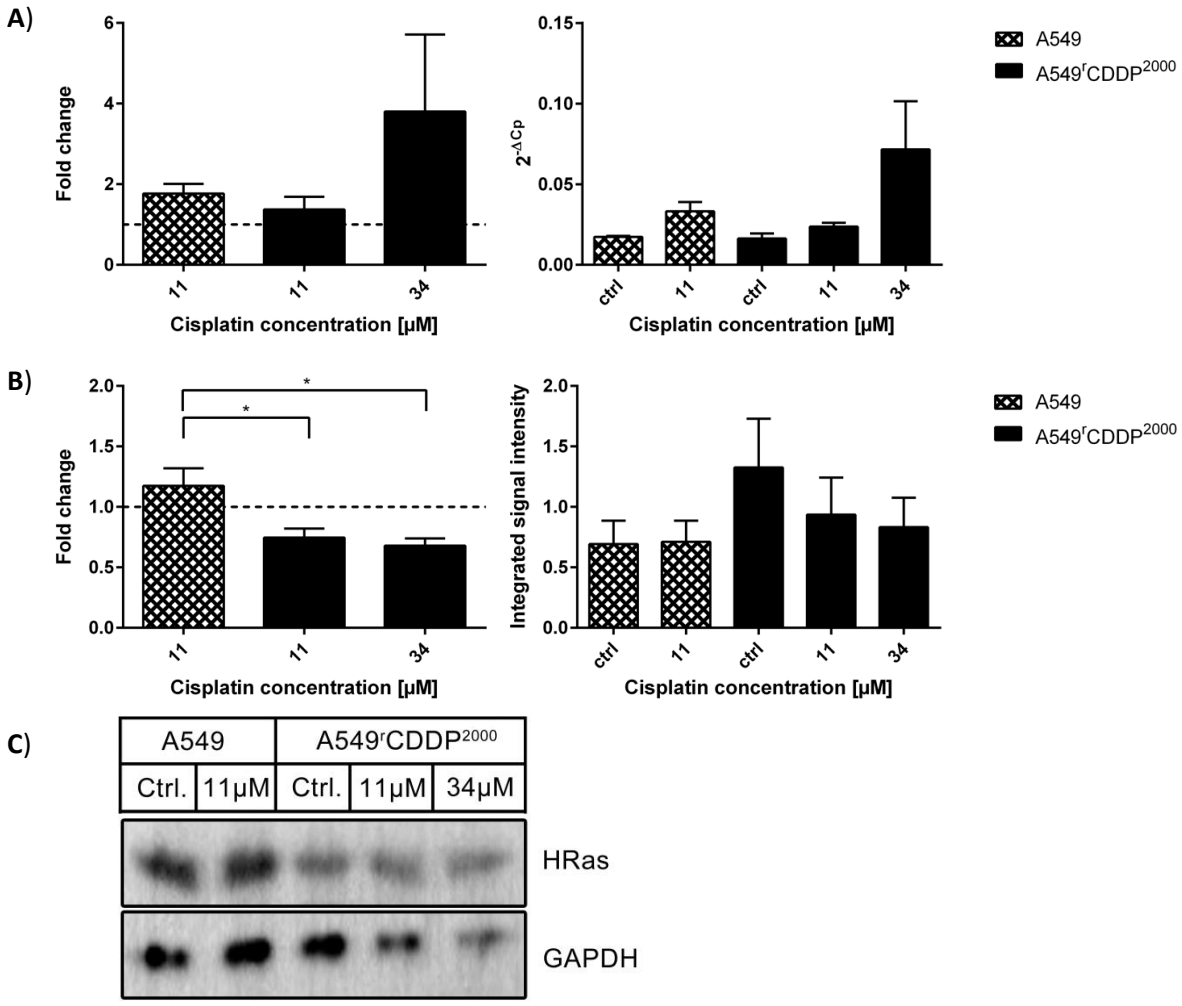

Figure 28 Analysis of **HRas** in **A**) RT-PCR (n = 3) as fold change related to untreated controls (ctrl) and absolute data, **B**) Western blot (n = 6) as fold change and integrated signal intensity, normalised to the housekeeper GAPDH in A549 and A549^{r}CDDP^{2000} cells, presented as mean ± SEM, **C**) one representative Western blot with A549 cells untreated, A549 cells treated with 11 µM cisplatin, A549^{r}CDDP^{2000} cells untreated, A549^{r}CDDP^{2000} cells treated with 11 µM cisplatin and A549^{r}CDDP^{2000} cells treated with 34 µM cisplatin.

JNK3, a protein kinase in context of apoptosis, which is directly connected to HRas (88), was down-regulated at the mRNA level upon all treatments. When cisplatin-resistant cells treated with high concentrations were compared to the low-concentration cisplatin treatment, the expression was significantly lower at the higher concentration. Moreover, this was also visible comparing the absolute data: JNK3 was significantly down-regulated at the protein level in the cisplatin-resistant cells treated with 34 µM cisplatin (Figure 29, see Appendix O). Remarkably, the basal mRNA level of JNK3 protein was significantly higher in untreated resistant cells than in the untreated sensitive ones. Differences at the mRNA level were not transferred to the protein level, where no changes were visible.

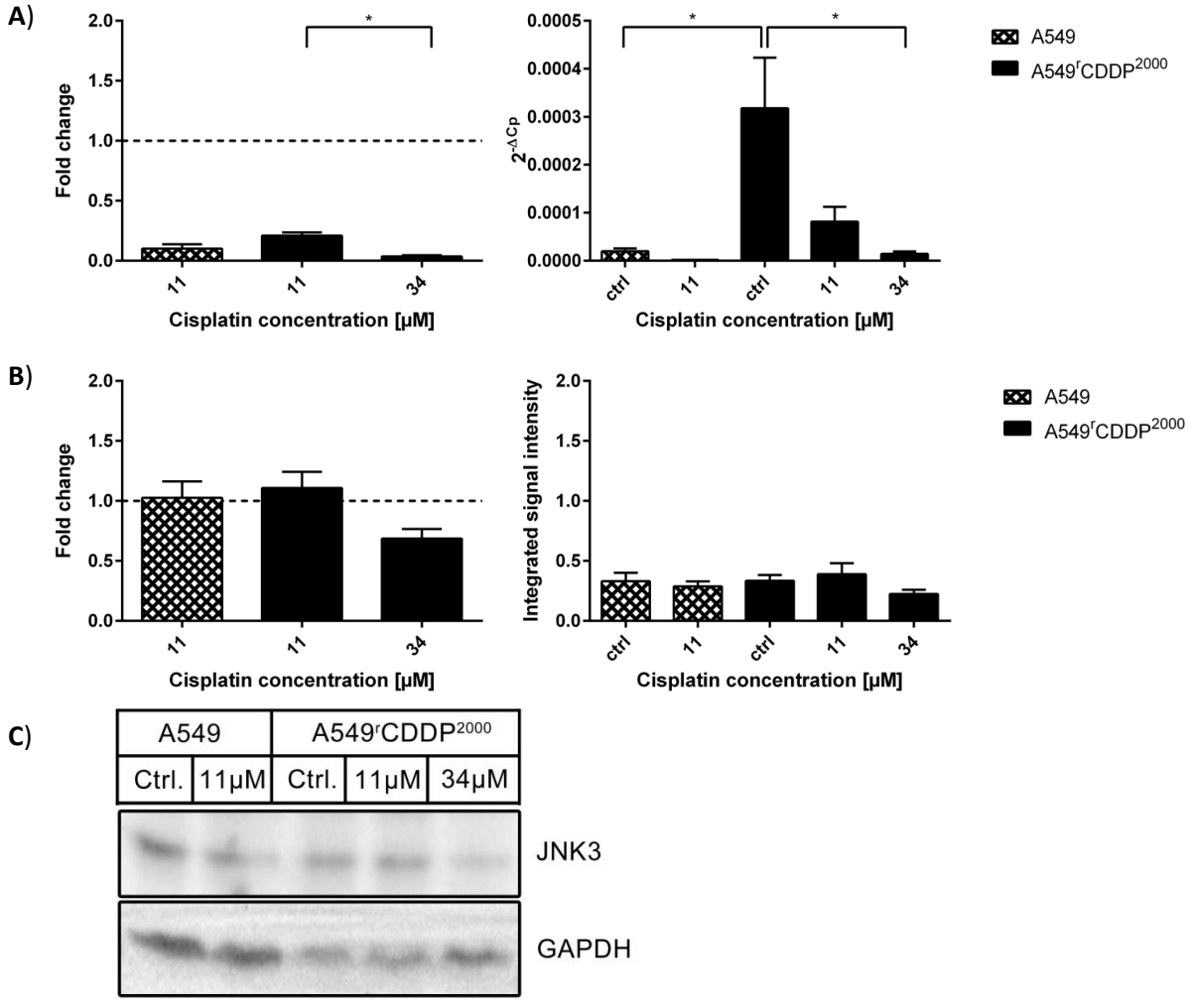

Figure 29 Analysis of **JNK3** in **A**) RT-PCR (n = 3) as fold change related to untreated controls (ctrl) and absolute data, **B**) Western blot (n = 9) as fold change and integrated signal intensity, normalised to the housekeeper GAPDH in A549 and A549^{r}CDDP^{2000} cells, presented as mean ± SEM, **C**) one representative Western blot with A549 cells untreated, A549 cells treated with 11 µM cisplatin, A549^{r}CDDP^{2000} cells untreated, A549^{r}CDDP^{2000} cells treated with 11 µM cisplatin and A549^{r}CDDP^{2000} cells treated with 34 µM cisplatin.

P38, a kinase involved in stress response and cell cycle alterations, was not differentially expressed at the mRNA level upon cisplatin treatment. Under equitoxic and equimolar treatment conditions in cisplatin-resistant cells, no up-regulation was observed (Figure 30A). Remarkably, the basal level of p38 protein was significantly higher in untreated resistant cells than in the untreated sensitive ones. No significant difference between treatments was found on protein level (Figure 30B, see Appendix P).

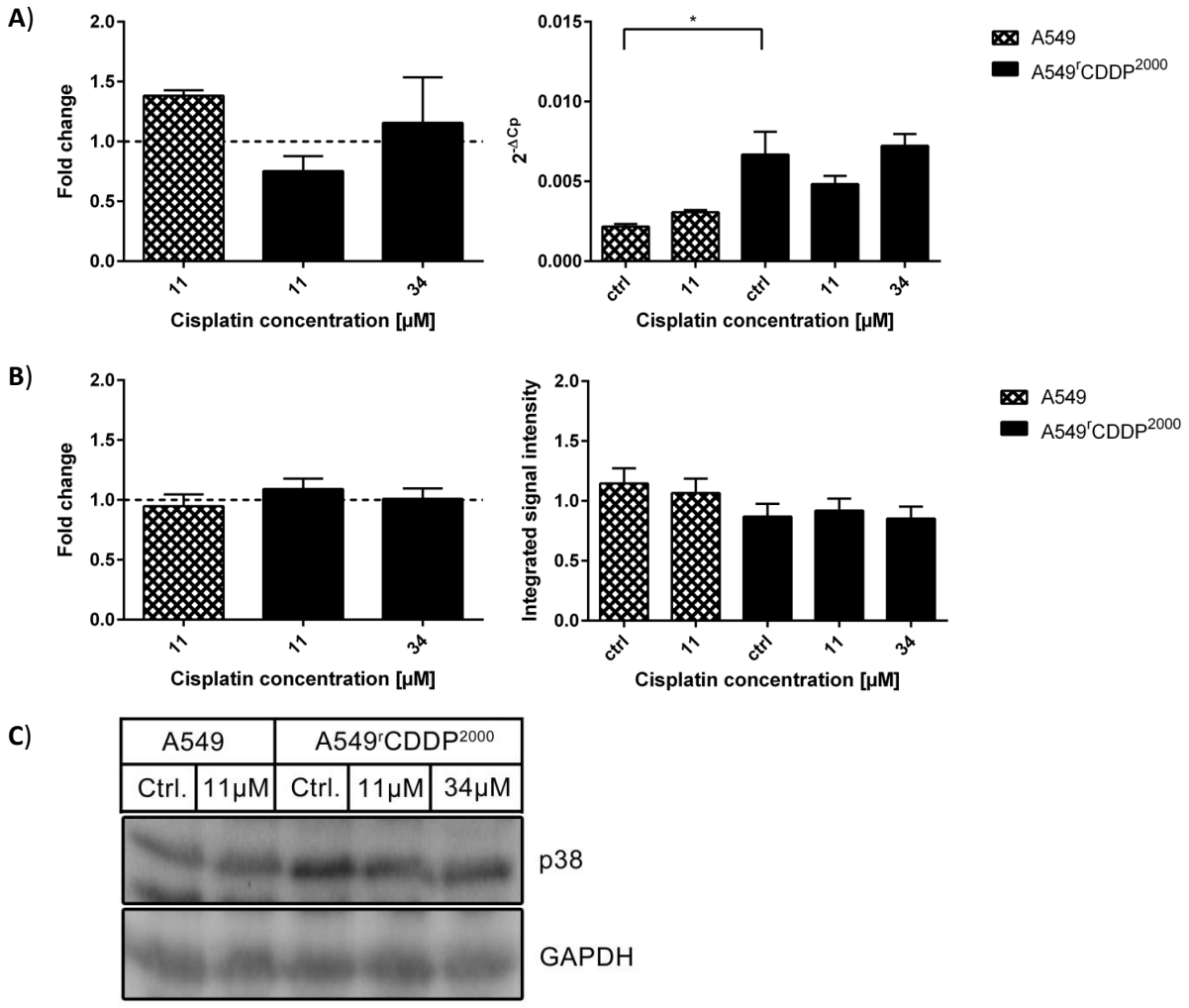

Figure 30 Analysis of **p38** in **A**) RT-PCR (n = 3) as fold change related to untreated controls (ctrl) and absolute data, **B**) Western blot (n = 6) as fold change and integrated signal intensity, normalised to the housekeeper GAPDH in A549 and A549^{r}CDDP^{2000} cells, presented as mean ± SEM, **C**) one representative Western blot with A549 cells untreated, A549 cells treated with 11 µM cisplatin, A549^{r}CDDP^{2000} cells untreated, A549^{r}CDDP^{2000} cells treated with 11 µM cisplatin and A549^{r}CDDP^{2000} cells treated with 34 µM cisplatin.

CCL2, a cytokine gene associated with invasion and metastasis, is connected to p38 (91, 92). No significant regulation either at mRNA or protein level could be observed in treated cells (Figure 31, see Appendix Q).

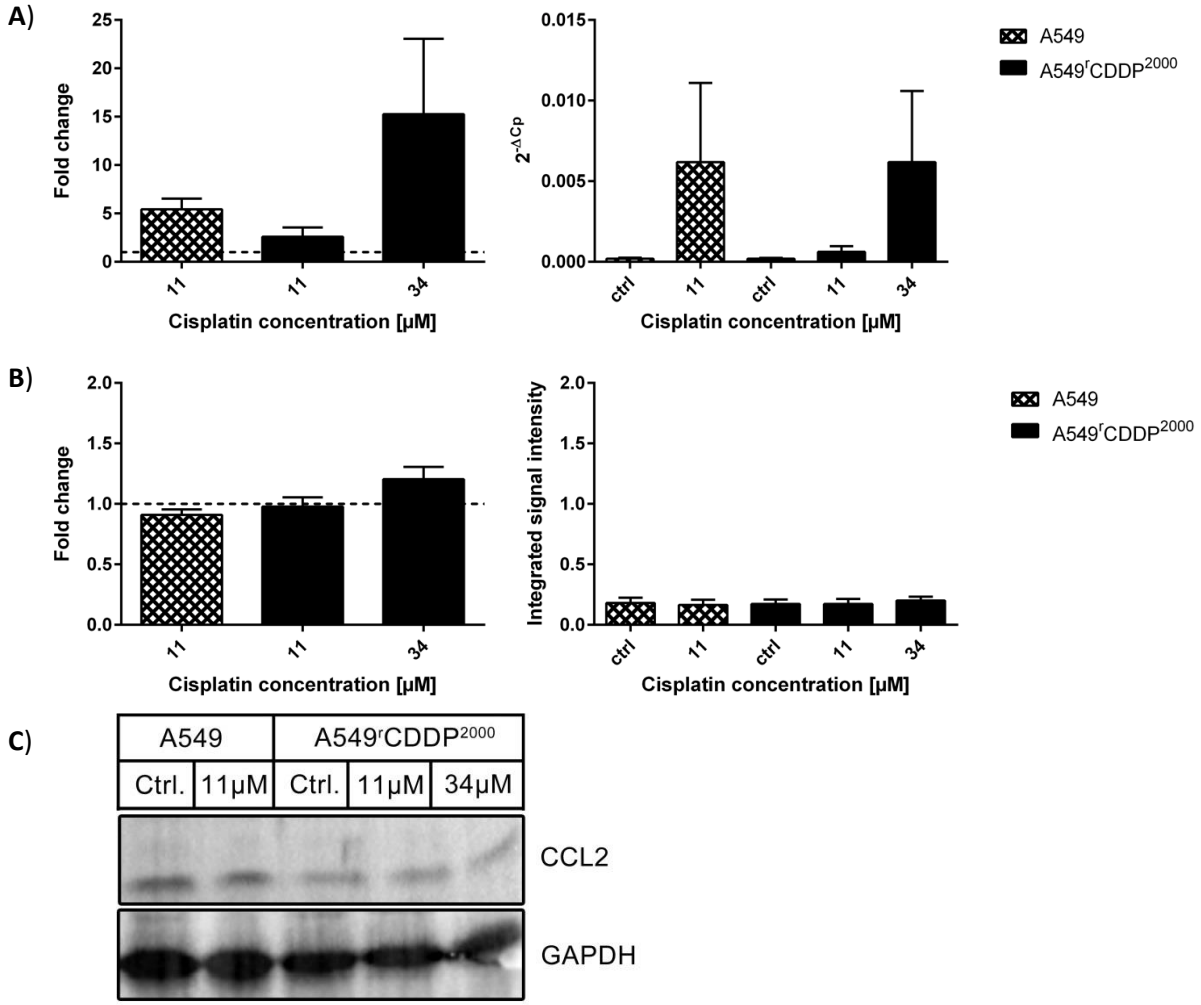

Figure 31 Analysis of **CCL2** in **A**) RT-PCR (n = 3) as fold change related to untreated controls (ctrl) and absolute data, **B**) Western blot (n = 4) as fold change and integrated signal intensity, normalised to the housekeeper GAPDH in A549 and A549^{r}CDDP^{2000} cells, presented as mean ± SEM, **C**) one representative Western blot with A549 cells untreated, A549 cells treated with 11 µM cisplatin, A549^{r}CDDP^{2000} cells untreated, A549^{r}CDDP^{2000} cells treated with 11 µM cisplatin and A549^{r}CDDP^{2000} cells treated with 34 µM cisplatin.

DOK1 is known as a tumour suppressor protein in epithelial ovarian cancer and negative regulator of tyrosine kinases in mitogen-activated kinase signalling (93). Several studies describe DOK1 as one of the upstream regulators of the Ras protein family (93, 94). Upon cisplatin treatment this candidate was regulated neither on mRNA nor on protein level in our study (Figure 32, see Appendix R).

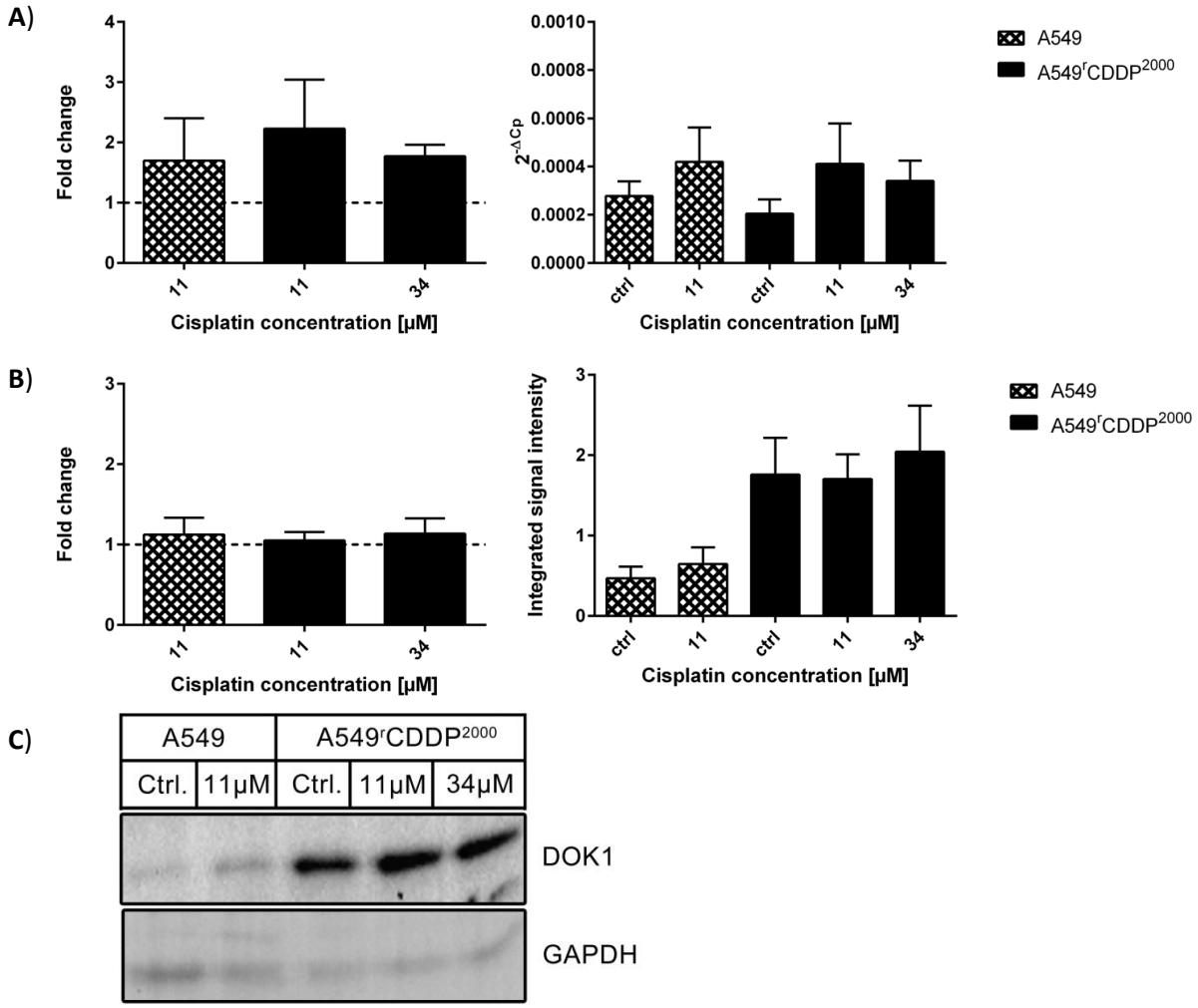

Figure 32 Analysis of **DOK1** in **A**) RT-PCR (n = 3) as fold change related to untreated controls and absolute data, **B**) Western blot (n ≤ 8) as fold change and integrated signal intensity, normalised to the housekeeper GAPDH in A549 and A549^{r}CDDP^{2000} cells, presented as mean ± SEM, **C**) one representative Western blot with A549 cells untreated, A549 cells treated with 11 µM cisplatin, A549^{r}CDDP^{2000} cells untreated, A549^{r}CDDP^{2000} cells treated with 11 µM cisplatin and A549^{r}CDDP^{2000} cells treated with 34 µM cisplatin.

4.9 Proposed model of resistance-associated signalling alterations

Cisplatin leads to DNA damage by forming DNA adducts. This toxic insult triggers cellular activation of several different pathways leading to survival or apoptosis, depending on the severity and extent of DNA damage. In chemoresistant cancer cells, these pathways are considered to be significantly dysregulated as one major mechanism of acquired resistance. Using the absolute data derived from the analysis of the DNA damage pathways and the data-driven approach based on the whole genome array, a preliminary model of resistance-associated signalling alteration is proposed to explain the observed differences in cell cycle analysis (Figure 33). Here significant differences among groups at the mRNA level are indicated in red and at the protein level in green. Differences resulting from 24 h treatment with cisplatin are indicated by coloured arrows, differences in basal levels between sensitive and resistant control cells are indicated by coloured forms in the background. Where the comparison of absolute data points between treated cells and control cells revealed a fold change > 2 and the error bars did not overlap, we included the propensity of a difference into the model, indicated with dotted arrows in the same colour scheme as mentioned before:

- P53 and pAtm showed significantly higher protein abundance in sensitive cells after cisplatin treatment (green arrows). Both additionally showed propensities for a concentration-dependent activation in resistant cells (green dotted arrows). P53 additionally had a higher basal mRNA level in resistant cells compared to sensitive ones (red background).
- MDM2 and P21 were equivalently activated at the mRNA level in both cells lines after cisplatin treatment (both indicated with red arrows).
- SIP activation was significantly increased at the mRNA level in sensitive cells after treatment (red arrows) and showed a higher basal protein level in resistant cells than in sensitive ones without treatment (green background).
- XPC only showed a propensity of a higher mRNA level in sensitive treated cells compared to the corresponding control. GADD45a showed this propensity in both cell lines after treatment with cisplatin (both indicated with red dotted arrows).

Two genes derived from the whole genome analysis, showing significant differences between both cell lines can be associated to the signalling connections proposed between the identified proteins from the DNA damage pathway.

- JNK3, a mitogen activated protein kinase involved in apoptosis (95–100) is downregulated at the mRNA level after cisplatin treatment in resistant cells (red arrows). There was only a propensity in the sensitive cells (red dotted arrow). JNK3 showed already a higher mRNA level in the untreated resistant cells compared to untreated sensitive cells (red background).

- P38, also a regulator of p53 (101–103), showed a significantly higher basal level in untreated cisplatin-resistant cells compared to untreated sensitive cells (red background).

CCL2, DOK1 and HRas were not included into the model, as the results did not reveal any significant differences following cisplatin treatment.

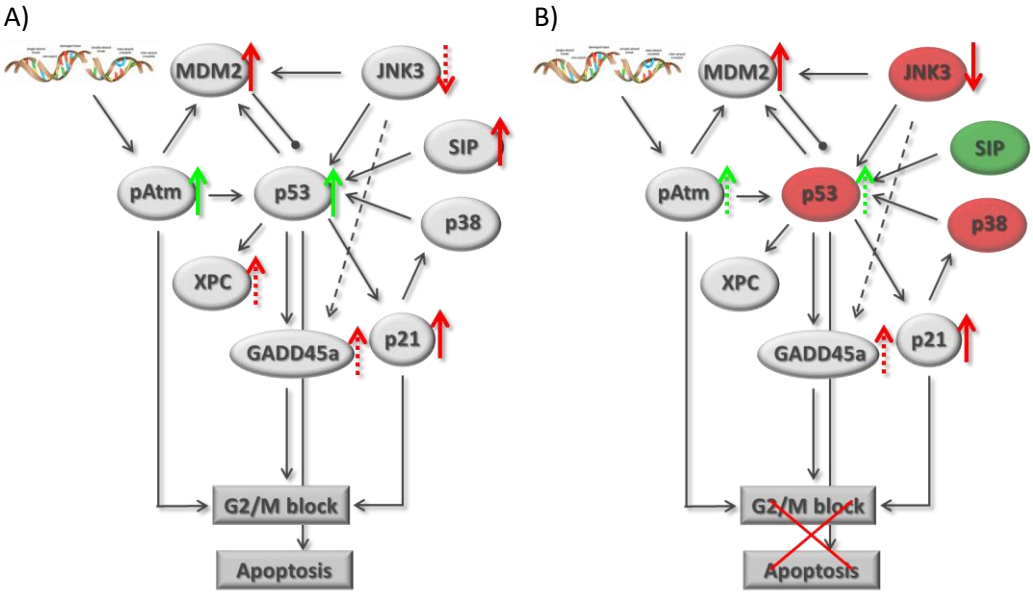

Figure 33 Model of resistance-associated signalling alterations compiling significant expression changes after cisplatin treatment in A) A549 and B) A549^{r}CDDP^{2000} cells based on mRNA data (red) or protein data (green). Significant changes after 24 h cisplatin treatment are indicated with arrows (→,→), significant differences of basal levels between the two cell lines are indicated with coloured forms in the background. Dotted arrows display propensities for differences in the same colour scheme.

5 Discussion

5.1 Systems pharmacology approach

This is our first step towards systems pharmacology, which connects several key players with each other, based on both transcriptome and proteome data. We think that a systems approach may be superior to address the problem of resistance to cisplatin. Contrary to approaches known from the literature, which mainly identify single proteins or a list of affected pathways (104–106) without displaying any functional connections, our approach establishes first steps depicting a part of the whole cell system. Additionally, we combined the analysis to the transcriptome and the protein level.

Galuzzi et al. studied the mRNA expression profile in cisplatin-sensitive cells without comparing them to the corresponding resistant ones and displaying a signalling network (107). They analysed the transcriptional changes after treatment with cisplatin in comparison to those after treatment with two known inducers of mitochondrial apoptosis, C2-ceramide and cadmium dichloride. They found, that cisplatin exerts apoptosis in a different way, through genes that are not induced in cell death signalling after treatment with C2-ceramide and cadmium dichloride. Among 19 transcriptional modulations, no overlap with our findings was found. The authors were also quite uncertain about the results, as unexpectedly little overlap was observed with 85 cisplatin response modifiers that the authors had previously reported in a siRNA screening (108). Zeng et al. compared the proteome between A549 and A549/CDDP cells and identified 12 cisplatin resistance-related proteins, without compiling the data in a network and discussing interactions (109). The identified proteins were different to our results, as the authors analysed the proteome level and we based our protein analysis on previously found differences at mRNA level. Here several factors like duration of treatment, other mechanisms of activation than translation may account for finding other candidates in our analysis. Yang et al. analysed the RNA expression profile of lung carcinoma cells and built up a signalling network between those specific RNAs but did not connect these data with protein expression in their cell system. Besides identifying a huge number of differentially expressed genes in A549 and A549/CDDP cells, the authors conclude that cisplatin resistance is also related to changes in non-coding RNAs. Interestingly, some of the 1471 identified mRNAs code for closely related proteins to those identified in our study, like CCL2 or several MAP-Kinases (110).

Consciously, we here follow a data-driven top-down approach, which involves iterative filtering of the massive amount of data of the whole genome microarray. This was done by statistical means without limiting the results by a predefined hypothesis. Here, the reduction was done by choosing those differentially expressed genes, which occur simultaneously in different GO and KEGG terms. This increased the a priori chance of these genes to play a major role in cisplatin-dependent response

of the cell. On the other hand, this way of reduction of genes could have led to the loss of relevant genes. The GO and KEGG terms, which were found by GSEA but not included into our study could be interesting for further analysis, as they may reveal completely new and unknown mechanisms of cell signalling alterations in response to cisplatin treatment.

5.2 Cell system

To elucidate the molecular mechanisms underlying acquired cisplatin resistance, we investigated the NSCLC cell line A549 and its cisplatin-resistant sub-line A549^{r}CDDP^{2000}. The resistant cells displayed a twofold higher EC_{50} value, reduced apoptosis, as well as alterations in intracellular platinum accumulation and DNA platination. The results displayed here are consistent with the two-fold lower sensitivity of resistant tumour cells to cisplatin in clinical studies for ovarian cancer (111) and the resistance in A549 cells measured by Yang et al. (112).

The EC_{10} concentrations used in the experiments were precautionary to prevent effects superimposing resistance mechanisms. Cisplatin concentrations used in our experiments were comparable to the clinically attainable concentrations. Milward et al. showed that patients treated with 75 – 100 mg/m^2 cisplatin in combination with docetaxel showed a C_{max} range from 8.1 µM to 28.9 µM total platinum (113). Tegeder et al. could determine cisplatin tumour concentration after intra-arterial administration as 37.6 ± 8.8 µmol/L (mean ± SEM, 11.3 ± 2.7 µg/mL) (114).

To compensate the effects of altered influx of cisplatin in resistant cells, equitoxic concentrations were studied showing similar Pt-DNA adduct formation but differences in drug accumulation. We previously demonstrated in other cell lines that reduced cisplatin accumulation may be one source of chemoresistance (115). At equimolar concentrations, platinum-DNA adduct formation was not significantly lower in A549^{r}CDDP^{2000} cells after 4 h treatment compared to sensitive cells and increased over time in A549 cells only. Equitoxic concentrations led to a subproportional increase of DNA-adduct levels in resistant cells compared to the intracellular platinum accumulation. After 24 h treatment with equitoxic concentrations, DNA adduct levels were similar in A549 and A549^{r}CDDP^{2000} cells suggesting that resistant cells exhibit a higher DNA-repair capacity than sensitive cells, as intracellular platinum accumulation was significantly higher in resistant cells. Other explanations for similar DNA-platination levels despite higher cellular platinum accumulation in A549^{r}CDDP^{2000} at equitoxic concentrations are increased sequestration in vesicles and an increased drug inactivation compared to the sensitive cells. Glutathione or for instance enzymes structurally similar to glutathione are known to act as detoxification agents for cisplatin (13, 27, 116–119).

5.3 DNA damage and repair

Although equitoxic cisplatin concentrations resulted in similar extent of DNA damage in sensitive and resistant cells, the cellular response showed significant differences. Apoptosis was only induced in sensitive cells pointing to an altered DNA-damage response in resistant cells. It was previously shown that resistant NSCLC cells have a higher repair capacity (120, 121). The impact of this phenomenon leading to resistance was documented in several studies. Chen et al. conducted a meta-analysis, where objective response or median survival were correlated with ERCC1 as a marker for DNA-repair capacity (27). The results showed that patients with high repair capacity featuring high expression of ERCC1 suffer from low median survival. The authors suggested ERCC1 expression as a marker for chemoresistance against cisplatin. Mountzios et al. drew a similar conclusion based on the observation that the benefit from cisplatin treatment was higher in patients with low expression of ERCC1 (122). Rosell et al. showed that NSCLC patients with a high DNA repair capacity had a poor survival after a combination treatment with cisplatin (123). This is in agreement with our results regarding phosphorylation of Atm, which is responsible for the recognition of DNA double-strand breaks, finally leading to a G_2/M arrest in sensitive cells. As expected, this protein shows nearly no activity in untreated control cells.

This DNA damage leads to activation of SIP which is a cofactor of p53. SIP is capable of modulating p53 activation and leads to the expression of antiproliferative and proapoptotic target genes of p53, like p21 (124, 125). This signalling pathway is activated by several different stress inducers in tumour cells (124, 126, 127). Activation of SIP by cisplatin promoting cell death was also shown in other cell lines (128). In line with this work SIP is activated after treatment for 24 h with cisplatin at the mRNA level in sensitive cells. Although showing higher basal SIP protein abundance, this mechanism seems to be blunted in resistant cells.

Furthermore, DNA damage tolerance may contribute to the cisplatin resistance of A549^{r}CDDP^{2000} cells. Cisplatin treatment significantly increased expression of XPC in fold change, a protein downstream of p53 and crucial for DNA damage recognition, in sensitive cells relative to resistant ones. This suggests higher activation of the global genome repair pathway and therefore a lower tolerance to cisplatin-DNA adducts in A549 cells. Beside its role in DNA damage recognition, XPC plays a major role in altering the cell cycle after treatment with cisplatin. In XPC-deficient cell lines, the p53 pathway is altered and cell cycle arrest, DNA repair and apoptosis are attenuated (129). XPC-deficient transgenic mice are highly predisposed to several types of cancer (130) and XPC/GADD45a knockout in mice leads to development of lung tumours (131). XPC expression is also reduced in the tumour tissue of resistant patients compared to normal lung tissue (132). Additionally, reduced XPC mRNA was suggested to predict a poor outcome for patients with NSCLC (133). Weaver et al. showed

that XPC correlates with chemoresistance in NSCLC (134). GADD45a, also enhancing NER (135), had a higher fold change in sensitive A549 cells after cisplatin treatment compared to XPC. This may support the hypothesis that the NER response is induced to a lower level in resistant cells. Overall, it can be seen that sensitive cells show stronger reactions in mRNA expression than resistant cells. They again seem to be more robust.

5.4 Cell cycle alterations

GADD45a is involved in cell cycle regulation and responsible for a G_2/M arrest to enhance DNA repair (136). If the reparation process is successful, the cell is able to survive; otherwise the cell is send into apoptosis. GADD45a may contribute to the G_2/M-phase cell cycle arrest in A549 cells in response to treatment with cisplatin. Fold change of GADD45a mRNA was significantly different in A549^{r}CDDP^{2000} cells treated with 11 µM cisplatin compared to sensitive cells after treatment. This could also be seen in the absolute data on mRNA level but, however, did not translate into a significant difference in GADD45a protein levels at the time point studied. Reduced expression of GADD45a has been associated with poor survival in oesophageal cancer patients (137). The cell cycle alterations are in agreement with previously published work (138), showing that tumour initiating cells are prone to less G_2/M-arrest after DNA-damaging treatment. Horibe et al. showed that cisplatin resistance is linked to loss of G_2/M-arrest in cisplatin-resistant cells (139). The p53 target gene product p21 that induces cell cycle arrest in G_2/M-phase was up-regulated in sensitive and resistant cells after treatment with cisplatin. Comparing the fold change to control, in sensitive and resistant cells treated with equitoxic cisplatin concentrations a higher expression of p21 was observed than in resistant cells treated with 11 µM cisplatin. This suggests a p53-mediated cell cycle arrest in sensitive cells that is less active in cisplatin-resistant cells. Activation of this mechanism needs higher concentrations in resistant cells. We assume that this adaptation to cisplatin treatment is part of the resistance phenotype in A549^{r}CDDP^{2000} cells.

MDM2 ubiquitinates p53 and regulates its activity and degradation in an autoregulatory feedback loop. MDM2 was significantly activated at the mRNA level in cisplatin-treated cells at equitoxic concentrations. The extent of activation in A549 cells was significantly higher in relation to A549^{r}CDDP^{2000} cells. At the protein level, no significant differences could be observed. One result of ubiquitination by MDM2 is destabilization of p53, diminishing the reservoir of p53 which could be easily and quickly activated if needed. This existing balance between MDM2 and ubiquitinated p53 would be disturbed if MDM2 protein levels are altered rapidly with high amplitudes, e.g. massive over-expression in short time. In consequence, a significant reduction of MDM2 would lead to an

overimposing activity of p53, which is physiologically unfavourable in resistant tumour cells. To avoid this, only moderate changes take place in this equilibrium. As MDM2 is also a downstream transcriptional target of p53 (140), p53 activation via phosphorylation, ubiquitination etc. may be altered in resistant cells. In the future, a closer look at the activation status of p53 after treatment with cisplatin should be taken, as this may be a key difference in p53 regulation influencing sensitivity against cisplatin.

5.5 Role of the identified key players

Cisplatin leads to DNA damage by forming Pt-DNA adducts. This toxic insult triggers activation of several different pathways for survival or apoptosis, depending on the extent of DNA damage. In chemoresistant cancer cells, these pathways are considered to be significantly dysregulated. HRas is one of the genes of the Ras oncogenic family and due to its prominent activity in the ERK1/2-pathway likely associated with cisplatin resistance. In contrast to our results, several studies revealed that HRas is activated by cisplatin treatment (79, 141, 142). Activating mutations of the Ras family in several cancer entities were held responsible for tumour development (141, 143–145). Reduced levels of HRas in our case could be responsible for the reduced levels of activated JNK. Several working groups showed that Ras signals, altering gene expression (e.g. fos- and jun- genes), reach the nucleus via phosphorylation of JNK (88–90). The observed reduced levels of JNK3 and potentially less phosphorylated JNK3 after treatment with equitoxic cisplatin concentrations could lead to reduced activation of p53 in the resistant cells. Fuchs et al. showed that JNK signalling is able to stabilise p53 by hindering MDM2 binding, increasing p53 activation and supporting p53-induced apoptosis (146). Additionally, JNKs appear to phosphorylate p53 at various sites after DNA damage (147). It is not really clear, why resistant cells show higher basal levels of JNK3 without any treatment. It was shown in mantle cell lymphoma that consecutive expression of JNK is required to promote proliferation (148). Alternatively, this could be an effect of the treatment with sub-toxic concentrations of cisplatin to maintain the resistant phenotype. In our case, this effect was abolished by cisplatin treatment for 24 h.

Another upstream effector of p53 is p38 which is not regulated at the mRNA level in both cells treated with cisplatin. Also in the Western blot experiments, no regulation under the different treatment conditions were seen in both cell lines. This result is in line with previously reported work, where no difference in expression of p38 protein was seen after cisplatin treatment (149–151). Remarkably, higher basal levels of p38 were observed in untreated resistant cells compared to untreated sensitive ones. This suggests that the longer lasting treatment with sub-toxic concentrations of cisplatin to maintain the resistance phenotype seems to have a greater effect on

p38 as the treatment with cisplatin for 24 h. This phenomenon in general is not uncommon in resistant cancer cells, where high levels of p38 were associated with poor prognosis (152). It seems that this difference at the mRNA level is not translated to the protein level at the time point measured in the conducted experiments. Future experiments should focus on phosphorylated p38, as activation could take place only by phosphorylation at the protein level. Activated p38 itself is capable of phosphorylating and activating p53 (153).

A previous study showed that expression of CCL2 in ovarian cancer cells seems to correlate with chemotherapy response and is reduced in cisplatin-resistant cells (154). Another study revealed that CCL2 expression rises after treatment with cisplatin (155). This effect was not observed in our cell line pair. Additionally, in contrast to our results, Ho et al. showed that the expression of CCL2 is induced by p38 (156). After treatment with equitoxic cisplatin concentrations, the results could suggest an increase of mRNA abundance in both cell lines. Due to the high variability of the results, significance was not reached.

According to the literature, DOK1 could play a role in response to cisplatin treatment as down-regulation of this protein increased cisplatin resistance in ovarian cancer cells (93). This could not be confirmed in our experiments, thus, the role of DOK1 remains unclear.

Following these results, proteins exhibiting significant differences (JNK3, p38) between both cell lines were included in our newly developed model. In contrast, those proteins where further evaluation is needed to explore their role in chemoresistance (CCL2, DOK1, HRas) were not included.

5.6 Proposed model of resistance-associated signalling alterations

Based on the results presented above we have developed a signalling model (Figure 33), which displays possible connections between the key players of cellular response to cisplatin exposure. We included knowledge-based evidence to draw the connections between our experimental results. This model reveals mechanisms accounting for a different reaction of the sensitive and resistant NSCLC cells to cisplatin treatment. It provides an overview of the possible roles of several cellular proteins; however, it represents only a very small part of the whole picture inside the cell. Results from mRNA level could not always be transferred to the protein level. This could be a matter of the time point of measurement. pAtm and p53 are activated after cisplatin exposure on protein level in sensitive cells, triggering G_2/M arrest. Activation at the mRNA level takes place at an earlier stage. P53 is now already capable of acting as a transcription factor to activate the other proteins in the signalling model. These are consequently activated at the mRNA level but possibly not yet at the protein level.

This lack of correlation between mRNA and protein data was discussed already in literature. A review from 2009 summarises several mechanisms possibly responsible for the quantitative differences of transcriptome and proteome: (1) post-transcriptional parameters, (2) post-translational parameters, and (3) noise and experimental error. It is still not clearly determinable to which extent biological factors, translation efficiency or protein half-life have impact on the mRNA levels (157). Half-life of proteins for example massively influences the correlation between mRNA and protein abundance as it may range between seconds and hours. An analysis in a space- and time- dependent manner could gain more insights and should be performed in the future. The model presented here is thus not comprehensive and can be extended by further players. Nevertheless, it serves as a good starting point for a systems pharmacology approach aiming at getting a full picture of protein interactions in the intracellular signalling network.

The greatest strength of the model is that the gene and protein alterations in the model are all based on experimental data. Within the model we displayed connections between the different candidates, which could serve as the origin for creating further hypotheses and for further investigations of the proteome. This could be limited by the fact that the model is so far not comprehensive and needs to be extended by further proteins, which could additionally account for the effects on cell cycle and apoptosis. In our study, we had to reduce the number of candidate genes and have so far not been able to process any distinct perturbations in the signalling network. This may be the focus of further projects based on these investigations.

In the future, our model should aim at depicting the whole proteome and transcriptome, allowing the description of the response of all relevant signalling pathways to cisplatin exposure. Thus, mathematical models could make it possible to forecast the effect of specific perturbations on the system, serving as a starting point for the development of novel therapeutic strategies.

6 Conclusions

The results of this work indicate clear differences between the response of cisplatin-resistant A549^{r}CDDP^{2000} and sensitive A549 cells to cisplatin treatment leading to the following conclusions:

- At equitoxic concentrations, cellular platinum accumulation was about 3-fold higher in A549^{r}CDDP^{2000} cells than in A549 cells. However, these increased intracellular cisplatin concentration did not result in enhanced cisplatin-DNA adduct formation. These data indicate that A549^{r}CDDP^{2000} cells acquired resistance mechanisms that reduce DNA-platination, e.g. by repair mechanisms, in comparison to A549 cells.

- A549^{r}CDDP^{2000} cells showed reduced apoptosis and a lack of G_2/M arrest compared to A549 cells. Different key candidates could be found to account for these differences:
    - p53 and pAtm play a major role in the induction of G_2/M arrest and apoptosis in A549 cells as they are significantly induced only in these cells at the protein level;
    - DNA damage recognition and signalling genes MDM2, XPC, SIP, p21 and GADD45a are induced by cisplatin at the mRNA level in sensitive cells to a higher extent as in resistant cells, where no or a reduced activation was observed;
    - JNK3 activation is reduced in resistant cells after cisplatin treatment compared to basal protein abundance which is significantly higher in untreated resistant cells compared to sensitive ones;
    - p38 only shows a higher basal mRNA level in resistant cells than in sensitive ones.

- The data-driven approach is appropriate to reduce the massive amount of data derived from a whole genome screening and to identify key candidates contributing to cisplatin resistance.

- In this work, the first step towards a systems pharmacology approach to cisplatin resistance has been taken and can be put forward in future experiments. A model has been built up describing resistance-associated signalling alterations in both cell lines. This model helps to comprehend how differences in gene and protein expression influence the G_2/M arrest and apoptosis and contribute to cisplatin resistance.

7 Outlook

The results of this thesis indicate that several key players are likely to be involved in cisplatin resistance in NSCLC cells at the transcriptome and proteome level, influencing apoptosis and cell cycle control. In future experiments, the analysis of the whole genome array should aim to include more involved players at the transcriptome level. Here, other overlaps of the identified GO terms or genes belonging to other GO terms should be evaluated more closely. Furthermore, connections between the identified players could be analysed in detail using targeted perturbations of our network. For this purpose, inhibitors of individual proteins or their knockdown would reveal their contribution to the whole network and its influence on other genes or proteins, respectively. In this piece of work, the cell lines were analysed at a defined time point. Additional work would be needed to characterise the kinetics of alterations in gene or protein expression in the network. Some changes in reaction to cisplatin, e.g. in the transcriptome, occur earlier than others, e.g. in the metabolome. Here, the focus at the vertical level (e.g. genome, transcriptome or proteome) in the systematic approach should be considered in defining the perfect time point for the experiments. Other aspects of resistance development could be revealed by investigating different stages during the development of the cisplatin-resistant cell line. Here, the analysis should be executed at every stage during the adaption of the parental cell line to cisplatin. Another focus could be placed at the protein level, where not only translation leads to active proteins but also phosphorylation activates several players. The analysis of the activation status could shed light on the mechanisms of resistance. In order to follow the systems pharmacology path, other levels of the cell physiology could be added on top of the defined model.

8 Summary

The efficacy of cisplatin-based chemotherapy in cancer is limited by the occurrence of innate and acquired drug resistance. In order to better understand the mechanisms underlying acquired cisplatin resistance, the adenocarcinoma-derived non-small cell lung cancer (NSCLC) cell line A549 and its cisplatin-resistant sub-line A549^{r}CDDP^{2000} were compared with regard to cellular platinum accumulation, DNA-adduct formation, cell cycle alterations, apoptosis induction and activation of key players of DNA-damage response.

In A549^{r}CDDP^{2000} cells, the cisplatin-induced G_2/M cell cycle arrest was lacking and apoptosis was significantly reduced compared to A549 cells, although equitoxic cisplatin concentrations resulted in comparable platinum-DNA adduct levels. These differences were accompanied by changes in the expression of proteins involved in DNA-damage response. In A549 cells, equimolar cisplatin exposure induced the expression of genes coding for proteins mediating G_2/M arrest and apoptosis (MDM2, p21, XPC, SIP and GADD45a) to a higher extent as in resistant cells. This was underlined by significantly higher protein levels of pAtm and p53 in A549 cells after cisplatin treatment compared to the respective untreated controls.

Additionally, a data-driven method was used to identify further key candidates responsible for the different response of the two cell lines to the drug. The cellular transcriptome was screened for relevant gene candidates using a whole genome array. By combining statistical methods with available gene annotation without previously defined hypothesis, HRas, JNK3, p38, CCL2 and DOK1 were identified as genes relevant for cisplatin resistance. These genes were further analysed at the transcriptome and proteome level to introduce a more systematic approach on different stages of cell signalling. Upon cisplatin exposure, JNK3 showed a lower mRNA expression only in A549^{r}CDDP^{2000} cells. In addition to these effects, p53, JNK3 and p38 showed higher basal mRNA abundance in resistant cells compared to the sensitive cells. This circumstance was also observed with SIP at the protein level and suggests a relevant long-lasting effect caused during the development of resistance. All results were compiled in a preliminary model of resistance-associated signalling alterations.

In conclusion, these findings suggest that acquired resistance of NSCLC cells against cisplatin is a consequence of altered signalling of the identified proteins leading to reduced G_2/M cell cycle arrest and apoptosis.

9 Literature

1. Robert Koch Institut. Lungenkrebs (Bronchialkarzinom): ICD-10 C33–34; 2015 [cited 2015 Jul 29]. Available from: http://www.krebsdaten.de/.

2. Krebs in Deutschland 2009/2010: Lunge; 2013 [cited 2015 Jul 29]. Available from: http://www.rki.de/.

3. Lungenkarzinom, nicht-kleinzellig (NSCLC); 2015 [cited 2015 Jul 29]. Available from: https://www.onkopedia.com/de/.

4. Buß I. Cellular Influx and Cytotoxicity of Oxaliplatin Analogues [Dissertation]. Bonn: Rheinische Friedrich-Wilhelms-Universität; 2010.

5. Kauffman GB, Pentimalli R, Doldi S, Hall MD. Michele Peyrone (1813-1883), Discoverer of Cisplatin. Platin Met Rev 2010; 54:250–6.

6. Rosenberg B, van Camp L, Krigas T. Inhibition of Cell Division in Escherichia coli by Electrolysis Products from a Platinum Electrode. Nature 1965; 205:698–9.

7. Rosenberg B, van Camp L, Trosko JE, Mansour VH. Platinum Compounds. Nature 1969; 222:385–6.

8. Ho AWY, Wong CK, Lam CWK. Tumor necrosis factor-alpha up-regulates the expression of CCL2 and adhesion molecules of human proximal tubular epithelial cells through MAPK signaling pathways. Immunobiology 2008; 213:533–44.

9. Graham J, Mushin M, Kirkpatrick P. Oxaliplatin. Nat Rev Drug Discov 2004; 3:11–2.

10. Kelland L. The resurgence of platinum-based cancer chemotherapy. Nat Rev Cancer 2007; 7:573–84.

11. Raymond E, Faivre S, Woynarowski JM, Chaney SG. Oxaliplatin: mechanism of action and antineoplastic activity. Semin Oncol 1998; 25:4–12.

12. Rabik CA, Dolan ME. Molecular mechanisms of resistance and toxicity associated with platinating agents. Cancer Treat Rev 2007; 33:9–23.

13. Galluzzi L, Senovilla L, Vitale I, Michels J, Martins I, Kepp O et al. Molecular mechanisms of cisplatin resistance. Oncogene 2012; 31:1869–83.

14. Kelland LR. New platinum antitumor complexes. Crit Rev Oncol Hematol 1993; 15:191–219.

15. Siddik ZH. Cisplatin: mode of cytotoxic action and molecular basis of resistance. Oncogene 2003; 22:7265–79.

16. Mohn C. Relevance of glutathione and MRP-mediated efflux for platinum resistance [Dissertation]. Bonn: Rheinische Friedrich-Wilhelms-Universität; 2013.

17. Kunkel TA, Erie DA. DNA mismatch repair. Annu Rev Biochem 2005; 74:681–710.

18. Crul M, Schellens J, Beijnen JH, Maliepaard M. Cisplatin resistance and DNA repair. Cancer Treat Rev 1997; 23:341–66.

19. Martin LP, Hamilton TC, Schilder RJ. Platinum resistance: the role of DNA repair pathways. Clin Cancer Res 2008; 14:1291–5.

20. Rosell R. Nucleotide excision repair pathways involved in Cisplatin resistance in non-small-cell lung cancer. Cancer Control 2003; 10:297.

21. Kandoth C, McLellan MD, Vandin F, Ye K, Niu B, Lu C et al. Mutational landscape and significance across 12 major cancer types. Nature 2013; 502:333–9.

22. Joerger AC, Fersht AR. Structural biology of the tumor suppressor p53. Annu Rev Biochem 2008; 77:557–82.

23. Di Stefano V, Soddu S, Sacchi A, D'Orazi G. HIPK2 contributes to PCAF-mediated p53 acetylation and selective transactivation of p21Waf1 after nonapoptotic DNA damage. Oncogene 2005; 24:5431–42.

24. Toledo F, Wahl GM. Regulating the p53 pathway: in vitro hypotheses, in vivo veritas. Nat Rev Cancer 2006; 6:909–23.

25. Galluzzi L, Vitale I, Michels J, Brenner C, Szabadkai G, Harel-Bellan A et al. Systems biology of cisplatin resistance: past, present and future. Cell Death Dis 2014; 5:e1257.

26. Olaussen KA, Dunant A, Fouret P, Brambilla E, André F, Haddad V et al. DNA repair by ERCC1 in non-small-cell lung cancer and cisplatin-based adjuvant chemotherapy. N Engl J Med 2006; 355:983–91.

27. Chen S, Zhang J, Wang R, Luo X, Chen H. The platinum-based treatments for advanced non-small cell lung cancer, is low/negative ERCC1 expression better than high/positive ERCC1 expression? A meta-analysis. Lung Cancer 2010; 70:63–70.

28. Vaisman A, Varchenko M, Umar A, Kunkel TA, Risinger JI, Barrett JC et al. The Role of hMLH1, hMSH3, and hMSH6 Defects in Cisplatin and Oxaliplatin Resistance: Correlation with Replicative Bypass of Platinum-DNA Adducts. Cancer Res 1998; 58:3579–85.

29. Bassett E, Vaisman A, Tropea KA, McCall CM, Masutani C, Hanaoka F et al. Frameshifts and deletions during in vitro translesion synthesis past Pt–DNA adducts by DNA polymerases β and η. DNA Repair 2002; 1:1003–16.

30. Shachar S, Ziv O, Avkin S, Adar S, Wittschieben J, Reissner T et al. Two-polymerase mechanisms dictate error-free and error-prone translesion DNA synthesis in mammals. EMBO J 2009; 28:383–93.

31. Wittschieben JP, Reshmi SC, Gollin SM, Wood RD. Loss of DNA polymerase zeta causes chromosomal instability in mammalian cells. Cancer Res 2006; 66:134–42.

32. Sakai W, Swisher EM, Karlan BY, Agarwal MK, Higgins J, Friedman C et al. Secondary mutations as a mechanism of cisplatin resistance in BRCA2-mutated cancers. Nature 2008; 451:1116–20.

33. Kirsch DG, Kastan MB. Tumor-suppressor p53: implications for tumor development and prognosis. JCO 1998; 16:3158–68.

34. Feldman DR, Bosl GJ, Sheinfeld J, Motzer RJ. Medical treatment of advanced testicular cancer. JAMA 2008; 299:672–84.

35. Millau J, Bastien N, Drouin R. P53 transcriptional activities: a general overview and some thoughts. Mutat Res 2009; 681:118–33.

36. Stewart DJ. Mechanisms of resistance to cisplatin and carboplatin. Crit Rev Oncol Hematol 2007; 63:12–31.

37. Fijolek J, Wiatr E, Rowinska-Zakrzewska E, Giedronowicz D, Langfort R, Chabowski M et al. p53 and HER2/neu expression in relation to chemotherapy response in patients with non-small cell lung cancer. Int J Biol Markers 2006; 21:81–7.

38. Kroemer G, Marino G, Levine B. Autophagy and the integrated stress response. Mol Cell 2010; 40:280–93.

39. Macleod K, Mullen P, Sewell J, Rabiasz G, Lawrie S, Miller E et al. Altered ErbB receptor signaling and gene expression in cisplatin-resistant ovarian cancer. Cancer Res 2005; 65:6789–800.

40. Berger SI, Ma'ayan A, Iyengar R. Systems pharmacology of arrhythmias. Sci Signal 2010; 3:ra30.

41. Van Der Graaf, Piet H, Gabrielsson J. Pharmacokinetic-pharmacodynamic reasoning in drug discovery and early development. Future Med Chem 2009; 1:1371–4.

42. Sorger PK, Allerheiligen SR. An NIH White Paper by the QSP Workshop Group. Quantitative and Systems Pharmacology in the Post-genomic Era: New Approaches to Discovering Drugs and Understanding Therapeutic Mechanisms 2011.

43. Wist AD, Berger SI, Iyengar R. Systems pharmacology and genome medicine: a future perspective. Genome Med 2009; 1:11.

44. Giard DJ, Aaronson SA, Todaro GJ, Arnstein P, Kersey JH, Dosik H et al. In Vitro Cultivation of Human Tumors: Establishment of Cell Lines Derived From a Series of Solid Tumors. J Natl Cancer Inst 1973; 51:1417–23.

45. Michaelis M, Rothweiler F, Barth S, Cinatl J, van Rikxoort M, Löschmann N et al. Adaptation of cancer cells from different entities to the MDM2 inhibitor nutlin-3 results in the emergence of p53-mutated multi-drug-resistant cancer cells. Cell Death Dis 2011; 2:e243.

46. A549 (ATCC® CCL-185™); 2014 [cited 2015 Jul 29]. Available from: http://www.lgcstandards-atcc.org/.

47. Alley MC, Scudiero DA, Monks A, Hursey ML, Czerwinski MJ, Fine DL et al. Feasibility of Drug Screening with Panels of Human Tumor Cell Lines Using a Microculture Tetrazolium Assay. Cancer Res 1988; 48:589–601.

48. Mueller H, Kassack MU, Wiese M. Comparison of the usefulness of the MTT, ATP, and calcein assays to predict the potency of cytotoxic agents in various human cancer cell lines. J Biomol Screen 2004; 9:506–15.

49. Motulsky H, Christopoulos A. Fitting models to biological data using linear and nonlinear regression: A practical guide to curve fitting. Oxford: Oxford Univ. Press; 2004.

50. Merck KGaA. User Protocol: BCA Protein Assay Kit (Novagen®); 2009.

51. Garmann D. Reaktivität und zelluläre Aufnahme albuminbindender Platinkomplexe und neuer Oxaliplatin-Analoga [Dissertation]. Bonn: Rheinische Friedrich-Wilhelms-Universität; 2007.

52. Kloft C, Appelius H, Siegert W, Schunack W, Jaehde U. Determination of platinum complexes in clinical samples by a rapid flameless atomic absorption spectrometry assay. Ther Drug Monit 1999; 21:631–7.

53. Pieck AC. Pharmakokinetik und Platin-DNA-Adduktbildung von Oxaliplatin [Dissertation]. Bonn: Rheinische Friedrich-Wilhelms-Universität; 2004.

54. Agilent Technologies. One-Color Microarray-Based Gene Expression Analysis: Low Input Quick Amp Labeling [Version 6.9.1]; 2015 [cited 2016 Dec 31]. Available from: http://www.agilent.com/.

55. Vogel C, Donat S, Döhr O, Kremer J, Esser C, Roller M et al. Effect of subchronic 2,3,7,8-tetrachlorodibenzo- p -dioxin exposure on immune system and target gene responses in mice. Arch Toxicol 1997; 71:372–82.

56. Schmittgen TD, Livak KJ. Analyzing real-time PCR data by the comparative CT method. Nat Protoc 2008; 3:1101–8.

57. Pfaffl MW. Real-time RT-PCR: Neue Ansätze zur exakten mRNA Quantifizierung. BIOspektrum 2004; 1:92–5.

58. Laemmli UK. Cleavage of Structural Proteins during the Assembly of the Head of Bacteriophage T4. Nature 1970; 227:680–5.

59. Smyth GK. Linear models and empirical bayes methods for assessing differential expression in microarray experiments. Stat Appl Genet Mol Biol 2004; 3:Article3.

60. Wang X, Terfve C, Rose JC, Markowetz F. HTSanalyzeR: an R/Bioconductor package for integrated network analysis of high-throughput screens. Bioinformatics 2011; 27:879–80.

61. Kanehisa M, Araki M, Goto S, Hattori M, Hirakawa M, Itoh M et al. KEGG for linking genomes to life and the environment. Nucleic Acids Res 2008; 36:D480-4.

62. Subramanian A, Tamayo P, Mootha VK, Mukherjee S, Ebert BL, Gillette MA et al. Gene set enrichment analysis: a knowledge-based approach for interpreting genome-wide expression profiles. Proc Natl Acad Sci USA 2005; 102:15545–50.

63. Harris MA, Clark J, Ireland A, Lomax J, Ashburner M, Foulger R et al. The Gene Ontology (GO) database and informatics resource. Nucleic Acids Res 2004; 32:D258-61.

64. Bolstad BM, Irizarry R, Astrand M, Speed TP. A comparison of normalization methods for high density oligonucleotide array data based on variance and bias. Bioinformatics 2003; 19:185–93.

65. Ritchie ME, Silver J, Oshlack A, Holmes M, Diyagama D, Holloway A et al. A comparison of background correction methods for two-colour microarrays. Bioinformatics 2007; 23:2700–7.

66. Goeman JJ, van de Geer, S. A., Kort F de, van Houwelingen HC. A global test for groups of genes. Bioinformatics 2004; 20:93–9.

67. Oren M. Regulation of the p53 Tumor Suppressor Protein. J Biol Chem 1999; 274:36031–4.

68. Liu J, Mao Z, Huang J, Xie S, Liu T, Mao Z. Blocking the NOTCH pathway can inhibit the growth of CD133-positive A549 cells and sensitize to chemotherapy. Biochem Biophys Res Commun 2014; 444:670–5.

69. McAuliffe SM, Morgan SL, Wyant GA, Tran LT, Muto KW, Chen YS et al. Targeting Notch, a key pathway for ovarian cancer stem cells, sensitizes tumors to platinum therapy. Proc Natl Acad Sci USA 2012; 109:E2939-48.

70. Aktaş S, Zadeoğlulari Z, Erçetin P, Olgun N. The effect of differentiating and apoptotic agents on notch signalling pathway in hepatoblastoma. Hepatogastroenterology 2010; 57:891–8.

71. Daenen LGM, Roodhart JML, van Amersfoort M, Dehnad M, Roessingh W, Ulfman LH et al. Chemotherapy enhances metastasis formation via VEGFR-1-expressing endothelial cells. Cancer Res 2011; 71:6976–85.

72. Sini P, Samarzija I, Baffert F, Littlewood-Evans A, Schnell C, Theuer A et al. Inhibition of multiple vascular endothelial growth factor receptors (VEGFR) blocks lymph node metastases but inhibition of

VEGFR-2 is sufficient to sensitize tumor cells to platinum-based chemotherapeutics. Cancer Res 2008; 68:1581–92.

73. Rho JK, Choi YJ, Choi YR, Kim SY, Choi SJ, Choi C et al. The Effect of Acquired Cisplatin Resistance on Sensitivity to EGFR Tyrosine Kinase Inhibitors in EGFR Mutant Lung Cancer Cells. Oncol Res 2011; 19:471–8.

74. Granados ML, Hudson LG, Samudio-Ruiz SL. Contributions of the Epidermal Growth Factor Receptor to Acquisition of Platinum Resistance in Ovarian Cancer Cells. PLoS ONE 2015; 10:e0136893.

75. Zhang P, Gao WY, Turner S, Ducatman BS. Gleevec (STI-571) inhibits lung cancer cell growth (A549) and potentiates the cisplatin effect in vitro. Mol Cancer 2003; 2:1.

76. Zhu H, Yun F, Shi X, Wang D. Inhibition of IGFBP-2 improves the sensitivity of bladder cancer cells to cisplatin via upregulating the expression of maspin. Int J Mol Med 2015; 36:595–601.

77. Tian Z, Yao G, Song H, Zhou Y, Geng J. IGF2R expression is associated with the chemotherapy response and prognosis of patients with advanced NSCLC. Cell Physiol Biochem 2014; 34:1578–88.

78. Juliachs M, Muñoz C, Moutinho CA, Vidal A, Condom E, Esteller M et al. The PDGFRβ-AKT pathway contributes to CDDP-acquired resistance in testicular germ cell tumors. Clin Cancer Res 2014; 20:658–67.

79. Woessmann W, Chen X, Borkhardt A. Ras-mediated activation of ERK by cisplatin induces cell death independently of p53 in osteosarcoma and neuroblastoma cell lines. Cancer Chemother Pharmacol 2002; 50:397–404.

80. Yang L, Zhou Y, Li Y, Zhou J, Wu Y, Cui Y et al. Mutations of p53 and KRAS activate NF-κB to promote chemoresistance and tumorigenesis via dysregulation of cell cycle and suppression of apoptosis in lung cancer cells. Cancer Lett 2015; 357:520–6.

81. Tao S, Wang S, Moghaddam SJ, Ooi A, Chapman E, Wong PK et al. Oncogenic KRAS confers chemoresistance by upregulating NRF2. Cancer Res 2014; 74:7430–41.

82. Yamamoto T, Tsigelny IF, Götz AW, Howell SB. Cisplatin inhibits MEK1/2. Oncotarget 2015; 6:23510-22.

83. Rane MJ, Coxon PY, Powell DW, Webster R, Klein JB, Pierce W et al. p38 Kinase-dependent MAPKAPK-2 activation functions as 3-phosphoinositide-dependent kinase-2 for Akt in human neutrophils. J Biol Chem 2001; 276:3517–23.

84. Cuenda A, Rousseau S. p38 MAP-kinases pathway regulation, function and role in human diseases. Biochim Biophys Acta 2007; 1773:1358–75.

85. Ben-Levy R, Hooper S, Wilson R, Paterson HF, Marshall CJ. Nuclear export of the stress-activated protein kinase p38 mediated by its substrate MAPKAP kinase-2. Curr Biol 1998; 8:1049–57.

86. Avraham H. Tyrosine Phosphorylation of the Related Adhesion Focal Tyrosine Kinase in Megakaryocytes upon Stem Cell Factor and Phorbol Myristate Acetate Stimulation and Its Association with Paxillin. J Biol Chem 1997; 272:10804–10.

87. Hiregowdara D, Avraham H, Fu Y, London R, Avraham S. Tyrosine phosphorylation of the related adhesion focal tyrosine kinase in megakaryocytes upon stem cell factor and phorbol myristate acetate stimulation and its association with paxillin. J Biol Chem 1997; 272:10804–10.

88. Deng T, Karin M. c-Fos transcriptional activity stimulated by H-Ras-activated protein kinase distinct from JNK and ERK. Nature 1994; 371:171–5.

89. Smeal T, Binetruy B, Mercola DA, Birrer M, Karin M. Oncogenic and transcriptional cooperation with Ha-Ras requires phosphorylation of c-Jun on serines 63 and 73. Nature 1991; 354:494–6.

90. Binétruy B, Smeal T, Karin M. Ha-Ras augments c-Jun activity and stimulates phosphorylation of its activation domain. Nature 1991; 351:122–7.

91. Lin S, Kok S, Yeh FT, Kuo MY, Lin C, Wang C et al. MEK/ERK and signal transducer and activator of transcription signaling pathways modulate oncostatin M-stimulated CCL2 expression in human osteoblasts through a common transcription factor. Arthritis Rheum 2004; 50:785–93.

92. Wong CK, Wang CB, Ip WK, Tian YP, Lam CWK. Role of p38 MAPK and NF-kB for chemokine release in coculture of human eosinophils and bronchial epithelial cells. Clin Exp Immunol 2005; 139:90–100.

93. Mercier P, Bachvarova M, Plante M, Gregoire J, Renaud M, Ghani K et al. Characterization of DOK1, a candidate tumor suppressor gene, in epithelial ovarian cancer. Mol Oncol 2011; 5:438–53.

94. Berger AH, Niki M, Morotti A, Taylor BS, Socci ND, Viale A et al. Identification of DOK genes as lung tumor suppressors. Nat Genet 2010; 42:216–23.

95. Sánchez-Pérez I, Perona R. Lack of c-Jun activity increases survival to cisplatin. FEBS Letters 1999; 453:151–8.

96. Yuan Z, Feldman RI, Sussman GE, Coppola D, Nicosia SV, Cheng JQ. AKT2 inhibition of cisplatin-induced JNK/p38 and Bax activation by phosphorylation of ASK1: implication of AKT2 in chemoresistance. J Biol Chem 2003; 278:23432–40.

97. Khatlani TS, Wislez M, Sun M, Srinivas H, Iwanaga K, Ma L et al. c-Jun N-terminal kinase is activated in non-small-cell lung cancer and promotes neoplastic transformation in human bronchial epithelial cells. Oncogene 2007; 26:2658–66.

98. Brozovic A, Fritz G, Christmann M, Zisowsky J, Jaehde U, Osmak M et al. Long-term activation of SAPK/JNK, p38 kinase and fas-L expression by cisplatin is attenuated in human carcinoma cells that acquired drug resistance. Int J Cancer 2004; 112:974–85.

99. Brozovic A, Osmak M. Activation of mitogen-activated protein kinases by cisplatin and their role in cisplatin-resistance. Cancer Lett 2007; 251:1–16.

100. Yan F, Wang X, Liu Z, Pan C, Yuan S, Ma Q. JNK1, JNK2, and JNK3 are involved in P-glycoprotein-mediated multidrug resistance of hepatocellular carcinoma cells. HBPD INT 2010; 9:287–95.

101. Galan-Moya EM, de la Cruz-Morcillo, Miguel A, Llanos Valero M, Callejas-Valera JL, Melgar-Rojas P, Hernadez Losa J et al. Balance between MKK6 and MKK3 mediates p38 MAPK associated resistance to cisplatin in NSCLC. PLoS ONE 2011; 6:e28406.

102. Hernández Losa J, Parada Cobo C, Guinea Viniegra J, Sánchez-Arevalo Lobo VJ, Ramón y Cajal S, Sánchez-Prieto R. Role of the p38 MAPK pathway in cisplatin-based therapy. Oncogene 2003; 22:3998–4006.

103. Refaat A, Aminullah, Zhou Y, Kawanishi M, Tomaru R, Abdelhamed S et al. Role of tyrosine kinase-independent phosphorylation of EGFR with activating mutation in cisplatin-treated lung cancer cells. Biochem Biophys Res Commun 2015; 458:856–61.

104. Wang X, Martindale JL, Holbrook NJ. Requirement for ERK activation in cisplatin-induced apoptosis. J Biol Chem 2000; 275:39435–43.

105. Wang M, Liu ZM, Li XC, Yao YT, Yin ZX. Activation of ERK1/2 and Akt is associated with cisplatin resistance in human lung cancer cells. J Chemother 2013; 25:162–9.

106. Shtivelman E, Hensing T, Simon GR, Dennis PA, Otterson GA, Bueno R et al. Molecular pathways and therapeutic targets in lung cancer. Oncotarget 2014; 5:1392–433.

107. Galluzzi L, Vitale I, Senovilla L, Eisenberg T, Carmona-Gutierrez D, Vacchelli E et al. Independent transcriptional reprogramming and apoptosis induction by cisplatin. Cell Cycle 2012; 11:3472–80.

108. Galluzzi L, Vitale I, Senovilla L, Olaussen KA, Pinna G, Eisenberg T et al. Prognostic impact of vitamin B6 metabolism in lung cancer. Cell Rep 2012; 2:257–69.

109. Zeng H, Qu Y, Zhang W, Xiu B, Deng A, Liang A. Proteomic analysis identified DJ-1 as a cisplatin resistant marker in non-small cell lung cancer. Int J Mol Sci 2011; 12:3489–99.

110. Yang Y, Li H, Hou S, Hu B, Liu J, Wang J. The noncoding RNA expression profile and the effect of lncRNA AK126698 on cisplatin resistance in non-small-cell lung cancer cell. PLoS ONE 2013; 8:e65309.

111. Schilder RJ, Ozols RF. New therapies for ovarian cancer. Cancer Invest 1992; 10:307–15.

112. Yang Y, Li H, Hou S, Hu B, Liu J, Wang J. The noncoding RNA expression profile and the effect of lncRNA AK126698 on cisplatin resistance in non-small-cell lung cancer cell. PLoS ONE 2013; 8:e65309.

113. Millward MJ, Zalcberg J, Bishop JF, Webster LK, Zimet A, Rischin D et al. Phase I trial of docetaxel and cisplatin in previously untreated patients with advanced non-small-cell lung cancer. J Clin Oncol 1997; 15:750–8.

114. Tegeder I, Brautigam L, Seegel M, Al-Dam A, Turowski B, Geisslinger G et al. Cisplatin tumor concentrations after intra-arterial cisplatin infusion or embolization in patients with oral cancer. Clin Pharmacol Ther 2003; 73:417–26.

115. Zisowsky J, Koegel S, Leyers S, Devarakonda K, Kassack MU, Osmak M et al. Relevance of drug uptake and efflux for cisplatin sensitivity of tumor cells. Biochem Pharmacol 2007; 73:298–307.

116. Rose MC, Kostyanovskaya E, Huang RS. Pharmacogenomics of cisplatin sensitivity in non-small cell lung cancer. Genomics Proteomics Bioinformatics 2014; 12:198–209.

117. Kasahara K, Fujiwara Y, Nishio K, Ohmori T, Sugimoto Y, Komiya K et al. Metallothionein content correlates with the sensitivity of human small cell lung cancer cell lines to cisplatin. Cancer Res 1991; 51:3237–42.

118. Hao XY, Bergh J, Brodin O, Hellman U, Mannervik B. Acquired resistance to cisplatin and doxorubicin in a small cell lung cancer cell line is correlated to elevated expression of glutathione-linked detoxification enzymes. Carcinogenesis 1994; 15:1167–73.

119. Meijer C, Mulder NH, Vries EG de. The role of detoxifying systems in resistance of tumor cells to cisplatin and adriamycin. Cancer Treat Rev 1990; 17:389–407.

120. Barr MP, Gray SG, Hoffmann AC, Hilger RA, Thomale J, O'Flaherty JD et al. Generation and characterisation of cisplatin-resistant non-small cell lung cancer cell lines displaying a stem-like signature. PLoS ONE 2013; 8:e54193.

121. Zeng-Rong N, Paterson J, Alpert L, Tsao MS, Viallet J, Alaoui-Jamali MA. Elevated DNA repair capacity is associated with intrinsic resistance of lung cancer to chemotherapy. Cancer Res 1995; 55:4760–4.

122. Mountzios G, Dimopoulos M, Papadimitriou C. Excision Repair Cross-Complementation Group 1 Enzyme as a Molecular Determinant of Responsiveness to Platinum-Based Chemotherapy for non Small-Cell Lung Cancer. Biomark Insights 2008; 3:219–26.

123. Rosell R, Taron M, Alberola V, Massuti B, Felip E. Genetic testing for chemotherapy in non-small cell lung cancer. Lung Cancer 2003; 41:97-102.

124. Okamura S, Arakawa H, Tanaka T, Nakanishi H, Ng CC, Taya Y et al. p53DINP1, a p53-Inducible Gene, Regulates p53-Dependent Apoptosis. Mol Cell 2001; 8:85–94.

125. Shahbazi J, Lock R, Liu T. Tumor Protein 53-Induced Nuclear Protein 1 Enhances p53 Function and Represses Tumorigenesis. Front Genet 2013; 4:80.

126. Tomasini R, Samir AA, Vaccaro MI, Pebusque MJ, Dagorn JC, Iovanna JL et al. Molecular and functional characterization of the stress-induced protein (SIP) gene and its two transcripts generated by alternative splicing. SIP induced by stress and promotes cell death. J Biol Chem 2001; 276:44185–92.

127. Jiang P, Motoo Y, Sawabu N, Minamoto T. Effect of gemcitabine on the expression of apoptosis-related genes in human pancreatic cancer cells. World Journal of Gastroenterology 2006; 12:1597–602.

128. Tomasini R, Seux M, Nowak J, Bontemps C, Carrier A, Dagorn J et al. TP53INP1 is a novel p73 target gene that induces cell cycle arrest and cell death by modulating p73 transcriptional activity. Oncogene 2005; 24:8093–104.

129. Wang G, Chuang L, Zhang X, Colton S, Dombkowski A, Reiners J et al. The initiative role of XPC protein in cisplatin DNA damaging treatment-mediated cell cycle regulation. Nucleic Acids Res 2004; 32:2231–40.

130. Friedberg EC, Cheo DL, Meira LB, Reis AM. Cancer predisposition in mutant mice defective in the XPC DNA repair gene. Prog Exp Tumor Res 1999; 35:37–52.

131. Hollander MC, Philburn RT, Patterson AD, Velasco-Miguel S, Friedberg EC, Linnoila RI et al. Deletion of XPC leads to lung tumors in mice and is associated with early events in human lung carcinogenesis. Proc Natl Acad Sci USA 2005; 102:13200–5.

132. Saviozzi S, Ceppi P, Novello S, Ghio P, Lo Iacono M, Borasio P et al. Non-small cell lung cancer exhibits transcript overexpression of genes associated with homologous recombination and DNA replication pathways. Cancer Res 2009; 69:3390–6.

133. Wu Y, Cheng Y, Chang JT, Wu T, Chen C, Lee H. Reduced XPC messenger RNA level may predict a poor outcome of patients with nonsmall cell lung cancer. Cancer 2007; 110:215–23.

134. Weaver DA, Crawford EL, Warner KA, Elkhairi F, Khuder SA, Willey JC. ABCC5, ERCC2, XPA and XRCC1 transcript abundance levels correlate with cisplatin chemoresistance in non-small cell lung cancer cell lines. Mol Cancer 2005; 4:18.

135. Smith M, Chen I, Zhan Q, Bae I, Chen C, Gilmer T et al. Interaction of the p53-regulated protein Gadd45 with proliferating cell nuclear antigen. Science 1994; 266:1376–80.

136. Wang XW, Zhan Q, Coursen JD, Khan MA, Kontny HU, Yu L et al. GADD45 induction of a G2/M cell cycle checkpoint. Proc Natl Acad Sci USA 1999; 96:3706–11.

137. Ishiguro H, Kimura M, Takahashi H, Tanaka T, Mizoguchi K, Takeyama H. GADD45A expression is correlated with patient prognosis in esophageal cancer. Oncol Lett 2016; 11:277–82.

138. Lundholm L, Hååg P, Zong D, Juntti T, Mörk B, Lewensohn R et al. Resistance to DNA-damaging treatment in non-small cell lung cancer tumor-initiating cells involves reduced DNA-PK/ATM activation and diminished cell cycle arrest. Cell Death Dis 2013; 4:e478.

139. Horibe S, Matsuda A, Tanahashi T, Inoue J, Kawauchi S, Mizuno S et al. Cisplatin resistance in human lung cancer cells is linked with dysregulation of cell cycle associated proteins. Life Sci 2015; 124:31–40.

140. Kruse J, Gu W. Modes of p53 regulation. Cell 2009; 137:609–22.

141. Arbiser JL, Moses MA, Fernandez CA, Ghiso N, Cao Y, Klauber N et al. Oncogenic H-ras stimulates tumor angiogenesis by two distinct pathways. PNAS 1997; 94:861–6.

142. Nikliński J, Niklińska W, Laudanski J, Chyczewska E, Chyczewski L. Prognostic molecular markers in non-small cell lung cancer. Lung Cancer 2001; 34:S53-S58.

143. To MD, Wong CE, Karnezis AN, Del Rosario R, Di Lauro R, Balmain A. Kras regulatory elements and exon 4A determine mutation specificity in lung cancer. Nat Genet 2008; 40:1240–4.

144. Karreth FA, Tuveson DA. Modelling oncogenic Ras/Raf signalling in the mouse. Curr Opin Genet Dev 2009; 19:4–11.

145. Prior IA, Hancock JF. Ras trafficking, localization and compartmentalized signalling. Semin Cell Dev Biol 2012; 23:145–53.

146. Fuchs SY, Adler V, Pincus MR, Ronai Z. MEKK1/JNK signaling stabilizes and activates p53. PNAS 1998; 95:10541–6.

147. Wu GS. The functional Interactions Between the MAPK and p53 Signaling Pathways. Cancer Biol Ther 2004; 3:156–61.

148. Wang M, Atayar C, Rosati S, Bosga-Bouwer A, Kluin P, Visser L. JNK is constitutively active in mantle cell lymphoma: cell cycle deregulation and polyploidy by JNK inhibitor SP600125. J Pathol 2009; 218:95–103.

149. Wang Z, Xu J, Zhou J, Liu Y, Wu GS. Mitogen-activated protein kinase phosphatase-1 is required for cisplatin resistance. Cancer Res 2006; 66:8870–7.

150. Tung C, Jian Y, Chen J, Wang T, Chen W, Zheng H et al. Curcumin downregulates p38 MAPK-dependent X-ray repair cross-complement group 1 (XRCC1) expression to enhance cisplatin-induced cytotoxicity in human lung cancer cells. Naunyn Schmiedebergs Arch Pharmacol 2016; 389:657–66.

151. Chen J, Solomides C, Parekh H, Simpkins F, Simpkins H. Cisplatin resistance in human cervical, ovarian and lung cancer cells. Cancer Chemother Pharmacol 2015; 75:1217–27.

152. Vega GG, Avilés-Salas A, Chalapud JR, Martinez-Paniagua M, Pelayo R, Mayani H et al. P38 MAPK expression and activation predicts failure of response to CHOP in patients with Diffuse Large B-Cell Lymphoma. BMC Cancer 2015; 15:1417.

153. Sanchez-Prieto R, Rojas JM, Taya Y, Gutkind JS. A Role for the p38 Mitogen-activated Protein Kinase Pathway in the Transcriptional Activation of p53 on Genotoxic Stress by Chemotherapeutic Agents. Cancer Res 2000; 60:2464–72.

154. Fader AN, RASOOL N, Vaziri SAJ, Kozuki T, Faber PW, ELSON P et al. CCL2 expression in primary ovarian carcinoma is correlated with chemotherapy response and survival outcomes. Anticancer Res 2010; 30:4791–8.

155. Levina V, Su Y, Nolen B, Liu X, Gordin Y, Lee M et al. Chemotherapeutic drugs and human tumor cells cytokine network. Int J Cancer 2008; 123:2031–40.

156. HO A, WONG C, LAM C. Tumor necrosis factor-α up-regulates the expression of CCL2 and adhesion molecules of human proximal tubular epithelial cells through MAPK signaling pathways. Immunobiology 2008; 213:533–44.

157. Maier T, Guell M, Serrano L. Correlation of mRNA and protein in complex biological samples. FEBS Letters 2009; 583:3966–73.

10 Appendix

Appendix A

Cisplatin cytotoxicity (MTT)

Values of a representative sigmoidal concentration-response curve of cisplatin in A549 and A549^{r}CDDP^{2000} cells. Survival is expressed in terms of % of absorbance of untreated cells as mean ± SD.

	A549				A549^{r}CDDP^{2000}			
	Absorption [%]		Absorption [units]		Absorption [%]		Absorption [units]	
log [conc.]	Mean	SD	Mean	SD	Mean	SD	Mean	SD
control	100.0	4.1	0.508	0.021	100.0	1.4	0.464	0.007
-6.301	107.2	8.6	0.544	0.044	91.2	1.1	0.423	0.005
-6.000	101.5	3.0	0.516	0.015	100.2	3.1	0.465	0.014
-5.301	107.7	3.8	0.547	0.019	98.3	4.1	0.456	0.019
-5.000	97.2	3.6	0.494	0.018	98.3	11.0	0.456	0.051
-4.523	40.4	3.9	0.205	0.020	89.4	3.1	0.414	0.014
-4.301	24.7	4.4	0.125	0.023	63.8	6.4	0.296	0.030
-4.155	23.4	2.5	0.119	0.012	37.0	5.2	0.171	0.024
-4.000	20.5	2.2	0.104	0.011	16.8	1.4	0.078	0.007
-3.301	12.1	0.4	0.061	0.002	9.4	0.9	0.044	0.004

Sensitivity of A549 and A549^{r}CDDP^{2000} cells towards cisplatin expressed as pEC_{50} (results of different testing days, n = 11-12).

Cell line	A549	A549^{r}CDDP^{2000}
pEC_{50}	-4.744	-4.667
	-4.554	-4.392
	-4.537	-4.234
	-4.671	-4.261
	-4.248	-4.024
	-4.329	-4.093
	-4.662	-4.066
	-4.500	-4.349
	-4.487	-4.307
	-4.511	-4.266
	-4.498	-4.288
		-4.196
Mean (SD)	-4.522 (0.144)	-4.626 (0.171)

Appendix B

Cellular platinum accumulation

Cellular platinum accumulation in A549 and A549^{r}CDDP^{2000} cells, treated with 11 µM or 34 µM cisplatin (results of different testing days, n = 29-33).

Cell line	A549		A549^{r}CDDP^{2000}
Treatment concentration	11 µM	11 µM	34 µM
Cellular platinum accumulation [µmol platinum/g protein]	0.108	0.083	0.212
	0.099	0.074	0.239
	0.108	0.105	0.257
	0.119	0.079	0.134
	0.103	0.057	0.128
	0.110	0.049	0.206
	0.083	0.059	0.198
	0.074	0.079	0.212
	0.078	0.073	0.207
	0.096	0.076	0.230
	0.087	0.046	0.156
	0.092	0.080	0.233
	0.062	0.061	0.250
	0.074	0.066	0.271
	0.071	0.064	0.104
	0.072	0.054	0.198
	0.100	0.035	0.217
	0.096	0.039	0.174
	0.030	0.042	0.155
	0.038	0.038	0.179
	0.050	0.039	0.067
	0.041	0.043	0.070
	0.052	0.025	0.085
	0.053	0.019	0.075
	0.026	0.037	0.068
	0.029	0.025	0.066
	0.031	0.030	0.068
	0.029	0.016	0.059
	0.034	0.023	0.072
	0.037	0.023	
	0.030	0.034	
	0.034		
	0.036		
Mean (SEM)	0.066 (0.005)	0.051 (0.004)	0.158 (0.013)

Appendix C

Cisplatin-DNA adduct formation

Cisplatin-DNA adduct formation in A549 and A549^{r}CDDP^{2000} cells, treated with 11 µM or 34 µM cisplatin for 4h and 24h as integrated signal intensity (results of different testing days, n = 3).

Cell line	A549			A549^{r}CDDP^{2000}		
Treatment duration	4 h			24 h		
Treatment concentration	11 µM	11 µM	34 µM	11 µM	11 µM	34 µM
	12.74	6.83	20.12	6.75	3.45	7.55
	13.91	8.56	11.39	30.87	12.13	23.14
	12.65	10.81	25.60	22.12	8.04	20.78
Mean (SEM)	13.10 (0.41)	8.73 (1.15)	19.04 (4.14)	19.91 (7.05)	7.87 (2.51)	17.16 (4.85)

Appendix D

Cell cycle analysis

Cell fraction in % in G_1/G_0-phase, S-phase and G_2/M-phase in A549 and A549^{r}CDDP^{2000} cells (results of different testing days, n = 3-5).

Cell line	A549		A549^{r}CDDP^{2000}		
Treatment concentration	control	11 µM	control	11 µM	34 µM
Cell phase	Cell fraction [%]	Cell fraction [%]	Cell fraction [%]	Cell fraction [%]	Cell fraction [%]
G_1/G_0	70.87	25.82	67.46	40.46	47.78
	72.30	18.59	66.79	50.97	47.58
	69.25	11.87	72.82	58.25	52.56
	68.38	11.68			50.54
	75.82	50.13			50.52
	75.89	47.38			51.94
Mean (SEM)	72.09 (1.31)	27.58 (7.03)	69.02 (1.91)	49.89 (5.16)	50.15 (0.85)
S	11.39	9.87	9.86	27.54	10.77
	7.81	8.66	13.35	21.43	16.07
	12.13	10.21	10.70	17.67	15.50
	12.50	6.68			13.23
	8.39	22.23			19.96
	9.92	24.91			15.98
Mean (SEM)	10.36 (0.80)	13.76 (3.16)	11.30 (1.05)	22.21 (2.88)	15.25 (1.26)
G_2/M	14.12	44.50	11.07	11.17	4.56
	15.36	54.99	10.69	10.43	4.13
	15.80	62.10	5.47	9.04	6.55
	16.61	62.74			6.26
	11.94	11.81			5.28
	11.14	12.93			6.45
Mean (SEM)	14.16 (0.90)	41.51 (9.60)	9.08 (1.81)	10.21 (0.62)	5.54 (0.42)

Appendix E

Apoptosis induction

Apoptosis analysis with FITC Annexin (n = 3-4) and cell count in the $SubG_1$-phase (n = 3-6) as fold change related to untreated controls in A549 and $A549^{r}CDDP^{2000}$ cells.

Cell line	A549	$A549^{r}CDDP^{2000}$	
Treatment concentration	11 µM	11 µM	34 µM
	FITC-Annexin [fold change to untreated control]		
	6.922	2.141	4.956
	4.994	2.114	2.811
	5.649	1.027	3.374
		2.516	
Mean (SEM)	5.856 (0.566)	1.950 (0.321)	3.714 (0.642)
	$SubG_1$-phase [fold change to untreated control]		
	5.470	1.948	3.347
	4.190	1.672	3.048
	5.296	1.380	2.288
	7.112		
	3.973		
	4.599		
Mean (SEM)	5.107 (0.468)	1.667 (0.164)	2.894 (0.315)

Appendix F

p53

Results of p53 in real-time RT-PCR (n = 3) as fold change relative to untreated control using the ΔΔCp method and absolute data calculated using the ΔCp method, and densitometric protein results in Western blot (n = 3) as fold change and integrated signal intensity; normalised to the housekeeper α-actin in A549 and A549^{r}CDDP^{2000} cells.

Cell line	A549		A549^{r}CDDP^{2000}		
Treatment concentration	control	11 µM	control	11 µM	34 µM
mRNA (fold change relative to untreated control)					
		1.015		1.140	0.979
		1.438		0.952	0.806
		0.907		1.024	1.227
Mean (SEM)		1.120 (0.162)		1.038 (0.055)	1.004 (0.122)
mRNA (absolute data)					
	0.024	0.024	0.041	0.047	0.040
	0.022	0.032	0.051	0.048	0.041
	0.026	0.023	0.045	0.046	0.055
Mean (SEM)	0.024 (0.001)	0.026 (0.003)	0.046 (0.003)	0.047 (0.001)	0.045 (0.005)
Protein (fold change relative to untreated control)					
		11.44		2.32	6.64
		11.05		2.55	3.19
		9.24		1.37	4.34
Mean (SEM)		10.58 (0.68)		2.08 (0.36)	4.72 (1.01)
Protein (integrated signal intensity)					
	0.48	5.54	0.90	2.08	5.95
	0.40	4.48	1.22	3.11	3.89
	0.25	2.32	0.55	0.75	2.39
Mean (SEM)	0.38 (0.07)	4.11 (0.95)	0.89 (0.19)	1.98 (0.68)	4.01 (1.03)

Appendix G

pAtm

Results of pAtm as densitometric protein results in Western blot (n = 3) as fold change and integrated signal intensity normalised to the housekeeper α-actin in A549 and A549^{r}CDDP^{2000} cells.

Cell line	A549		A549^{r}CDDP^{2000}		
Treatment concentration	control	11 µM	control	11 µM	34 µM
Protein (fold change relative to untreated control)					
		1.92		2.04	2.87
		15.35		3.50	2.17
		2.34		1.59	2.90
Mean (SEM)		6.54 (4.41)		2.38 (0.58)	2.65 (0.24)
Protein (integrated signal intensity)					
	1.12	2.15	0.93	1.90	2.67
	0.26	3.99	0.30	1.05	0.65
	1.32	3.09	1.18	1.88	3.42
Mean (SEM)	0.90 (0.33)	3.08 (0.53)	0.80 (0.26)	1.61 (0.28)	2.25 (0.83)

Appendix H

MDM2

Results of MDM2 in real-time RT-PCR (n = 3) as fold change relative to untreated control calculated using the ΔΔCp method and absolute data calculated using the ΔCp method and densitometric protein results in Western blot (n = 7) as fold change and integrated signal intensity; normalised to the housekeeper GAPDH in A549 and A549^{r}CDDP^{2000} cells.

Cell line	A549		A549^{r}CDDP^{2000}		
Treatment concentration	control	11 µM	control	11 µM	34 µM
mRNA (fold change relative to untreated control)					
		4.785		1.520	3.125
		4.719		1.535	1.973
		3.998		1.429	2.596
Mean (SEM)		4.501 (0.252)		1.495 (0.033)	2.565 (0.333)
mRNA (absolute data)					
	0.003	0.020	0.007	0.011	0.027
	0.004	0.025	0.010	0.017	0.023
	0.003	0.018	0.005	0.007	0.015
Mean (SEM)	0.003 (0.0002)	0.021 (0.002)	0.007 (0.002)	0.012 (0.003)	0.022 (0.003)
Protein (fold change relative to untreated control)					
		2.87		0.94	1.27
		0.86		0.91	0.83
		1.76		1.11	1.77
		0.87		0.95	0.91
		1.96		1.50	1.16
		1.01		1.08	0.61
		0.97		0.65	0.56
Mean (SEM)		1.47 (0.29)		1.02 (0.10)	1.01 (0.16)
Protein (integrated signal intensity)					
	0.21	0.18	0.23	0.21	0.19
	0.15	0.43	0.33	0.31	0.42
	1.47	2.58	2.30	2.56	4.07
	0.46	0.40	0.81	0.77	0.74
	0.71	1.39	0.96	1.44	1.11
	2.32	2.35	3.85	4.14	2.33
Mean (SEM)	1.14 (0.39)	1.42 (0.41)	2.21 (0.93)	2.00 (0.68)	1.82 (0.62)

Appendix I

p21

Results of p21 in real-time RT-PCR (n = 3) as fold change relative to untreated control calculated using the ΔΔCp method and absolute data calculated using the ΔCp method and densitometric protein results in Western blot (n = 3) as fold change and integrated signal intensity; normalised to the housekeeper α-actin in A549 and A549^{r}CDDP^{2000} cells.

Cell line	A549		A549^{r}CDDP^{2000}		
Treatment concentration	control	11 µM	control	11 µM	34 µM
mRNA (fold change relative to untreated control)					
		9.496		2.534	8.619
		6.239		2.611	5.199
		6.713		1.921	5.206
Mean (SEM)		7.483 (1.016)		2.355 (0.218)	6.341 (1.139)
mRNA (absolute data)					
	0.013	0.162	0.025	0.070	0.271
	0.023	0.174	0.033	0.096	0.205
	0.013	0.107	0.018	0.038	0.115
Mean (SEM)	0.016 (0.003)	0.148 (0.021)	0.026 (0.004)	0.068 (0.017)	0.197 (0.045)
Protein (fold change relative to untreated control)					
		1.73		1.16	1.76
		1.56		0.89	1.04
		1.29		1.18	1.15
Mean (SEM)		1.53 (0.13)		1.08 (0.09)	1.32 (0.22)
Protein (integrated signal intensity)					
	1.84	3.19	1.59	1.84	2.80
	0.95	1.48	1.49	1.33	1.55
	1.32	1.70	1.43	1.69	1.65
Mean (SEM)	1.37 (0.26)	2.12 (0.54)	1.50 (0.05)	1.62 (0.15)	2.00 (0.40)

Appendix J

SIP

Results of p21 in real-time RT-PCR (n = 3) as fold change relative to untreated control using the ΔΔCp method and absolute data calculated using the ΔCp method and densitometric protein results in Western blot (n = 5) as fold change and integrated signal intensity; normalised to the housekeeper GAPDH in A549 and A549^{r}CDDP^{2000} cells.

Cell line	A549		A549^{r}CDDP^{2000}		
Treatment concentration	control	11 µM	control	11 µM	34 µM
mRNA (fold change relative to untreated control)					
		7.836		1.569	1.811
		5.633		1.229	1.171
		3.601		1.495	2.695
Mean (SEM)		5.690 (1.223)		1.431 (0.103)	1.892 (0.442)
mRNA (absolute data)					
	$2.6\cdot10^{-4}$	$2.2\cdot10^{-3}$	$7.8\cdot10^{-4}$	$1.3\cdot10^{-3}$	$1.5\cdot10^{-3}$
	$5.0\cdot10^{-4}$	$3.0\cdot10^{-3}$	$1.2\cdot10^{-3}$	$1.5\cdot10^{-3}$	$1.4\cdot10^{-3}$
	$3.8\cdot10^{-4}$	$1.4\cdot10^{-3}$	$6.0\cdot10^{-4}$	$9.1\cdot10^{-4}$	$1.7\cdot10^{-3}$
Mean (SEM)	$3.8\cdot10^{-4}$ ($7.0\cdot10^{-5}$)	$2.2\cdot10^{-3}$ ($4.6\cdot10^{-4}$)	$8.5\cdot10^{-4}$ ($1.6\cdot10^{-4}$)	$1.2\cdot10^{-3}$ ($1.5\cdot10^{-4}$)	$1.5\cdot10^{-3}$ ($9.3\cdot10^{-5}$)
Protein (fold change relative to untreated control)					
		1.40		0.87	0.84
		1.26		1.22	1.31
		0.58		1.31	1.35
		0.74		0.63	0.73
		0.84		0.73	0.75
Mean (SEM)		0.96 (0.16)		0.95 (0.13)	0.99 (0.14)
Protein (integrated signal intensity)					
	0.47	0.65	1.50	1.30	1.25
	0.40	0.51	1.12	1.36	1.47
	0.59	0.34	0.90	1.18	1.22
	0.60	0.45	1.79	1.13	1.30
	0.47	0.39	0.98	0.72	0.73
Mean (SEM)	0.51 (0.04)	0.47 (0.05)	1.26 (0.17)	1.14 (0.11)	1.20 (0.12)

Appendix K

XPC

Results of XPC in real-time RT-PCR (n = 3) as fold change relative to untreated control using the ΔΔCp method and absolute data calculated using the ΔCp method and densitometric protein results in Western blot (n = 5) as fold change and integrated signal intensity; normalised to the housekeeper GAPDH in A549 and A549^{r}CDDP^{2000} cells.

Cell line	A549		A549^{r}CDDP^{2000}		
Treatment concentration	control	11 µM	control	11 µM	34 µM
mRNA (fold change relative to untreated control)					
		3.385		1.572	1.586
		2.783		1.005	0.849
		2.505		1.414	2.210
Mean (SEM)		2.891 (0.260)		1.331 (0.167)	1.548 (0.393)
mRNA (absolute data)					
	0.008	0.032	0.021	0.034	0.034
	0.009	0.030	0.023	0.023	0.019
	0.007	0.020	0.011	0.016	0.026
Mean (SEM)	0.008 (0.001)	0.027 (0.004)	0.018 (0.004)	0.024 (0.005)	0.026 (0.004)
Protein (fold change relative to untreated control)					
		1.38		0.80	0.97
		1.77		1.39	1.71
		1.33		1.25	1.25
		1.47		0.68	1.32
		1.09		1.56	1.66
Mean (SEM)		1.41 (0.11)		1.13 (0.17)	1.38 (0.14)
Protein (integrated signal intensity)					
	0.93	1.28	1.21	0.97	1.18
	0.83	1.48	0.96	1.33	1.64
	0.93	1.23	1.07	1.34	1.34
	0.72	1.06	1.15	0.78	1.52
	1.20	1.31	1.33	2.08	2.22
Mean (SEM)	0.92 (0.08)	1.27 (0.07)	1.15 (0.06)	1.30 (0.22)	1.58 (0.18)

Appendix L

GADD45a

Results of GADD45a in real-time RT-PCR (n = 3) as fold change relative to untreated control using the ΔΔCp method and absolute data calculated using the ΔCp method and densitometric protein results in Western blot (n = 4) as fold change and integrated signal intensity; normalised to the housekeeper GAPDH in A549 and A549^{r}CDDP^{2000} cells.

Cell line	A549		A549^{r}CDDP^{2000}		
Treatment concentration	control	11 µM	control	11 µM	34 µM
mRNA (fold change relative to untreated control)					
		5.497		1.719	2.727
		3.014		1.667	1.770
		3.036		1.306	2.088
Mean (SEM)		3.849 (0.824)		1.564 (0.130)	2.195 (0.282)
mRNA (absolute data)					
	0.005	0.034	0.018	0.034	0.058
	0.010	0.037	0.024	0.043	0.046
	0.007	0.027	0.012	0.017	0.029
Mean (SEM)	0.007 (0.002)	0.033 (0.003)	0.018 (0.003)	0.031 (0.008)	0.044 (0.008)
Protein (fold change relative to untreated control)					
		0.67		0.95	0.81
		1.30		0.91	0.89
		0.76		1.03	0.90
		0.75		1.05	0.73
Mean (SEM)		0.87 (0.15)		0.98 (0.03)	0.83 (0.04)
Protein (integrated signal intensity)					
	1.15	0.77	1.51	1.44	1.22
	0.81	1.05	0.86	0.77	0.76
	0.78	0.59	0.87	0.89	0.78
	0.94	0.70	1.22	1.28	0.88
Mean (SEM)	0.92 (0.09)	0.78 (0.10)	1.12 (0.16)	1.10 (0.16)	0.91 (0.11)

Appendix M

Validation of the micro array data

Fold change of the 10 significantly up- or down-regulated genes on the microarray.

Cell line	A549	$A549^{r}CDDP^{2000}$	
Treatment concentration	11 µM	11 µM	34 µM
Gene	mRNA (fold change relative to untreated control on microarray)		
HRas	n.s.	n.s.	2.34
MDM2	5.22	2.15	3.25
p21	8.60	2.65	6.82
JNK3	n.s.	-4.77	-3.80
Wnt4	-2.62	n.s.	6.08
CCL2	5.76	n.s.	5.33
SLC9A9	n.s.	-7.43	-36.57
DOK1	n.s.	n.s.	n.s.
p38	n.s.	n.s.	n.s.
DNER	-4.83	-.206	-5.39

Appendix N

HRas

Results of HRas in real-time RT-PCR (n = 3) as fold change relative to untreated control using the ΔΔCp method and absolute data calculated using the ΔCp method and densitometric protein results in Western blot (n = 6) as fold change and integrated signal intensity; normalised to the housekeeper GAPDH in A549 and A549^{r}CDDP^{2000} cells.

Cell line	A549		A549^{r}CDDP^{2000}		
Treatment concentration	control	11 µM	control	11 µM	34 µM
mRNA (fold change relative to untreated control)					
		2.230		1.410	2.470
		1.430		1.900	7.570
		1.640		0.810	1.360
Mean (SEM)		1.767 (0.240)		1.373 (0.315)	3.800 (1.912)
mRNA (absolute data)					
	0.018	0.045	0.014	0.023	0.046
	0.018	0.028	0.013	0.028	0.131
	0.016	0.028	0.023	0.020	0.0380
Mean (SEM)	0.007 (0.002)	0.033 (0.003)	0.018 (0.003)	0.031 (0.008)	0.044 (0.008)
Protein (fold change relative to untreated control)					
		1.23		0.93	0.73
		1.58		0.70	0.75
		1.19		0.71	0.66
		0.76		0.87	0.90
		1.51		0.42	0.51
		0.76		0.84	0.52
Mean (SEM)		1.17 (0.14)		0.75 (0.08)	0.68 (0.06)
Protein (integrated signal intensity)					
	0.13	0.16	0.15	0.14	0.11
	0.12	0.19	0.20	0.14	0.15
	0.77	0.92	1.21	0.86	0.80
	1.19	0.91	1.69	1.47	1.52
	0.80	1.21	2.24	0.93	1.15
	1.15	0.87	2.46	2.07	1.27
Mean (SEM)	0.69 (0.19)	0.71 (0.18)	1.33 (0.40)	0.94 (0.31)	0.83 (0.24)

Appendix O

JNK3

Results of JNK3 in real-time RT-PCR (n = 3) as fold change relative to untreated control using the ΔΔCp method and absolute data calculated using the ΔCp method and densitometric protein results in Western blot (n = 9) as fold change and integrated signal intensity; normalised to the housekeeper GAPDH in A549 and A549^{r}CDDP^{2000} cells.

Cell line	A549		A549^{r}CDDP^{2000}		
Treatment concentration	control	11 µM	control	11 µM	34 µM
mRNA (fold change relative to untreated control)					
		0.160		0.240	0.020
		0.110		0.160	0.050
		0.030		0.230	0.040
Mean (SEM)		0.100 (0.038)		0.210 (0.025)	0.037 (0.009)
mRNA (absolute data)					
	$1.0\cdot10^{-5}$	$1.9\cdot10^{-6}$	$3.3\cdot10^{-4}$	$9.1\cdot10^{-5}$	$1.1\cdot10^{-5}$
	$1.7\cdot10^{-5}$	$2.2\cdot10^{-6}$	$1.3\cdot10^{-4}$	$2.4\cdot10^{-5}$	$7.5\cdot10^{-6}$
	$3.1\cdot10^{-5}$	$1.2\cdot10^{-6}$	$4.9\cdot10^{-4}$	$1.3\cdot10^{-4}$	$2.4\cdot10^{-5}$
Mean (SEM)	$1.9\cdot10^{-5}$ ($6.1\cdot10^{-6}$)	$1.7\cdot10^{-6}$ ($2.9\cdot10^{-7}$)	$3.1\cdot10^{-4}$ ($1.0\cdot10^{-4}$)	$8.1\cdot10^{-5}$ ($3.0\cdot10^{-5}$)	$1.4\cdot10^{-5}$ ($5.1\cdot10^{-6}$)
Protein (fold change relative to untreated control)					
		0.67		0.76	0.73
		0.60		1.54	0.58
		0.65		0.86	0.48
		0.76		0.66	0.72
		0.80		1.47	0.72
		1.34		0.63	0.34
		1.29		1.45	0.72
		1.64		1.00	0.67
		1.50		1.61	1.22
Mean (SEM)		1.17 (0.14)		0.75 (0.08)	0.68 (0.06)
Protein (integrated signal intensity)					
	0.54	0.36	0.37	0.28	0.27
	0.63	0.38	0.59	0.91	0.34
	0.20	0.13	0.21	0.18	0.10
	0.21	0.16	0.32	0.21	0.23
	0.64	0.51	0.53	0.78	0.38
	0.18	0.24	0.32	0.20	0.11
	0.28	0.36	0.29	0.42	0.21
	0.11	0.18	0.15	0.15	0.10
	0.18	0.27	0.23	0.37	0.28
Mean (SEM)	0.33 (0.07)	0.29 (0.04)	0.33 (0.05)	0.39 (0.09)	0.22 (0.03)

Appendix P

p38

Results of p38 in real-time RT-PCR (n = 3) as fold change relative to untreated control using the ΔΔCp method and absolute data calculated using the ΔCp method and densitometric protein results in Western blot (n = 6) as fold change and integrated signal intensity; normalised to the housekeeper GAPDH in A549 and A549^{r}CDDP^{2000} cells.

Cell line	A549			A549^{r}CDDP^{2000}	
Treatment concentration	control	11 µM	control	11 µM	34 µM
mRNA (fold change relative to untreated control)					
		1.310		0.800	0.990
		1.460		0.940	1.880
		1.380		0.520	0.600
Mean (SEM)		1.383 (0.043)		0.753 (0.124)	1.157 (0.379)
mRNA (absolute data)					
	$2.4\cdot10^{-3}$	$3.3\cdot10^{-3}$	$6.9\cdot10^{-3}$	$5.7\cdot10^{-3}$	$7.7\cdot10^{-3}$
	$1.8\cdot10^{-3}$	$2.8\cdot10^{-3}$	$4.1\cdot10^{-3}$	$4.0\cdot10^{-3}$	$8.2\cdot10^{-3}$
	$2.3\cdot10^{-3}$	$3.2\cdot10^{-3}$	$9.1\cdot10^{-3}$	$4.8\cdot10^{-3}$	$5.8\cdot10^{-3}$
Mean (SEM)	$2.2\cdot10^{-3}$ ($1.6\cdot10^{-5}$)	$3.1\cdot10^{-3}$ ($1.3\cdot10^{-5}$)	$6.7\cdot10^{-3}$ ($1.4\cdot10^{-3}$)	$4.8\cdot10^{-3}$ ($5.0\cdot10^{-5}$)	$7.2\cdot10^{-3}$ ($7.3\cdot10^{-4}$)
Protein (fold change relative to untreated control)					
		0.93		1.10	1.08
		0.97		1.39	1.27
		0.90		1.06	0.81
		1.39		0.93	0.83
		0.82		1.26	1.23
		0.68		0.81	0.83
Mean (SEM)		0.95 (0.10)		1.09 (0.09)	1.01 (0.09)
Protein (integrated signal intensity)					
	0.82	0.73	0.78	0.83	0.64
	0.91	0.75	0.42	0.53	0.52
	1.09	1.52	0.97	0.90	0.80
	1.13	1.10	0.92	1.28	1.16
	1.70	1.16	1.22	0.98	1.01
	1.22	1.14	0.91	1.00	0.99
Mean (SEM)	1.15 (0.13)	1.07 (0.12)	0.87 (0.11)	0.92 (0.10)	0.85 (0.10)

Appendix Q

CCL2

Results of CCL2 in real-time RT-PCR (n = 3) as fold change relative to untreated control using the ΔΔCp method and absolute data calculated using the ΔCp method and densitometric protein results in Western blot (n = 4) as fold change and integrated signal intensity; normalised to the housekeeper GAPDH in A549 and A549^{r}CDDP^{2000} cells.

Cell line	A549		A549^{r}CDDP^{2000}		
Treatment concentration	control	11 µM	control	11 µM	34 µM
mRNA (fold change relative to untreated control)					
		7.630		2.410	14.220
		4.150		4.320	29.230
		4.510		1.050	2.320
Mean (SEM)		5.430 (1.105)		2.593 (0.948)	15.260 (7.786)
mRNA (absolute data)					
	$8.5\cdot10^{-5}$	$1.2\cdot10^{-3}$	$1.2\cdot10^{-4}$	$3.0\cdot10^{-4}$	$3.1\cdot10^{-3}$
	$2.6\cdot10^{-4}$	$1.6\cdot10^{-2}$	$2.8\cdot10^{-4}$	$1.3\cdot10^{-3}$	$1.5\cdot10^{-2}$
	$2.3\cdot10^{-4}$	$1.3\cdot10^{-3}$	$1.9\cdot10^{-4}$	$2.2\cdot10^{-3}$	$6.1\cdot10^{-4}$
Mean (SEM)	$1.9\cdot10^{-4}$ ($5.5\cdot10^{-5}$)	$6.2\cdot10^{-4}$ ($4.9\cdot10^{-4}$)	$1.9\cdot10^{-4}$ ($4.5\cdot10^{-5}$)	$6.1\cdot10^{-4}$ ($3.5\cdot10^{-4}$)	$6.1\cdot10^{-3}$ ($4.4\cdot10^{-3}$)
Protein (fold change relative to untreated control)					
		1.00		0.90	1.50
		0.80		0.85	1.15
		0.96		0.96	1.12
		0.88		1.20	1.05
Mean (SEM)		0.91 (0.05)		0.98 (0.08)	1.21 (0.10)
Protein (integrated signal intensity)					
	0.11	0.11	0.10	0.09	0.15
	0.10	0.08	0.13	0.11	0.15
	0.27	0.26	0.26	0.25	0.29
	0.24	0.21	0.20	0.24	0.21
Mean (SEM)	0.18 (0.04)	0.17 (0.04)	0.17 (0.36)	0.17 (0.04)	0.20 (0.03)

Appendix R

DOK1

Results of CCL2 in real-time RT-PCR (n = 3) as fold change relative to untreated control using the ΔΔCp method and absolute data calculated using the ΔCp method and densitometric protein results in Western blot (n ≤ 8) as fold change and integrated signal intensity; normalised to the housekeeper α-actin in A549 and A549^{r}CDDP^{2000} cells.

Cell line	A549		A549^{r}CDDP^{2000}		
Treatment concentration	control	11 µM	control	11 µM	34 µM
mRNA (fold change relative to untreated control)					
		0.670		1.780	1.810
		3.050		3.810	2.080
		1.370		1.090	1.430
Mean (SEM)		1.697 (0.706)		2.227 (0.816)	1.773 (0.189)
mRNA (absolute data)					
	$2.0\cdot10^{-4}$	$1.4\cdot10^{-4}$	$9.9\cdot10^{-5}$	$1.7\cdot10^{-4}$	$1.7\cdot10^{-4}$
	$2.4\cdot10^{-4}$	$6.0\cdot10^{-4}$	$2.1\cdot10^{-4}$	$7.3\cdot10^{-4}$	$4.1\cdot10^{-4}$
	$4.0\cdot10^{-4}$	$5.2\cdot10^{-4}$	$3.0\cdot10^{-4}$	$3.4\cdot10^{-4}$	$4.4\cdot10^{-4}$
Mean (SEM)	$2.7\cdot10^{-4}$ ($6.1\cdot10^{-5}$)	$4.2\cdot10^{-4}$ ($1.4\cdot10^{-4}$)	$2.0\cdot10^{-4}$ ($5.8\cdot10^{-5}$)	$4.1\cdot10^{-4}$ ($1.6\cdot10^{-4}$)	$3.4\cdot10^{-4}$ ($8.4\cdot10^{-5}$)
Protein (fold change relative to untreated control)					
		1.28		1.37	2.06
		0.70		1.06	1.12
		1.02		1.16	1.78
		2.00		1.17	1.07
		0.55		1.40	0.81
		1.19		0.61	0.91
				1.01	0.41
				0.63	0.93
Mean (SEM)		1.12 (0.21)		1.05 (0.11)	1.14 (0.19)
Protein (integrated signal intensity)					
	0.60	0.77	1.13	1.55	2.33
	1.20	0.84	1.40	1.48	1.57
	0.63	0.64	2.66	3.09	4.74
	0.07	0.14	1.35	1.58	1.44
	0.26	1.71	1.20	1.68	0.97
	0.31	0.17	4.63	2.81	4.23
	0.21	0.25	0.99	1.00	0.41
			0.70	0.44	0.65
Mean (SEM)	0.47 (0.14)	0.65 (0.21)	1.76 (0.46)	1.70 (0.31)	2.04 (0.57)